Modelling of potential energy savings of solar powered smart windows

Patrick Kwee

Technische Universiteit Delft

TU Delft

Modelling of potential energy savings of solar powered smart windows

by

Patrick Kwee

to obtain the degree of Master of Science
at the Delft University of Technology,
to be defended publicly on Friday August 21, 2020 at 2:00 PM.

Student number: 4646592

Thesis committee:		
	Dr. O. Isabella,	TU Delft, supervisor
	Prof. dr. ir. A.A.J.F. van den Dobbelsteen,	TU Delft
	Dr. ir. M.J. Tenpierik,	TU Delft
	J.C. Ortiz Lizcano,	TU Delft, daily supervisor

An electronic version of this thesis is available at http://repository.tudelft.nl/.

TU Delft

Abstract

The built environment is among the highest energy consuming sectors worldwide. However, buildings have large surface areas that can be used to improve the building energy performance. One example is by integration of photovoltaic systems in roofs and facades, which can reduce the carbon footprint of the built environment. An emerging field that could lead to energy savings involves the glazing. Switchable or smart windows allow for a variable transparency which affects the amount of incoming daylight and solar heat. Manually controlled smart windows however, require electricity to function and could thus be powered by solar energy to function autonomously. Smart windows have been shown to improve the building energy performance by reducing heating, cooling and lighting loads and can also be used to optimize the visual and thermal comfort conditions of occupants. In this thesis project the energy performance of three types of switchable glazing has been compared to different window technologies including electricity generating photovoltaic windows. Additionally, the hourly and yearly electricity requirements of each smart window and the corresponding minimal photovoltaic system requirements have been determined.

Acknowledgements

During my thesis project many people from both the PVMD group as well as the architecture department at TU Delft have helped me and I am very grateful for their time and help. First of all I would like to thank my supervisor Dr. Olindo Isabella for his feedback and suggestions on my work. This encouraged me to find details which I did not search before. I also would like to thank my daily supervisor Juan Camilo Ortiz Lizcano for introducing me to the thesis topic, for his recommendations and tips throughout the project duration and for the daily support he gave me even when he was in hospital. My project involved coding which I did in Matlab and I am grateful for the help I got with this from Andres Calcabrini and Maarten Verkou. Besides I got to work in the simulation tool Grasshopper which I never used before and I am grateful for the help I got with this from Tiantian Du and Dr. Martin Tenpierik. I would also like to thank Dr. Tenpierik for being part of the thesis committee. Although in the end I did not build a prototype of a solar powered smart window, I learned and practiced the steps to do so from laser cutting solar cells to laminating PV modules. I would like to thank Arturo Martinez Lopez and Martijn Tijssen for teaching me these steps.

I had an amazing time while being part of the PVMD group and as a student of Sustainable Energy Technology. I shared many wonderful memories with people from all around the world who taught me more about different countries and cultures. Besides I had the privilege to be part of the MOR team which gave me new insights on the various aspects which are involved in designing and realizing a building. I would like to thank Prof. Andy van den Dobbelsteen for supporting me while being in the team and for being part of the thesis committee.

At last I would like to thank my parents for all their support and love and for giving me every opportunity to broaden my knowledge and skills.

Patrick Kwee
Delft, August 2020

Contents

List of symbols

a-Si	Amorphous Silicon
AC	Alternating Current
ACH	Air Change per Hour
AM	Air Mass
AOI	Angle Of Incidence
ASHRAE	American Society of Heating, Refrigerating and Air-Conditioning Engineers
BPIE	Buildings Performance Institute Europe
c-Si	Crystalline Silicon
CdTe	Cadmium Telluride
DC	Direct Current
DHI	Diffuse Horizontal Irradiance
DHI_{lux}	Diffuse Horizontal Illuminance
DNI	Direct Normal Irradiance
DNI_{lux}	Direct Normal Illuminance
DOY	Day of the Year
DSF	Double-Skin Facade
DSSC	Dye Sensitized Solar cell
EC	Electrochromic
EU	European Union
EVA	Ethylene Vinyl Acetate
GHI	Global Horizontal Irradiance
GHI_{lux}	Global Horizontal Illuminance
FF	Fill Factor
G	Solar Irradiance
GMST	Greenwich Mean Sidereal Time
HVAC	Heating, Ventilation and Air Conditioning
I	Current
IR	Infrared
LC	Liquid Crystal
LSC	Luminescent Solar Concentrators
low-e	Low Emissivity
mpp	Maximum Power Point
MPPT	Maximum Power Point Tracking
NIR	Near Infrared
oc	Open Circuit
OPV	Organic Photovoltaic
P	Power
PC	Photochromic
PDLC	Polymer Dispersed Liquid Crystal
PV	Photovoltaic
Q	Heat
sc	Short Circuit
SAM	System Advisor Model
SHGC	Solar Heat Gain Coefficient
SOC	State Of Charge
SPD	Suspended Particle Device
STC	Standard Test Conditions
STPV	Semi-Transparent Photovoltaic
T	Temperature
TC	Thermochromic
UV	Ultraviolet
V	Voltage
VT	Visible Light Transmittence
WIPV	Window Integrated Photovoltaic
WWR	Window-to-Wall Ratio
α	Albedo
η	Efficiency

1 Introduction

Since the industrial revolution began a few centuries ago, humans began to build advanced engines and machines in rapid pace to get faster to a destination, to make products faster than before and to provide electricity and gas to more and more households for cooking and using electronic appliances. The invention of the many technologies which are used in the daily life today have caused a significant decrease in natural resources such as forests, oil fields and gas fields. When burning fossil fuels such as coal, oil or gas for energy which is required to build machines or run engines, greenhouse gases are emitted and reach the atmosphere. This leads to global warming. In the Paris Agreement in 2015, most of the countries worldwide agreed that global warming caused by human activity should be limited and this could be possible if the global temperature rise would be kept below 2°C compared to average pre-industrial temperature. The Climate Action Tracker [96] is an independent scientific organisation which analyses government climate action and predicted that due to the current policies of countries worldwide, the global temperature will rise by up to 3.2°C by the year 2100 with respect to the average pre-industrial temperature. This indicates that serious measures should be taken to reduce the global greenhouse gas emissions in order to keep the global temperature rise below 2°C. Because greenhouse gas emissions and energy consumption are related, reducing the worldwide energy consumption needs will lower the greenhouse gas emissions. Besides it can be reduced by decreasing the dependence of energy production on fossil fuel sources and to produce more energy using renewable energy sources. All countries within the European Union (EU) have agreed to make a transition towards renewable energy sources and set energy goals. In the Netherlands for example, the target is to reduce the CO2 emissions by 50% with respect to 2019 by the year 2030, to produce 70% of the electricity using renewable energy sources in 2030 and to be energy neutral by 2050 [70]. In 2019 however only 8.34% of the energy consumption originated from renewable energy sources which indicates that the Netherlands has a long way to go reach their energy targets [32].

1.1. Current state and potential of renewable energy production

Renewable energy is currently consumed for electricity, heat and transport. According to the Center for Big Data Statistics of the Netherlands, biomass had the highest share among the renewable energy sources in the energy production for heat and transport in 2019, while for electricity wind energy had the highest share [31]. This is because solar energy is generated during the day while wind energy can be generated during the night as well. The electrical capacity of wind turbines installed in the Netherlands at the end of 2018 was 4393 MW and the electrical capacity of photovoltaic (PV) panels installed was 4522 MW, while at the end of 2019 this was 4463 MW for wind and 6924 MW for solar [31]. These numbers indicates that the share of solar energy is growing. A reason why the capacity of PV panels increases more than for wind turbines, is because of the relative ease to transport and install solar panels compared to wind turbines. Another advantage of solar energy over wind energy is that it can be generated close to where energy is required, which saves losses in the cabling and decreases dependency on the large energy grid. However the advantage of wind energy over solar energy is that the wind energy production is larger than that of solar energy per installed capacity [31]. Regarding solar energy there is a large potential for building integrated photovoltaic (BIPV) systems, because of

the large unused surface areas on roofs and facades of buildings. To put this in perspective, in 2013 the installed solar power capacity in the built environment was 0.7 GW and it was estimated in 2014 based on the technology available at that time that the potential for solar power in the built environment was 66 GW [2]. However the efficiency of PV technologies has improved since 2014 [67] as shown in figure 1.1, thus it can be expected that this potential is even higher. Crystalline silicon (c-Si) PV cells can reach efficiencies above 20% and is currently the leading technology.

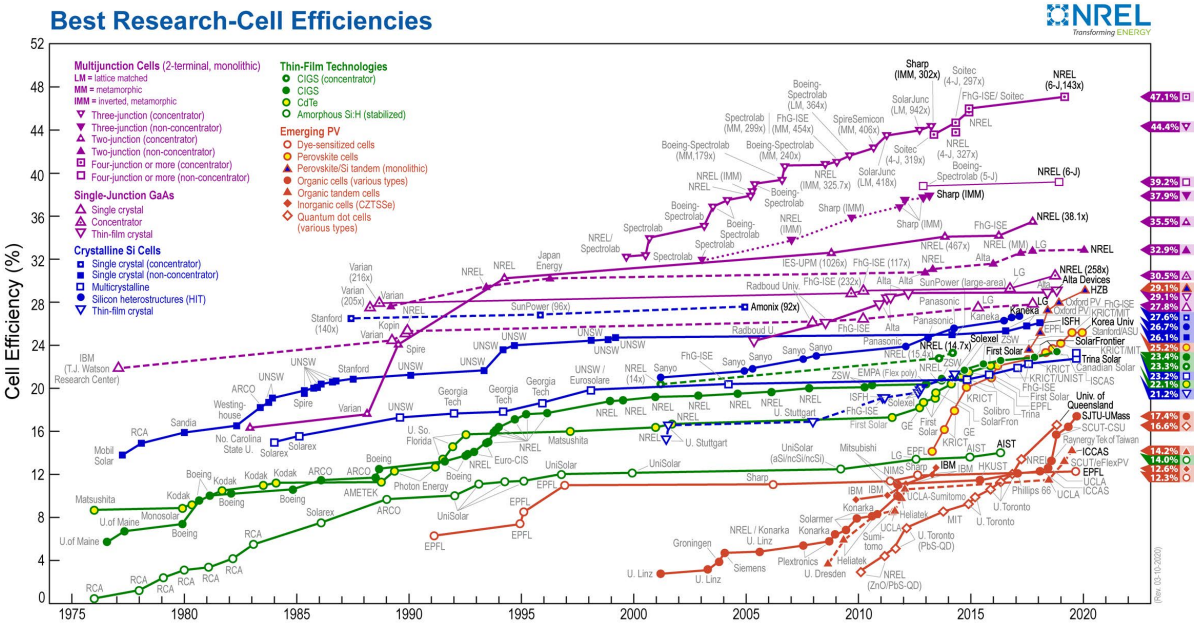

Figure 1.1: The evolution of PV cell technology efficiency [67].

1.2. Build environment consumption

Energy is consumed in different sectors and the largest sectors are the industry, transport and buildings as shown in figure 1.2a, other sectors include the agriculture and energy generation sector [27]. To determine how to reduce energy consumption and greenhouse gas emissions in the different sectors, it is investigated in which sector the largest potential savings are possible. According to the Buildings Performance Institute Europe (BPIE) which assesses the energy performance of buildings located in the continent, buildings contributed to 36% of the total CO2 emissions and to around 40% of the total energy consumption in 2018 [28]. The BPIE has defined three types of buildings, namely old buildings (build before 1960), modern buildings (build between 1961 and 1990) and recent buildings (build between 1991 and present) [27]. They found that on average modern buildings are currently the most abundant buildings in countries within Europe. Old and modern buildings are often poorly insulated because these were build before the introduction of strict requirements and regulations in terms of energy performance. These buildings thus have the highest potential for improvement. Buildings are also distinguished between residential buildings which include all types of households such as family houses and apartments, and non-residential buildings which include offices, hospitals, shops, sport facilities and other buildings which are shown in figure 1.2b. Although residential buildings consume 68% of the total energy consumption of buildings in Europe, which is more than non-residential buildings, non-residential buildings consume 40% more energy per floor area than residential buildings. This indicates that there is a higher potential for energy savings for non-residential buildings than for residential buildings. Figure 1.2b shows that offices are among the highest energy consuming non-residential buildings. Research has shown that on average, lighting, heating, cooling and ventilation contribute the most to the total energy consumption of offices in the Netherlands. It was found that 22% is consumed for lighting and 49% for heating, cooling and ventilation (HVAC) [63]. In total this accounts for 71% of the energy consumption of an office. Because of the high contribution of heating, cooling and lighting to the total energy consumption of an office, it is important to investigate how these

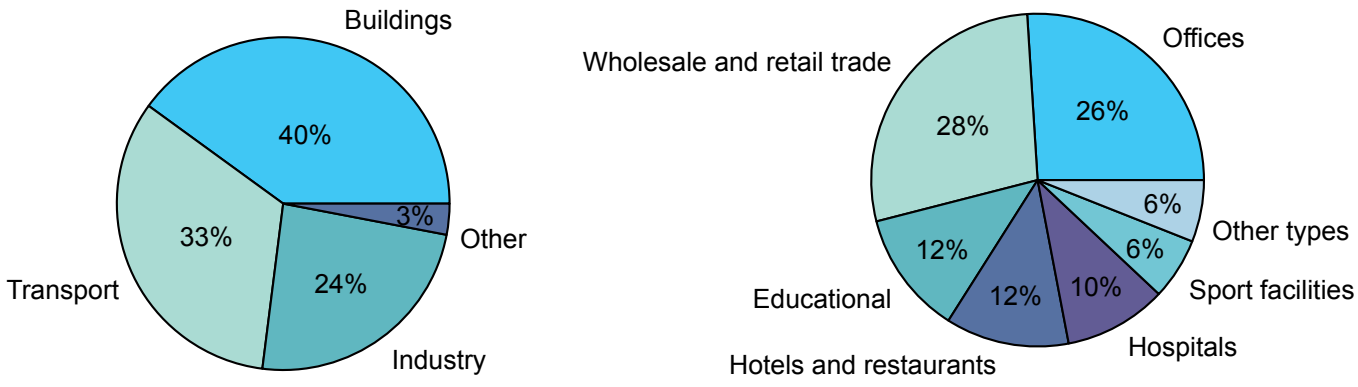

(a) Final energy consumption by sector in Europe.

(b) Total energy use per building type in Europe.

Figure 1.2: Energy consumption per sector and per building type in Europe [27].

can be reduced. By 1 January 2023 all buildings in the Netherlands need to meet the requirements set by the Dutch building regulations (Building decree 2012) [66], but currently 52% of all offices do not meet these requirements [3]. A way to improve the energy performance of a building is by reducing thermal losses on their facade system. In [51] it was namely stated that 50% of the total building energy is lost because it is dissipated through the facade. The facade of buildings thus shows potential for energy loss reduction and energy generation by implementing BIPV. Besides the possibilities to reduce energy losses and to generate energy, the facade has the potential to be used to optimize the indoor comfort conditions for occupants which includes thermal and visual comfort. This is because the facade consists of glazing which affects how much solar heat and natural daylight can enter a room. Thermal comfort is reached when the indoor temperature is within the ideal comfort temperature limits and visual comfort is reached when the indoor illuminance is within the ideal comfort illuminance limits. When using a smart window which can change its transparency, it is possible to control the incoming heat and light of an office room. To determine the energy performance of a smart window and its effect on the indoor comfort conditions, the window-to-wall ratio (WWR) should be considered. This is defined as the ratio between the area of the window and the area of the whole facade. This namely affects how much natural sunlight and heat is transmitted through the window.

1.3. Project motivation

A lot of research has been done already on the potential energy savings of buildings with smart windows and other window technologies with respect to conventional windows. [59] compared the thermal and optical properties of multiple glazed windows with different cavity fillings. Studies on different existing and developing passive window technologies which require no electricity to function are summarized by [83]. Research has also been done on different window integrated photovoltaic (WIPV) technologies to compare the energy performance of these technologies to a reference window and to determine the PV power generation potential in each case. Research groups in Dublin, Ireland [35],[36],[37],[40],[38],[39], Berkeley, the United States [55], and Inchon, South Korea [72],[71] have investigated active smart windows which require an applied voltage to control its transparency. The research group in Inchon did simulations on EnergyPlus software package to investigate smart windows, while the research group in Dublin used a different approach and did measurements on functioning devices to validate their simulation models. The smart window which was used in [40] and [38] was powered by solar energy. In Delft, the Netherlands a method was found to visibly [75] and more invisibly integrate solar energy and glass with a smart window film [34]. However here no analysis on the potential energy savings with respect to a conventional window was done. In the papers found on the energy performance of different types of window technologies, the reference window to which the energy performance of the window technology is compared is not the same in all cases or only referred to as ”conventional windows”. In some cases it is thus not clear if the energy performance of a window technology is compared to a single glazed window or a double glazed window and this would significantly affect the outcome. This report therefore aims to determine and compare the energy performance of different types of window technologies to a defined conventional double glazed window which meets the Dutch

building regulations [66]. To determine the potential energy savings, the heating, cooling and lighting loads of an office room are considered. Additionally the energy generation potential is included for some window types. Besides the indoor comfort conditions with respect to incoming natural daylight are considered. A trade off between minimizing the energy consumption of a building and maximizing the indoor comfort conditions needs to be made when controlling the transparency of a window. By changing the transparency, the amount of incoming natural daylight and solar heat changes and the higher the transparency the more sunlight and solar heat is transmitted through the window. Some smart window technologies are relatively easy to add to an existing structure and could thus be used in renovation projects of buildings which do currently not meet the standards for buildings. In the cases where smart windows show potential energy savings, it will be investigated what is the optimal way to integrate solar energy and the smart window such that it functions autonomously. The smart window technologies which will be investigated in this project are the following switchable glazing windows: Electrochromic (EC) glazing, suspended particle device (SPD) glazing and polymer dispersed liquid crystal (PDLC) glazing. These smart windows are active windows because these require a voltage to change the transparency and can be manually controlled. A functioning PDLC window powered by PV cells was build by [75]. This system included a battery, charge controller, maximum power point tracker and inverter. The PV cells which were used are based on monocrystalline silicon with a back surface field and different patterns of PV cells for aesthetic comparison and functionality were tested. Similar demonstrators have been build and tested by [40] and [38] for the SPD window and for the EC window [24].

1.4. Aim of thesis project

The aim of this project is to provide an energy model which gives the potential energy savings of smart window technologies with respect to conventional and other window technologies, to give an overview of the advantages and disadvantages of the technologies and to determine the minimum PV system requirements needed to power a smart window.

1.5. Tasks and objectives

The following research question will be investigated:
- What are the potential savings of smart window technologies compared to reference double window and to other window technologies?
- What are the minimal PV system requirements to power an active smart window for an entire year?

Multiple locations with different climates will be investigated. The weather data for these locations are taken from the database corresponding to a simulation tool called EnergyPlus.

1.6. Overview thesis report

The structure of the project is as follows: In chapter 2 a current status on different types of energy saving window technologies and the WIPV technologies is discussed. Then in chapter 3 a model is presented to determine the energy performance of an office room and to determine a PV requirements to power a smart window. This model is made in Matlab, and will be referred to as ”Model” in chapter 5. In chapter 4 a concept design for a solar powered smart window is discussed. In chapter 5 the validation of the energy performance model using a simulation program and the simulation results will be discussed. Here the model will be used to compare the energy performance of different window technologies.

2

Technology

In this chapter the current research on different window technologies and PV applications in windows will be given and the window properties will be discussed. The most relevant window properties to consider to determine heating, cooling and lighting loads are the thermal insulation, solar heat gain and visible light transmittance. These are the properties normally provided by manufacturers. The thermal insulation is expressed by a U-value in $\frac{W}{m^2K}$, the higher the U-value the more heat can be exchanged and thus how much heat can be lost. The solar heat gain coefficient (SHGC) or solar factor is a dimensionless value between 0 and 1 and this is a measure of how much solar heat is transmitted through the window which causes a room to heat up. The higher the SHGC value is, the more solar heat is transmitted through the window and this affects the need for heating and cooling loads. The heat gains and losses through the window contribute significantly to the energy balance of buildings. According to [81] the solar heat gain accounts for 37% of the total cooling demand of buildings while the heat which is dissipated through the window accounts for 40% of the total building energy which is lost. The visible light transmittance (VT) is a value between 0 and 1 and this represents the fraction of the visible light which is transmitted through the window. For low VT values the visible transmittance is low which can lead to an increase of artificial lighting demands. In table 2.1 the suggested window properties for a cool, temperate and hot climate are given to minimize heating loads during the winter and cooling loads during the summer. For a cool climate a window with good insulating properties is recommended and this corresponds to a U-value lower than 2 $\frac{W}{m^2K}$. This is to minimize heat losses through the window when the outdoor temperature is significantly lower than the indoor temperature. Besides a low U-value, it would be expected that a relatively high SHGC is preferred for a cool climate such that relatively more solar heat can enter a room which then decreases the demand for heating load. For a hot climate a lower SHGC is preferred to reduce the demand for cooling. Here the U-value can be relatively higher because the average outdoor temperature is higher and thus closer to the designed indoor temperature. This means that the temperature difference is less and thus less heat will be lost. Single glazed windows used in office buildings typically have a U-value of around 5.8 $\frac{W}{m^2K}$ which indicates poor thermal insulation.

Climate	VT [-]	SHGC [-]	U-value [$\frac{W}{m^2K}$]
Cool climate	>0.70	>0.60	<2
Temperate climate	>0.70	>0.50	<2.5
Hot climate	>0.60	<0.40	<4

Table 2.1: Suggested window properties in different climates according to [81].

2.1. Multiple pane glazing

There are many window technologies which allow for energy reduction compared to a single glazed window. The easiest way to improve the energy performance of a window is by improving the thermal insulation, which can be achieved by replacing a single glazed window with a double or triple glazed window. For a window with better thermal insulation properties, less heat will leak away from the indoor space. It is thus expected that compared to the double glazed window defined for the reference office, a single glazed window would have a higher U-value. When replacing a single glazing by a double or triple glazed window, the cavity gap can be filled with air, but also with argon, krypton or xenon gas which have better thermal insulation properties compared to air [83]. It is also possible to fill the gap with aerogel which consists of air and silica, an example of such a window is given in figure 2.1. An

Figure 2.1: Aerogel window. Adapted from [58].

energy performance simulation has been done by [33] in EnergyPlus for double glazed windows filled with either aerogel and air in the gap for Oslo, Norway which has a cold climate. It was found that filling the gap in the double glazed window with aerogel could save up to 21% of the energy building consumption with respect to the double glazed window filled with air. Here a building was used with windows in north, east, south and west directions. It should be mentioned that the U-value, SHGC and VT of the reference window in this case were 2.86 $\frac{W}{m^2K}$, 0.76 and 0.81 while these of the most insulating aerogel window were 0.6 $\frac{W}{m^2K}$, 0.34 and 0.17. For the scope of this project, the SHGC and VT properties of the aerogel window as determined by [59] are used. This is because the VT of the aerogel window in this article is higher than in [33]. In the research done by [59], it was found that the U-value of a double glazed aerogel window is lower than that of a triple glazed window with argon gas fill. This implies a higher thermal insulation for the aerogel window. In the same article a life cycle analysis was done. Here it was determined that the usage of the double glazed aerogel window in the building would give up to 9% less greenhouse gas emissions than the usage of its triple glazed counterpart. In this report, the thermal properties of double glazed windows with different cavity fills will be calculated using equation (3.51) which will be explained in section 3.8.5. These are calculated using the conductivity of air, argon, krypton, xenon and aerogel which are given by [83], [12] and shown in table 2.2. The conductivity of glass is considered to be 0.98 $\frac{W}{mK}$ [53]. The double glazed windows consist of three layers, namely two of glass with a defined thickness of 4 mm and a gap of 16 mm in between. These thicknesses correspond to commercially available windows [83]. The SHGC and VT of air and argon are found in literature for these layer thicknesses. However the SHGC and VT for double glazed windows with krypton or xenon gas fill were not found and it is therefore assumed that these have the same SHGC and VT values as the windows with air and argon gas fill. The SHGC and VT of aerogel are given by [59] for a double glazed window with a 14 mm gap between the glass panes and it is assumed that these are remain the same if the gap is increased to 16 mm. The calculated and assumed window properties are given in table 2.2.

Cavity filling in double glazed window	Air	Argon	Krypton	Xenon	Aerogel
Conductivity of filling [$\frac{W}{mK}$]	0.026	0.018	0.0095	0.0055	0.011
U-value of window [$\frac{W}{m^2K}$]	1.26	0.94	0.54	0.32	0.61
SHGC of window [-]	0.73	0.73	0.73	0.73	0.74
VT of window [-]	0.81	0.81	0.81	0.81	0.5

Table 2.2: The thermal and optical properties of double glazed windows with different cavity fillings [83].

2.2. Low emissivity coating

A way to reduce the cooling energy consumption of an office during summer is by using windows with a low emissivity (low-e) coating on the roomside glass which reflects infrared (IR) and ultraviolet (UV) radiation while transmitting radiation in the visible light region [43]. The visible light region corresponds to light particles or photons with wavelengths between 380 nm and 740 nm and light outside of this region cannot be perceived by the human eye. IR corresponds to the low energy photons with wavelengths between 740 nm and 1 mm while UV corresponds to high energy photons with wavelengths between 10 nm and 380 nm. The blocking of UV light does not affect the energy consumption but is rather to protect the human skin against long exposure of UV light which could lead to skin cancer. IR light is associated with the solar heat gain and can be transmitted through the glass. Besides it can be absorbed as heat in the glass surface, which increases the glass surface temperature. If the emissivity of the window is high, then most of the absorbed heat is re-radiated on the inside of the glass and reaches the indoor space. The emissivity is thus a measure of how much of the light which is absorbed by the glass is radiated as heat into the indoor space. For a conventional glass the emissivity is 0.84 and this means that 84% of light absorbed on the outside surface of the window is radiated as heat on the inside and exchanged with the indoor space. When decreasing the emissivity of IR radiation by reflecting light in this region the SHGC can be lowered. This is illustrated in figure 2.2 where the transmittance of light with different wavelengths is plotted for low-e windows with a high, moderate and low SHGC. The lower the transmission the higher the reflectance. In table 2.3 the VT, SHGC and U-value corresponding to these window are given [29]. The first window has a relatively high SHGC value of 0.62 and a VT of 0.77, the second window has a moderate SHGC value of 0.41 and a VT of 0.70, and the last one has a low SHGC value of 0.27 and a VT of 0.63. All windows have argon gas as cavity fill.

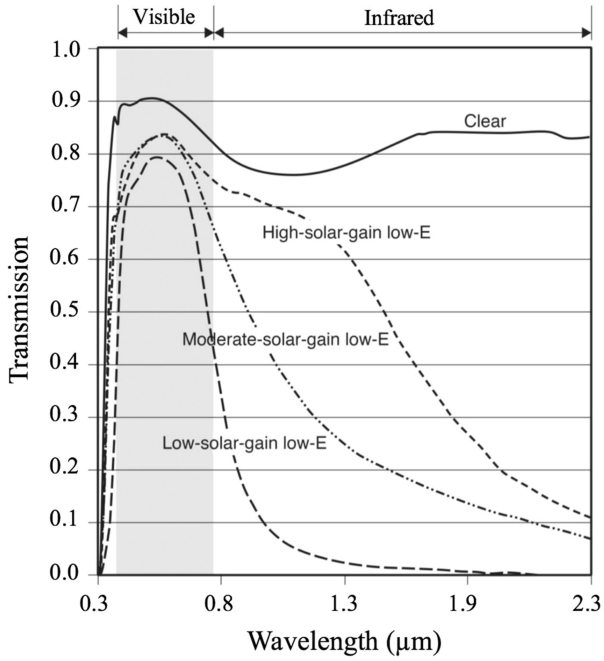

Figure 2.2: Transmittance spectra of low-e windows. Adapted from [83].

Type of double glazed window	High SHGC + low e	Moderate SHGC + low e	Low SHGC + low e
U-value [$\frac{W}{m^2K}$]	1.19	1.36	1.31
SHGC [-]	0.62	0.41	0.27
VT [-]	0.77	0.70	0.63

Table 2.3: The thermal and optical properties of three types of double glazed windows with low-e coating [29].

2.3. Window integrated photovoltaic technologies

Besides improving the thermal insulation of windows or adding a coating to reduce the consumption of an office, there are so called window integrated photovoltaic (WIPV) technologies available which show promising results in reducing the energy consumption of a building while generating energy. Examples of these are semi-transparent photovoltaic (STPV) windows and ventilated photovoltaic double-skin facades (PV-DSF). For the scope of this project only STPV windows are simulated in the model. The solar heat gain of STPV and PV-DSF technologies is relatively lower compared to other single or multiple pane windows, but the visible light transparency is lower as well. This is because visible light which is absorbed by the integrated solar cells for power generation is not transmitted through the window and this lowers the visible light transparency of such a window. Therefore for such WIPV technologies, a trade off between light to electricity conversion and visible light transmission should be made. Another PV integrated window technology features luminescent solar concentrators (LSC), where solar energy is generated in the edge of the window. An overview of different types of PV applications in glazing is shown in figure 2.3. In the left figure, opaque PV cells are cut in small pieces such that the parts which are not covered by PV are transparent. In the second figure a thin film semitransparent PV module is shown which is colored because it partly absorbs visible light. Here a trade off between power conversion efficiency and visible light transmittance has to be made. In the third configuration light is absorbed in the part which is described as ”concentrator” and is re-emitted at different wavelengths and absorbed by PV cells which are located in the edge of the glazing. The fourth configuration from left shows a semitransparent PV window which absorbs mainly near infrared (NIR) and UV light for power generation while transmitting light in the visible light region. In the final configuration UV and NIR light only are absorbed by a concentrator which emits the absorbed light at longer wavelengths which reaches the PV cells which are again in the edge of the window. For the scope of this report only the first two configurations are considered because these are available on the market or in an advanced developing stage.

2.3.1. Semitransparent photovoltaic technologies

STPV technologies which are currently on the market include crystalline silicon (c-Si), amorphous silicon (a-Si) and cadmium telluride (CdTe). In literature and in datasheets from manufacturers the thermal, optical and electrical properties of these STPV technologies have been extensively described. Research is currently also conducted on organic PV (OPV), dye sensitized solar cells (DSSC) and perovskite solar cells, but most results found in literature regarding these technologies were for medium small to small novel PV cells. This indicates that these technologies are promising but need to be further developed to be implemented on a larger scale. Although copper indium selenide (CIS) and copper indium gallium selenide (CIGS) do have a market share among the thin film technologies for standard PV applications, little research appears to be done on semitransparent CIS or CIGS. Only in [62], CIS was investigated for its potential in window applications and found that the CIS had a higher power output than for a-Si. The thermal and electrical properties of CIS are similar to CdTe and CIS is therefore not considered in the model. In general the efficiency of PV modules is found to be lower in semitransparent glass applications compared to PV modules used for roofs for example. This is because of the trade off made between visible light transmittance and light absorbed for power conversion. For c-Si the efficiency of the best performing PV modules can be up to 26% according to [11], while it was simulated to be 7% and measured to be 5.4% for a laminated semitransparent PV module by [78]. It should be mentioned that this lower efficiency was reached because only a third of the laminate was covered by PV cells and that the efficiency when considering the solar cell area only would thus be approximately 15%. Two types of c-Si semitransparent PV windows with different transparencies are shown in figures 2.4a and 2.4b for comparison. In the model the c-Si PV window with relatively higher transparency is considered because this is aesthetically more appealing. The

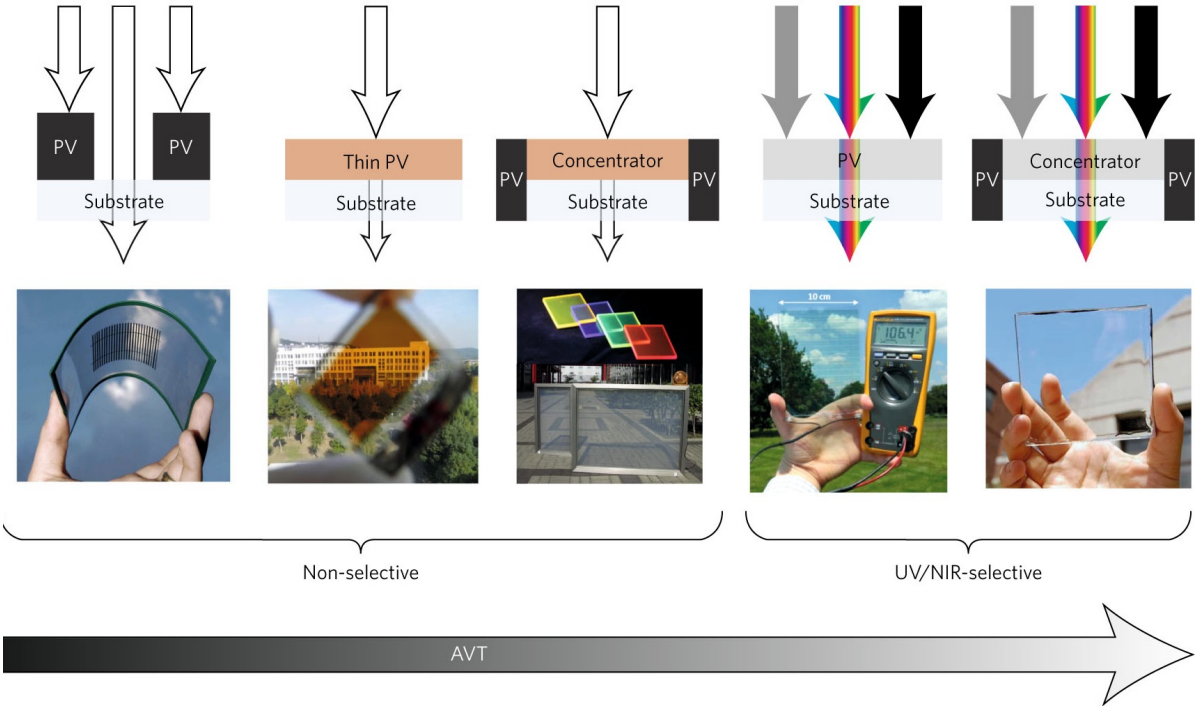

Figure 2.3: Different types of PV applications. Adapted from [14].

solar cells in this laminated PV module were cut into narrow strips to achieve a transparency of 0.628 [77]. The U-value of this c-Si PV module was simulated to be 2.675 $\frac{W}{m^2K}$. The potential energy savings were determined to be 15.9% with respect to a double glazed window with a SHGC, VT of respectively 0.275, 0.640 and a U-value of 1.623 $\frac{W}{m^2K}$ for Berkeley, California. It should be noted here that these savings were mainly achieved after including the PV energy generation in the calculation of the energy performance and by subtracting this contribution from the total consumption loads. This means that the net energy consumption of a building can be negative if the energy generated is higher than the total energy consumption. In this work the energy savings of the PV window technologies will be calculated while considering the energy generation. Although in [77] the U-value of c-Si was simulated to be 2.675 $\frac{W}{m^2K}$, in the presented work a U-value of 1.65 $\frac{W}{m^2K}$ is considered. This assumption will also be considered for other window technologies for which a higher U-value is found in literature. The reason behind this will be discussed in chapter 3.

For the thin film technologies a-Si and CdTe integrated in windows, the efficiency was found to be 5.6% [101] and 6.0% [9] respectively in literature, while the efficiency of the highest performing conventional PV module of these types can be up to respectively 11.9% and 22.1% [11]. The U-value corresponding to the CdTe window was found to be 1.812 $\frac{W}{m^2K}$. It should be noted that the efficiency of CdTe semitransparent windows can be up to 10% but then the VT would be lower and is therefore not selected. For OPV the efficiency of a semitransparent PV cell was found to be 4.8% [61] while for PV modules of this type this could be up to 11.2% according to [11]. In figure 2.6a this OPV cell is shown and how this could be integrated in glazing is demonstrated in figure 2.6b. In a study by [73] a semitransparent a-Si based PV module with a 5% efficiency and U-value of 2.783 $\frac{W}{m^2K}$ was found to save energy by 18% (for a WWR of 0.33) up to 59% (for a WWR of 0.88) compared to a double glazed window with a U-value, VT and SHGC of 2.783 $\frac{W}{m^2K}$, 0.461 and 0.473 respectively. This was determined in a simulation done for a south facing facade in Madrid, Spain and the simulation tools which were used for the simulations were DesignBuilder, EnergyPlus, PVsyst, and COMFEN. In a different study carried out by Didoné and Wagner [25], simulations were done by for two locations in Brazil where the energy performance of two semitransparent PV technologies were compared to a double glazed window with a U-value, VT and SHGC of 2.73 $\frac{W}{m^2K}$, 0.81 and 0.76 respectively. The PV technologies which were investigated in this study were OPV and a-Si. These were integrated in

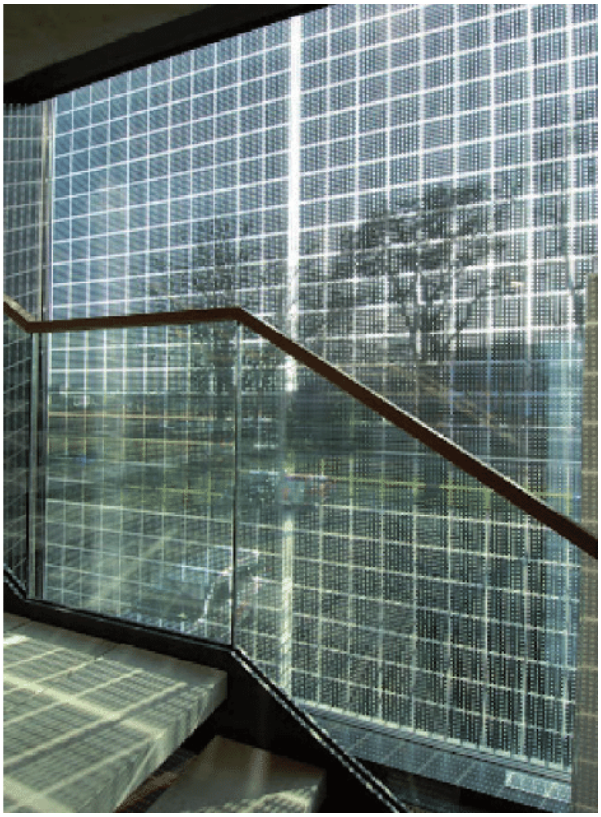

(a) c-Si semitransparent PV window. Adapted from [45].

(b) c-Si semitransparent PV window with higher transparency. Adapted from [77].

Figure 2.4: c-Si semitransparent PV windows.

double glazed windows consisting of two glass layers of 3 mm with in between a 12 mm gap filled with air. The outside facing glass was made of low iron glass which has a higher transparency compared to clear glass and the PV cell was attached to the inside of this glass layer. The inside facing glass had a low-e coating. The U-value of both window technologies was 1.67 $\frac{W}{m^2K}$. The SHGC and VT of the OPV were 0.22 and 0.23 and for the a-Si PV windows these were 0.13 and 0.09 respectively. It was found that for a WWR higher than 0.5, the savings were up to 13% and 21% for OPV and a-Si PV with respect to the double glazed window of the article. The electrical and thermal properties of the a-Si are extensively described by [101] and these properties are used in the model. The savings with respect to double glazed windows were found in this article to be up to 50% for locations in China. A dye sensitized solar module has been investigated by [20] and [19] and its performance has been compared to that of a double glazed window for three locations in Italy. The energy savings of DSSC with respect to a double glazed window were found by [19] to be up to 34.7% in Rome. The DSSC was measured to have a SHGC of 0.2 and a U-value of 3.6 $\frac{W}{m^2K}$ and the reference glazing in this case had a SHGC of 0.82 and a U-value of 2.8 $\frac{W}{m^2K}$. The power conversion efficiency under standard test conditions (STC) was 3.28% and was measured to be 2.49% during an outdoor test period of 9 days in Italy. Because the appearance is similar to OPV and the power conversion efficiency of this technology is lower than found for the semitransparent OPV cell, DSSC is not considered in this work. Neutral colored perovskite solar cells with an active area of 0.71 cm^2 have been made by [16]. Here a visible light transparency of 42.4% and a power conversion efficiency of 6.64% was reached. An example of such a PV cell is shown in figure 2.7b. In a building simulation the hypothetical yearly energy yield for these PV cells implemented in a window was determined to be between 10 and 30 kWh/m^2 under ideal conditions. Here a south facing room with a floor area of 20 m^2 and a height of 3.5 m was simulated for different locations. Two WWR values were considered, namely 0.19 and 0.32.

Each WIPV technology has its advantages and disadvantages. Currently the highest power conversion efficiency in standard PV modules is reached for c-Si with a relatively low VT of around 0.2.

(a) a-Si semitransparent PV window. Adapted from [83].

(b) CdTe semitransparent PV window. Adapted from [85].

Figure 2.5: Examples of a-Si and CdTe PV windows.

(a) Organic PV film. Adapted from [61].

(b) Organic PV window. Adapted from [17].

Figure 2.6: Semitransparent organic PV.

This means that more electricity can be produced on the same area compared to thin film technologies. However such c-Si window application is more noticeable compared to the thin film solar window technologies and arguably less aesthetically appealing. When making the c-Si less visible by decreasing the effective PV area, the VT increases as done by [77]. However by doing this the efficiency of the laminate decreases significantly and can thus be lower even than for thin film technologies. Thin film technologies such as CdTe are cheaper and aesthetically more appealing than c-Si and current CdTe semitransparent windows on the market allow for VT values up to 50%. Besides these are less affected by shading and high temperatures and lighter compared to c-Si based technologies because these can be made thinner. The effect of temperature on the efficiency is given by the temperature coefficient κ_{temp} in table 2.4. The lower the value, the less the temperature affects the efficiency. For most PV technologies κ_{temp} is negative which indicates that higher temperatures reduce the efficiency. For OPV the temperature coefficient was found to be positive by [25]. The disadvantage of CdTe is that consists of materials which are scarce and toxic.

OPV cells consist of organic materials and are flexible and lightweight, but are vulnerable when getting into contact with water and oxygen which lead to a decreasing stability and degradation issues and thus a shorter life time. OPV and DSSC are similar, but the difference is that OPV is fully organic

(a) Dye sensitized solar module. Adapted from [20].

(b) Neutral colored perovskite solar cell. Adapted from [14].

Figure 2.7: Semitransparent dye sensitized PV module and neutral colored perovskite solar cell.

while DSSC consists of organic and inorganic parts.

Perovskite solar cells have shown to reach relatively high power conversion efficiencies while reaching a high visible light transmittance, however this technology is also known for its limited long term stability which makes it currently unfavorable to integrate in windows.

In this work the electrical properties of OPV determined in [61] are used, while the SHGC and VT from [25] are considered. OPV is selected to compare the potential of a third generation WIPV technology to other existing WIPV technologies although these are not yet commercially available. For CdTe the properties are taken from [9]. All semitransparent solar window technologies are double glazed and have a low-e coating on the roomside glass pane. The properties of the four types of semitransparent PV windows are given in table 2.4. For c-Si, a-Si and CdTe these properties were found for relatively large PV modules, while for OPV the properties were given for a small/medium sized PV cell.

PV technology	c-Si [78][77]	a-Si [101]	CdTe [9]	OPV [25][61]
U-value [$\frac{W}{m^2K}$]	1.65	1.621	1.65	1.65
VT [-]	0.628	0.221	0.297	0.23
SHGC [-]	0.314	0.212	0.271	0.22
L_{PV} [m]	1.7637	1.245	1.2	0.14
W_{PV} [m]	1.4478	0.635	0.6	0.14
V_{oc} [V]	23.9	89	122.1	24
I_{sc} [A]	7.6	0.77	0.64	0.0658
V_{mpp} [V]	19.6	69	96.1	18.95
I_{mpp} [A]	7	0.64	0.56	0.05
P_{mpp} [W]	137.2	44.16	53.8	0.95
FF [-]	0.76	0.64	0.69	0.6
η [%]	5.4	5.6	6.0	4.8
κ_{temp} [%/°C]	-0.35	-0.2	-0.214	0.05

Table 2.4: Properties of semitransparent PV double glazing technologies considered in model. The properties of OPV are given for a single cell.

2.3.2. Luminescent solar concentrators

Luminescent solar concentrators (LSC) in windows allow for VT, SHGC and U-values similar to conventional glazing while generating electricity. The PV modules in such device are placed in the edge of the window and light reaches the PV module after being absorbed and re-emitted at longer wavelengths by molecules which are present in a special coating in the glazing. A LSC window with PV modules in the edge based on CIGS was investigated by [18] and is shown in figure 2.8. The energy yield was estimated to be 1.4 kWh per year in the Netherlands for LSC model with a window area of 1 m^2. Here the PV cells were placed in one edge while the other edges are perfect mirrors. CIGS was selected because it has a direct and relatively low bandgap of 1.05 eV and can absorb visible light as well as NIR light for energy generation. The absorption coefficient is higher than for c-Si which has an indirect bandgap [87]. A similar calculation was done by [74] for a LSC device based on monocrystalline silicon. Here it was found that the annual electricity generation was around 386 kWh/m^2 for a southwest facing facade in Delft in the Netherlands when using a window of 50 cm x 50 cm and a PV area of 0.0088 m^2. This corresponds to a yearly energy generation of 3.4 kWh or 13.6 kWh/m^2 when dividing by the window area. This indicates that the energy generation per PV area is large, but relatively low when calculated per window area. Because of the annual energy generation is relatively low and because the VT, SHGC and U-values of LSC windows are expected to be similar to double glazed windows with low-e coating because of the absorption of NIR for energy generation, these type of windows are not simulated in this model.

Figure 2.8: LSC window taken from [86].

2.3.3. Photovoltaic double skin facade

A technique which is used to improve the energy performance of existing buildings is to add a second skin to the existing facade. This concept is called a double skin facade (DSF) and can be used to passively reduce heating or cooling loads of buildings. Besides it can be used to improve thermal and acoustic insulation and aesthetic appearance of buildings. The difference between a DSF and a multiple pane window, is that the width of the cavity gap of a DSF is larger. Besides the cavity filling of a DSF is air while for a double glazed window this can be another gas with higher thermal insulating properties. Passive strategies for which the DSF can be used are for pre-cooling the indoor space during a summer night to reduce cooling loads of the next day and to hold heat in the cavity space during the winter. The concept of the DSF has been extended by integrating semitransparent solar modules in the second skin to create a photovoltaic double skin facade (PV-DSF). This was found by [76] to improve the energy performance if the cavity gap is larger than 200 mm while for a double glazed PV window also defined as a photovoltaic insulating glass unit (PV-IGU) the cavity gap is between 9 and 16 mm. Above and below the PV module in a PV-DSF there are ventilation louvres. When opened these allow for air to flow in and out to passively remove heat from the cavity and when closed these keep the heat in the cavity. By removing the heat from the cavity during hot days, the cooling consumption of a building can be reduced and the PV modules are cooled. On average the PV module temperature of the PV-DSF

was found by [99] to be 7.7°C lower than that of the PV-IGU which improved the efficiency by 1.8%. These results were determined for a south facing facade in Hong Kong. It was found by [76] that a

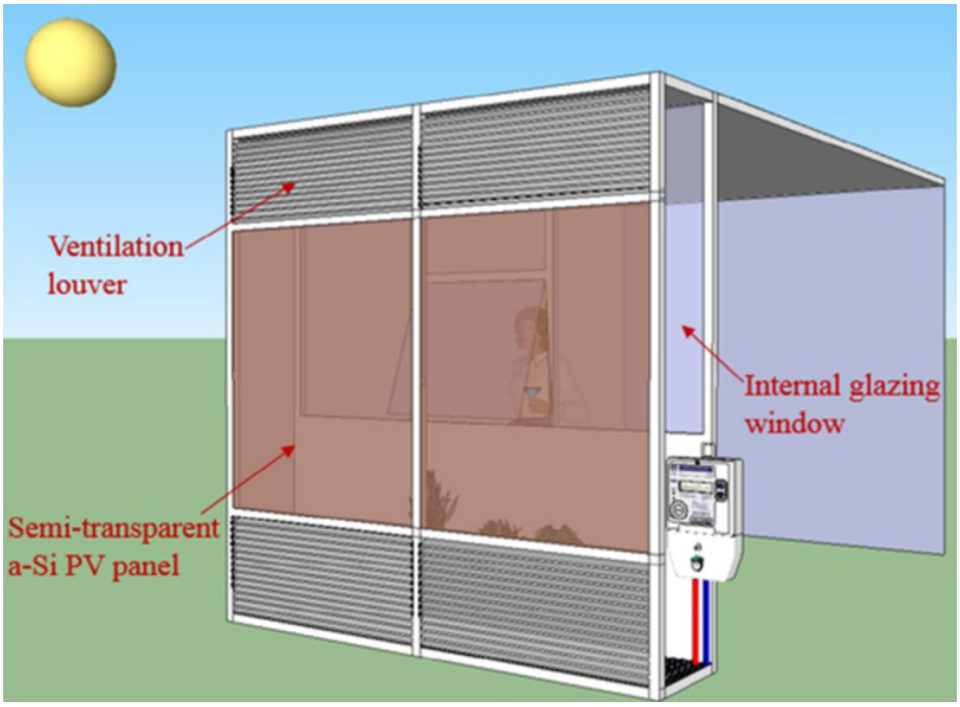

Figure 2.9: PV-DSF concept taken from [76].

PV-DSF based on a-Si improves the thermal insulation and reduces the solar heat gain. Such facade was investigated with an orientation towards 30° southwest in Berkeley, California. It was determined here that saving on the net electricity consumption due to the PV-DSF could be up to 50% compared to a double glazed windows which are clear or have a low-e coating. It was also stated that when using CdTe with a power conversion efficiency of approximately 10% and a VT of 0.2 instead of a-Si, the energy generation output could be doubled. The yearly power generation of an a-Si based PV-DSF was determined to be 65 kWh/m^2 PV area in Berkeley, which means that for CdTe an annual power generation of 130 kWh/m^2 PV area could be expected. Research on the PV-DSF and PV-IGU was also done by [99] for a south facing facade in different locations in China. Here it was found that on average PV-IGU could save 30% compared to the same type of glazing without PV, while the PV-DSF could save 28.4% compared to the conventional glazing. The savings of the PV-DSF were thus 2% less than the PV-IGU. It was concluded in the article that the performance of PV-DSF would be better than for PV-IGU if the ventilation would be controlled more appropriately. In the work presented here, the PV-DSF is not simulated. This is because of the complex heat exchange and ventilation requirements and because PV-IGU was found to have higher potential savings than PV-DSF.

2.4. Passive smart window technologies

In the previous sections methods of reducing the building consumption loads and energy generation possibilities were discussed. However these technologies have in common that the transmittance of solar heat and visible light cannot be adjusted to the preferred settings. For smart windows this option is possible and various research have shown that this leads to potential energy savings with respect to conventional windows. Smart windows can be active or passive, passive smart windows change transparency passively while for active smart windows energy is required. Passive window technologies with switchable glazing features are available in the form of thermochromic (TC) and photochromic (PC) windows. Thermochromic window properties depend on the temperature which affect the transparency of the window and the solar heat gain. For a TC window the visible light transmittance and SHGC are respectively 0.5 and 0.29 at 25°C while at 65°C these are respectively 0.12 and 0.13. In its initial state the TC window is transparent but under higher temperatures it darkens. PC glazing is also

transparent in its initial state but darken when exposed to UV light. The advantage of the mentioned passive window technologies is that no energy is required to make them function. However the disadvantage it that is not possible to manually control the amount of transmitted light and heat through the window [83].

2.5. Active smart window technologies

Active window technologies with switchable glazing features require the usage of power but this allows for manual control of the transparency of the window. Active window technologies are available in the form of suspended particle device (SPD), electrochromic (EC) and liquid crystal (LC) windows. The optical and thermal properties of these active smart windows are discussed in the following sections.

2.5.1. Electrochromic

An EC coating consists of multiple layers namely an electrolyte in the middle which can conduct ions, an active EC layer, a passive counter-electrode layer and two outer layers of transparent conductors [55]. EC in its initial state is transparent or clear until a voltage is applied to the transparent conductors for a short period of time. Under applied voltage a potential difference is induced. This causes lithium ions which are present in the counter-electrode layer to move to electrochromic layer through the electrolyte which darkens the coating. When reversing the voltage the ions move back to the counter-electrode and the glazing becomes clear again. In its dark or colored state more light is absorbed in the EC layer than transmitted and this way the solar heat and visible light transmittance decreases. The working principle of the EC window is illustrated in figure 2.10. The switching time between transparent and

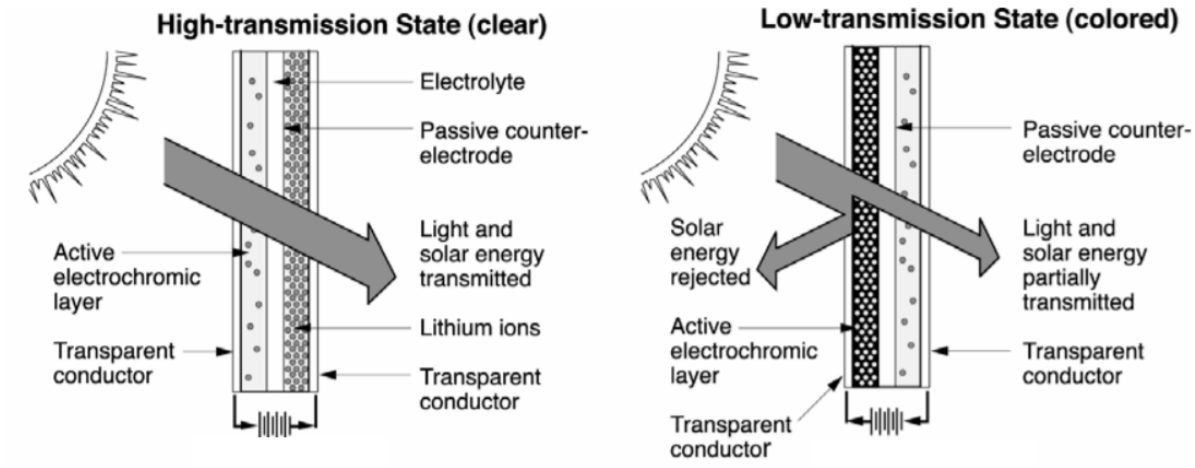

Figure 2.10: Working principle schematic of EC window. Adapted from [55].

opaque states takes relatively long. Some studies mention a switching time up to 15 minutes while others mention a switching time between 30 seconds up to two minutes. A long switching time is a disadvantage when using it in a location with intermittent cloudy skies. Another disadvantage of EC windows is that in its dark state light is absorbed rather than reflected by the EC layer which causes the surface temperature of the glass to increase according to [54]. When switching the EC window from its initial transparent state to an opaque state it can stay in this state for 24 hours without any applied voltage. This smart window therefore does not require a constant supply of voltage to maintain the current state of transparency. EC windows run on DC power while SPD and LC windows run on AC power. This means that if PV systems are to be used for their electrical needs, LC and SPD will require an inverter. According to research done by the Lawrence Berkeley National Laboratory [55], EC windows allow for lighting energy savings of 48 up to 68% while saving cooling consumption loads by 19 up to 26% when compared to a low-e coated windows with a SHGC and VT of respectively 0.42 and 0.22. The applied DC voltage which is required to turn the initial transparent state into an opaque state or the other way around was found by [7] to be 5 V for commercially available EC windows. The EC window which is considered in the model has three opaque states. The scenarios for these different states will be discussed in chapter 3. In figure 2.11 the EC window is shown for different

Figure 2.11: EC window in different opaque states. Adapted from [65].

opaque states. The properties of a commercially available double glazed EC window are selected for the energy consumption assessment and these are given in table 2.5. The U-value of the window is 1.1 W/m^2K and the cavity fill is krypton.

Applied DC voltage [V]	0	1	3	5
SHGC [-]	0.40	0.12	0.07	0.05
VT [-]	0.60	0.17	0.05	0.01

Table 2.5: SHGC and VT of EC window under given and assumed applied voltages, taken from [84].

2.5.2. Suspended particle devices

The initial state of SPD windows when no voltage is applied is the opaque state and this is because the particles are in random positions and absorb light similarly to the EC window. The working principle of the SPD window is shown in figure 2.12. Under applied voltage the particles in the SPD layer align which

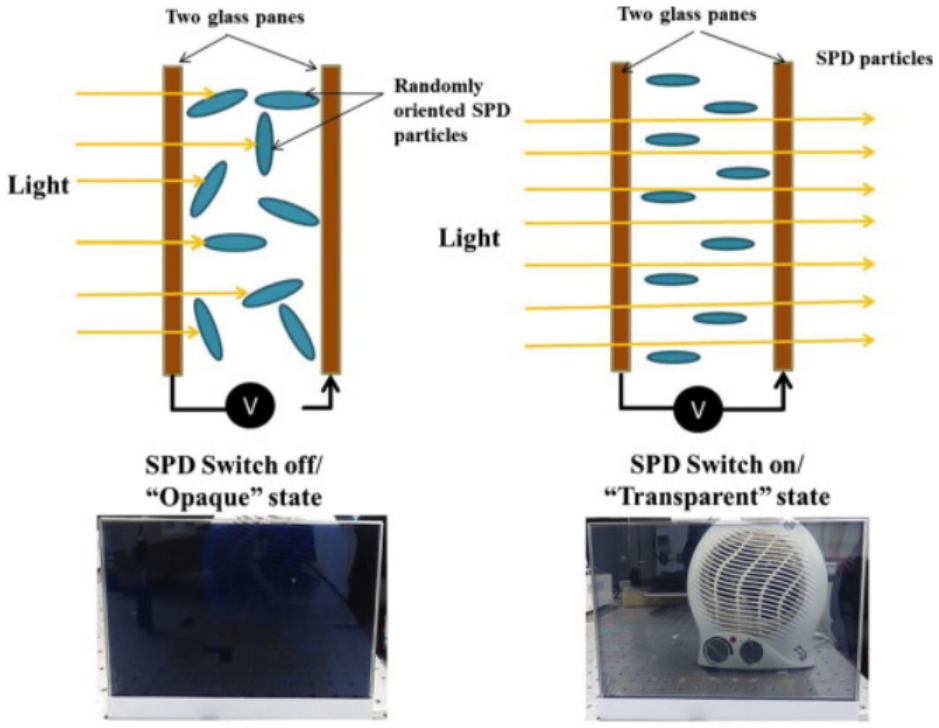

Figure 2.12: Working principle schematic of SPD window. Adapted from [39].

increases the transparency of the window. In figure 2.13 the SPD window is plotted for two different applications and for different states. In literature 100 V AC was applied to switch to the transparent state, to switch back to the opaque state the voltage should be 0 V. To maintain the transparent state

a continuous load is required, when this load is turned of the window go back to its initial state. In commercially available SPD window technologies the color of the window in its opaque state is dark blue. It should be noted that depending on the value of the applied voltage the transparency of the SPD window can be adjusted similarly to the EC window according to [39]. However because in literature only the SHGC and VT of the window at 0 V and 100 V were found, only these states are considered in the model. The U-value of a SPD window was measured to be 1.99 $\frac{W}{m^2K}$ by [39].

Applied AC voltage [V]	0	100
SHGC [-]	0.05	0.35
VT [-]	0.05	0.55

Table 2.6: SHGC and VT of SPD window in opaque or transparent state.

Figure 2.13: SPD application examples taken from [83].

2.5.3. Liquid crystal

The principle of LC is similar to that of SPD but instead of suspended particles in an organic fluid which absorb light in its initial state, LC consist of liquid crystals in a polymer which scatter light until a voltage is applied. The working principle is illustrated in figure 2.14. In its initial state, light is thus transmitted through the window but the window itself is not see through due to haze. When in its transparent state there is still some haze and this is not the case for the SPD window according to [41]. Among the LC windows, PDLC types are the ones which are mostly present in real life applications. In commercially available PDLC windows, the color of the window in its translucent state is white. M. Cordoba Parra (2019) [75] found that switchable glazing based on PDLC technologies are preferred over EC and SPD technologies. This is because PDLC allows for faster changing of transparency than EC and because the transmittance of light for transparent mode is higher for PDLC compared to SPD. The switching between translucent/opaque and transparent states takes around 400 ms for PDLC and SPD windows. The transparency of the windows in transparent state for PDLC and SPD can be up to respectively 80% and 60% [75], depending on the applied voltage in AC. Also because a PDLC window in its translucent state is not see through it could be used for privacy applications. The disadvantage of PDLC however is that the SHGC in both the transparent as translucent state is relatively higher compared to EC and SPD technologies, thus it is expected to have limited potential for reduction of cooling load. Besides it was found by [37] that PDLC glazing was able to control glare on intermittent cloudy and overcast cloudy days but not on clear days. In some literature sources it is therefore recommended to use PDLC only for privacy applications. The PDLC window in different states is shown in figure 2.15.

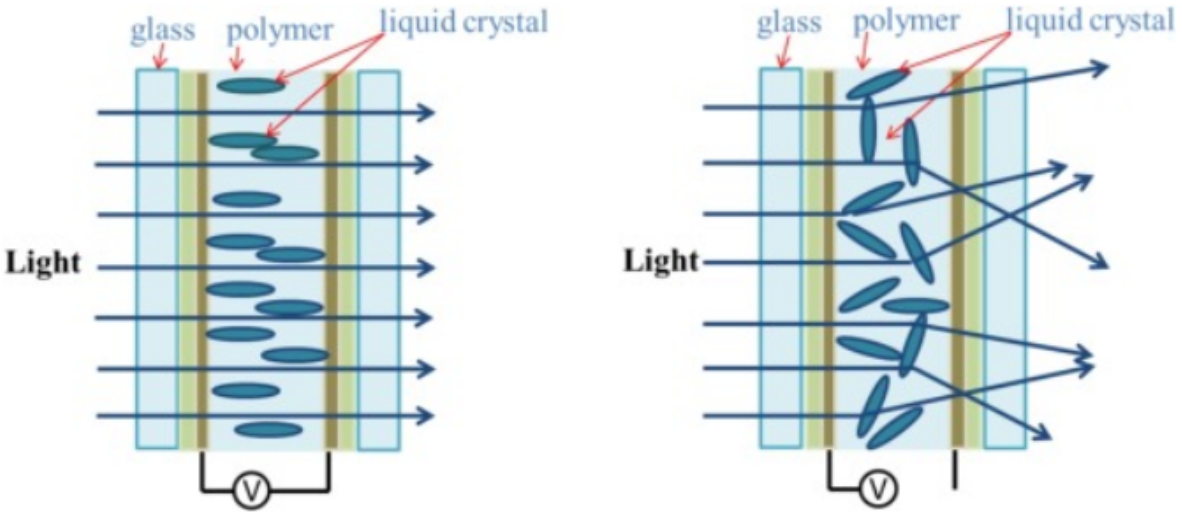

Figure 2.14: Working principle schematic of PDLC window. Adapted from [37].

There are two types of PDLC smart windows: Self-adhesive and non-adhesive. A self-adhesive PDLC film can be applied to a new or existing glass and thus does not require extra installation equipment. A non-adhesive PDLC film is sandwiched between two layers of EVA (Ethylene vinyl acetate) and two layers of glass.

In literature different values are found for the U-value, VT and SHGC of a PDLC window types. As mentioned before, the VT depends on the applied voltage and this is also the case for the SHGC. In research done by [37], a spectrophotometer was used to measure the light and solar transmittance of a PDLC glazing for wavelengths in the 300-2500 nm range. This was measured in indoor conditions and under different applied voltages. From this the VT and SHGC of the PDLC were calculated and these are shown in table 2.7. The highest calculated transparency and SHGC are reached for the highest applied AC voltage (20 V) as expected and the VT and SHGC for this applied voltage are respectively 0.71 and 0.53. The VT and SHGC for zero applied voltage are respectively 0.27 and 0.39. In later research done by the same group [46], the SHGC, VT and U-value were determined using a

Applied AC voltage [V]	0	5	10	15	20
SHGC [-]	0.39	0.45	0.48	0.51	0.53
VT [-]	0.27	0.52	0.68	0.7	0.71

Table 2.7: Thermal and optical properties of PDLC window under different applied voltages [37].

solar simulator. The SHGC for 20 V and 0 V were 0.68 and 0.63 respectively and the corresponding VT values were 0.79 and 0.44. The U-value was measured by [37] to be 2.79 $\frac{W}{m^2}$ for the PDLC in transparent state and 2.44 $\frac{W}{m^2}$ in translucent state. Regarding the applied voltage range, it should be noted that the rate applied voltage according to some literature sources and in the data sheet of a manufacturer is around 65 V AC to reach lower haze levels. However in this model the applied voltages from 0 up to 20 V AC are considered because [37] did measurements on both the VT and SHGC for these voltages.

Oh et al. (2019) [72] did simulations on PDLC added to an existing curtain wall in Energyplus using the optical and thermal properties of PDLC which are given in tables 2.8 and 2.9. The existing glazing was a double glazing type (6 mm clear glass + 14 mm air + 6 mm clear) with a VT of 0.771, SHGC of 0.697 and U-value of 2.813 W/m^2K. In table 2.8 the optical and thermal properties of four types of PDLC films are shown when added to the existing glazing. Table 2.8 shows the optical and thermal properties of laminated glass with the same types of PDLC films which are added to the existing double glazing. Figure 2.16 shows how the PDLC film and window is added to the existing glazing. The office room which was considered in [72] is different from the office room which will be discussed in section 3.1. The sizes of the room considered by [72] are 50 m x 50 m x 3 m, on each side are windows and

Figure 2.15: PDLC window. Adapted from [42].

the WWR is 0.6. Besides the ventilation and infiltration rates, the assumed lighting consumption per floor area, and assumed occupancy of the room are different. The simulations were done for Incheon, Korea. It was concluded from the simulations that when attaching PDLC film types A, B, C and D to the existing double glazed window, this would save the energy consumption by respectively 17.1%, 15.8%, 7.3%, and 3.1% compared to the existing double glazing. When adding the PDLC windows types A, B, C and D to the existing double glazed window, the energy savings were determined to be 22.4%, 21.3%, 20.5%, and 18.8% respectively. It should be noted here that the SHGC of the reference window to which the results of the PDLC configurations were compared was relatively high.

	26 mm Double Glazing	Existing Double Glazing + PDLC Film							
		A Type		B Type		C Type		D Type	
		On	Off	On	Off	On	Off	On	Off
U-Value [W/m^2K]	2.813	2.811	2.811	2.811	2.811	2.811	2.811	2.811	2.811
SHGC [-]	0.697	0.475	0.402	0.498	0.47	0.633	0.567	0.68	0.633
VT [-]	0.771	0.408	0.346	0.563	0.487	0.555	0.373	0.747	0.65

Table 2.8: Optical and thermal properties of PDLC films added to an existing glazing (adapted from [72]).

	26 mm Double Glazing	Existing Double Glazing + PDLC Window							
		A Type		B Type		C Type		D type	
		On	Off	On	Off	On	Off	On	Off
U-Value [W/m^2K]	2.813	1.758	1.758	1.758	1.758	1.758	1.758	1.758	1.758
SHGC [-]	0.697	0.541	0.536	0.557	0.551	0.566	0.549	0.584	0.575
VT [-]	0.771	0.301	0.255	0.418	0.361	0.419	0.280	0.570	0.492

Table 2.9: Optical and thermal properties of PDLC windows added to an existing glazing. Adapted from [72].

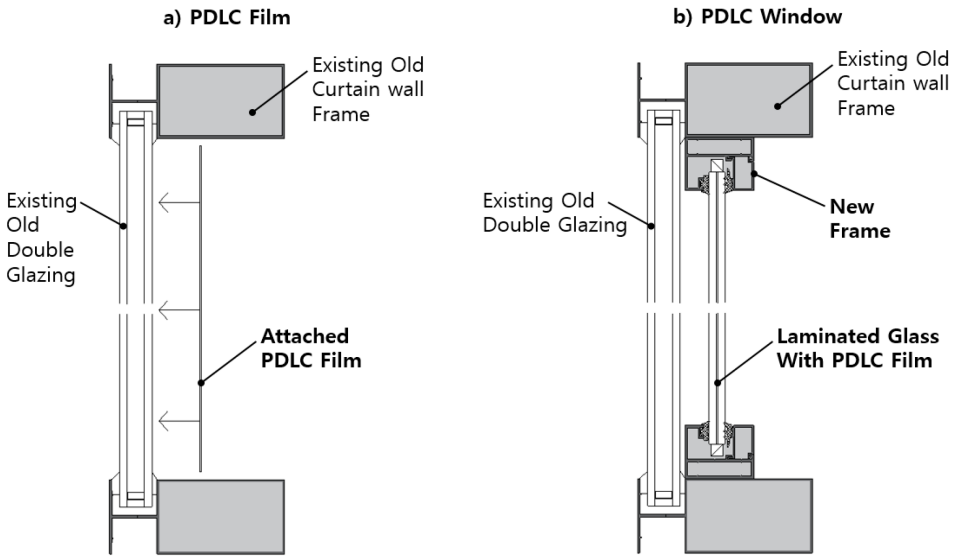

Figure 2.16: Two methods of adding PDLC to existing glazing. Adapted from [36].

2.5.4. PV integrated smart window

In some articles found in literature, an active smart window was built which was powered by solar energy. A functioning PDLC window powered by c-Si PV cells which were attached to the glazing layer was build by [75] and this demonstrator is shown for its translucent and a transparent state in figure 2.17. In this case the solar cells are visible. A semitransparent a-Si PV cell with an average VT of 20.04% and a power conversion efficiency of 6.94% and an PDLC film layer added to this PV cell was produced by [34]. This PV cell is shown for the PDLC film in its translucent and transparent states in figure 2.18 and is more invisibly integrated.

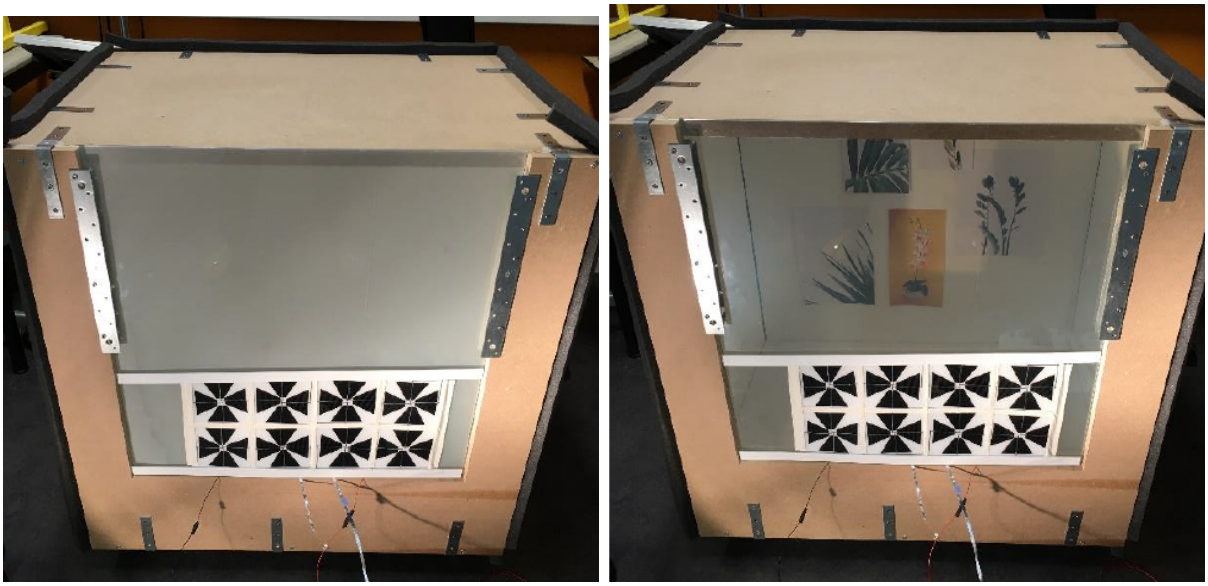

(a) PDLC in translucent state.

(b) PDLC in transparent state.

Figure 2.17: PDLC window with visibly integrated solar cells. Adapted from [75].

In [40] and [38], a SPD window was investigated which was powered by a standard c-Si PV module. This module was not integrated in the window. The integration of EC glazing and DSSC has been demonstrated by [30] on a small sized cell. Here a visible light transmittance between 16.9% and 31.5% was reached for an opaque and transparent state. In another study by [15], EC glazing was integrated with a neutral colored perovskite solar cell. Here an average visible transmittance between 8.4 and 26%

(a) PDLC in translucent state, camera behind glazing is not visible.

(b) PDLC in transparent state, camera behind glazing is now visible.

Figure 2.18: PDLC window with invisibly integrated solar cells. Adapted from [34].

was reached for the opaque and transparent state and the corresponding power conversion efficiencies were 5.5% and 3.7%. In the transmission spectrum of this device in its transparent and opaque states it was shown that the transmittance of light in the near-IR was relatively low in both cases and this indicates that this device is not suitable for controlling the solar heat gain when applied in an actual window. In [23] EC glazing was integrated with neutral colored OPV which uses mainly near-UV light to generate electricity to allow for solar heat gain control and for a high transmittance of visible light when in its transparent state. Here a relatively low power conversion efficiency of up to 1.5% was reached, which is because 93% of the spectral irradiance of AM1.5 was neglected. Because smart windows with invisibly integrated PV technologies have not yet been demonstrated on large scale and because not all required information on these devices was found to implement these in the model, these are not considered in the model.

3

Model

This chapter discusses how the model determines the heating, cooling and lighting consumption of a reference office room and how the PV area is calculated which is needed to power the smart window. The model consists of a solar irradiance part and illuminance part where the solar irradiance and illuminance on the window respectively are estimated as a function of the position of the Sun. With this the state of the smart window can be determined and the consumption of energy for lighting. Furthermore the model consists of a thermal part from which the consumption of heating and cooling will be determined. At last the solar power generation part of the model will be discussed.

3.1. Reference office

Reinhart et al. [82] defined the properties and dimensions of a reference office room such that the effect of changing one parameter to the energy performance of the office room can be determined and compared to a baseline. This is relevant when comparing different types of glazing technologies. In some articles found in literature, it is namely stated how much energy savings are expected for investigated window technologies, but it is then unclear to what type of ”conventional window” it is compared, if the WWR value is similar as used in other research and if the same room dimensions are used. The office room is facing south and its height, depth and width are respectively 2.8 m, 8.2 m and 3.6 m. The reference window has a width of 3 m and height of 1.5 m and is located 1 m above ground and the WWR of the reference office room is 0.45. Although the reference office room is located in Boston, USA, for this research project different locations will be considered with different climates. Besides the energy performance of the the office room will be investigated for four different orientations, namely for a facade facing north, east, south and west respectively.

The working hours in the reference office are between 8 AM and 6 PM, from Monday until Friday for every week during a whole year, thus not considering national holidays. The office consists of four six surfaces, namely three interior walls, an exterior wall with glazing, a ceiling and a floor. To calculate the energy performance of the office room, the properties of the walls are kept constant while the window properties are changed. Besides all surfaces except for the facade are assumed to be adiabatic which means that no heat is transferred through the interior walls and that the indoor temperatures of different office rooms next to each other are identical. The reference window is a double glazed window with a VT of 0.65, a SHGC of 0.28 and a U-value of 1.6 $\frac{W}{m^2K}$ and no low-e coating. It should be noted that when comparing these properties to the European reference glazing standards [22] or to commercially available double glazed windows without low-e coating, the SHGC of the reference window defined by [82] is significantly lower than these windows. The thicknesses of the glass panes and the width of the gap in the reference window are not specified in the article. However when calculating the U-value of a double glazed window with air filling using equation 3.51, this is equal to 1.55 $\frac{W}{m^2K}$. Here two glass panes of 4 mm and a gap of 12 mm are considered. It can thus be assumed that the reference window consists of two glass panes with a thickness of 4 mm which are 12 mm apart with air gas fill. The lighting requirements when considering a constant light source are 10.1 W/m^2 floor area and the equipment heat load is 8 W/m^2 floor area. The infiltration rate is the rate at which air leaks through the wall and is determined to be 0.5 ac/h (air change per hour) in the reference office. This can be expressed in m^3/s

using the equation

$$q_{filt} = V_{room} ACH/3600, \tag{3.1}$$

where ACH is the air change per hour and V_{room} is the volume of the office room. q_{filt} is equal to 0.0315 m^3/s or 31.5 L/s is the volume of air which is added or removed per second. The ventilation rate is the rate at which fresh air is supplied to the room and these are taken according to the American Society of Heating, Refrigerating and Air-Conditioning Engineers (ASHRAE) standards [6]. There are two ventilation rates which are considered for an office room and these are per floor area and per person who is using the room. The ventilation rate per person is 2.5 L/s which needs to be added to the ventilation rate of 0.3 L/s per floor area.

An overview of the considered properties of the reference office room is given in table 3.1. There are some differences between the values used in the model and the reference room defined by [82]. The first difference is that in this model the indoor illuminance should be between 500 lux and 2000 lux, while in the article 300 lux is the desired indoor illuminance. Besides the average indoor illuminance is calculated differently. Also in the article heating and cooling set points of 20°C and 26°C and setbacks of temperatures of 15°C and 30°C respectively are defined during occupied and unoccupied hours. This means that during occupation of the room the indoor temperature can fluctuate between 20°C and 26°C and heating or cooling will activate if the indoor temperature falls outside of this range during occupation. Outside of the working hours the temperature can fluctuate between 15°C and 30°C. In this model however the indoor temperature is fixed at 23°C to maintain a constant temperature throughout the year.

Albedo (α) [-]	0.2
Depth office room [m]	8.2
Height office room [m]	2.8
Infiltration rate (q_{filt}) [L/s]	31.5
Internal heat gain equipment per floor area (q_{equip}) [W/m^2]	8
Power consumption lighting per floor area (P_{light}) [W/m^2]	10.1
Reflectance internal walls (R_{wall}) [-]	0.5
Reflectance internal floor (R_{floor}) [-]	0.2
Reflectance internal ceiling ($R_{ceiling}$) [-]	0.8
SHGC reference window [-]	0.28
U-value of reference window [$\frac{W}{m^2K}$]	1.6
U-value of exterior wall [$\frac{W}{m^2K}$]	0.365
Ventilation rate per person ($q_{vent,pers}$) [L/s]	2.5
Ventilation rate per floor area ($q_{vent,floor}$) [$L/s/m^2$]	0.3
VT reference window [-]	0.65
Width office room [m]	3.6
Window to wall ratio (WWR) [-]	0.45

Table 3.1: Parameters of reference office room. Taken from [82].

3.2. Constants and assumptions

Table 3.2 shows the considered constants in the simulation model. The designed indoor temperature is fixed at 23°C in the model. The power requirement to power one square meter of PDLC window is given in the datasheet to be 3.7 W [47]. The current density is calculated by dividing the power requirement by an applied AC voltage of 65 V which is also given in the datasheet. The current density is thus 57 $mA/m2$, and it is assumed that this is the same for every applied voltage. In literature the SHGC and VT values for different applied voltages were found (see table 2.7) and these are considered in this work. For the SPD window, it was found in literature that 0.07 W was required for this technology to become transparent. The area of the tested SPD window was 0.0345 m^2, and it is assumed that the power requirements to power one square meter of SPD window is therefore 2.0 W [38]. The applied AC voltage required to power the SPD window is 100 V, thus the corresponding current density is calculated to be 20 mA/m^2. For a commercial EC window, the DC voltage required to switch the transparency

of the EC window is given by [7] to be 5 V. In [84] an EC window with three colored states is given. However the required applied voltage to reach the two intermediate states is not given in the source. These corresponding applied voltage are therefore approximated. Besides it is assumed that to switch to any opaque state a voltages needs to be applied for one minute. It is mentioned in [24] that the current density required to switch transparency in a monolithic device where EC and PV are integrated was 0.1 mA/cm^2, which is equal to 1 A/m^2. This current density is assumed for each applied DC voltage when switching between states.

In chapter 2 it was mentioned that the U-value found in literature for some of the window technologies was relatively high. For these window technologies a U-value of 1.65 $\frac{W}{m^2K}$ will be considered in this work. The reason is that window technologies should at least have a high thermal insulation to be implemented in a building such that the thermal losses are minimized. Furthermore, in the Dutch building regulation standard regarding thermal insulation of windows the maximum allowed U-value of windows is 1.65 $\frac{W}{m^2K}$ [66]. As explained earlier, the U-value can be lowered by using a cavity filling with high insulating properties such as argon, krypton or xenon. Increasing the width of the cavity gap would also lower the U-value, because the layer of insulation then becomes thicker. The assumption made regarding the U-value is thus reasonable.

Regarding the HVAC requirements calculations, it is assumed that the conductive heat transfer depends on a temperature independent U-value. Besides it is assumed that the internal walls, floor and ceiling of the office room are adiabatic. This means that no heat is exchanged between the rooms and floors of an office building. The only heat exchange which is considered in the model is thus through the external facade which contains the window. This assumption is reasonable if the designed indoor temperature of each office room in the building is the same such that the temperature difference between the rooms is small. The SHGC is a factor which accounts for solar heat transmittance through the window and heat absorbed in the glass layers. In the solar heat gain calculation of the model, the definition of the SHGC as defined by [36] is used. Here only the solar heat transmittance through the window and not the solar heat absorbed in the glass is considered. The SHGC affects the heat balance and thus the need for energy consumption of heating and cooling in an office room. The amount of solar heat which enters the indoor space also depends on the area of the window. A variable which could thus be considered in the simulation model is the WWR. A general rule for the WWR is that for a small WWR value, the energy efficiency and the thermal insulation of the building are higher than for large WWR values. This is because the thermal insulation properties of brick are better than for glass which means that more heat can be lost through the window. On the other hand for larger WWR values there is more daylight availability which has been found in various research papers to be more healthy for occupants.

In this model the WWR is considered as a constant. The specific heat capacity and density of dry air are considered in the model and are equal to 1005 $\frac{J}{kgK}$ and 1.204 kg/m^3 at 20 °C and 1 atmospheric pressure [92][93]. These values are assumed to be constant in the model. Although the heat radiated by a person varies depending on the activity, it is assumed that on average 120 W is radiated per person during the working hours based on [90]. Besides it is assumed that the office room constantly has six occupants during the working hours. In the model it is possible to select a constant light source where the lighting loads are always the same when turned on, or a adaptable light source where the lighting consumption depends on the illuminance. In this model the adaptable light source is considered. The model also allows to design a HVAC system based on a single optimal indoor temperature or based on a minimum and maximum indoor temperature range. For the simulations the single optimal indoor temperature is considered. Regarding energy generation there are some assumptions made as well. The state of charge (SOC) limits of the battery should be between 10% and 95% and the maximum current through the wires is 10 A. For the PV generation part to power the smart windows, the PV technology can be varied but only c-Si is considered because of its relatively higher efficiency. The simulations are done for the year 2017 because this is used for the validation model. In the model no holidays are considered for simplicity. When simulating the energy consumption loads in terms of heating, cooling and lighting for semitransparent PV windows, the energy yield is subtracted from these loads to determine a net energy consumption. Here the maximum input voltage of the charge controller is raised to 600 V, which is given in the electrical specifications of a commercially available c-Si glass.

Capacity of single Li ion rechargable battery ($I_{batt,1}$) [Ah]	0.4
Costs of battery [€/Wh]	2.73
Costs of electricity [€/kWh]	0.18
Costs of c-Si solar cells [€/piece]	0.10
Current density EC (I_{EC}) [A/m^2]	1
Current density PDLC (I_{PDLC}) [mA/m^2]	57
Current density SPD (I_{SPD}) [mA/m^2]	12
Density of air (ρ) [kg/m^3]	1.204
Designed indoor temperature (T_{in}) [°C]	23
Efficiency inverter (η_{inv}) [-]	0.90
Efficiency MPPT tracker (η_{MPPT}) [-]	0.95
Efficiency charge controller (η_{CC}) [-]	0.93
Exchange rate USD to euro [€/$]	0.89
Exchange rate GBP to euro [£/$]	1.11
Heat emission coefficient LED light (q_{light}) [$W_{heat}/W_{electricity}$]	0.08
Human body heat radiation (Q_{person}) [W]	120
Luminous efficacy LED light ($l_{l,smart}$) [$lumen/W$]	172.1
Maximum DC input voltage charge controller ($V_{cc,max}$) [V]	28
Maximum input current charge controller ($I_{cc,max}$) [A]	10
Minimum DC input voltage charge controller ($V_{cc,min}$) [V]	8
Minimum input current charge controller ($I_{cc,min}$) [mA]	3
Maximum state of charge (SOC_{max}) [%]	95
Minimum state of charge (SOC_{min}) [%]	10
Nominal voltage of battery V_{nom} [V]	12
Occupants office room during working hours (n_{person}) [-]	6
Resistance when (dis)charging the battery (R_{batt}) [Ω]	0.1
Self-discharge factor per hour (D_{self}) [1/hr]	2.2831e-05
Sizing factor (SF) [-]	1.1
Solar irradiance under STC (G_{stc}) [W/m^2]	1000
Specific heat capacity of air (C_{air}) [$J/(kgK)$]	1005
Tilt angle (θ_m) [°]	90
Voltage of single Li ion rechargable battery (V_{batt}) [V]	3.2

Table 3.2: Considered constants in model.

3.3. Variables considered in the model

To find the minimal area of PV required to power the active smart window, it is required to know the solar irradiance and illuminance that reaches the facade. For this the direct normal irradiance, diffuse horizontal irradiance, global horizontal irradiance, direct normal illuminance, diffuse horizontal illuminance and global horizontal illuminance are required. To calculate the consumption of heating and cooling, the outdoor temperature is required because this determines how much heat is exchanged between the indoor space and outdoor environment. The irradiance and illuminance components as well as the outdoor temperature can be found in weather data for a given location for a typical meteorological year. This is a set of weather data determined through actual measurements for several years from which representative values are selected. The weather data used in this model is an ".epw" file extracted from the EnergyPlus website [68].

The daylight illuminance and solar heat which are transmitted through the window depend on VT and SHGC and these change as a function of the angle of incidence. In the case of smart windows the VT and SHGC can be varied, thus the indoor illuminance and solar heat gain depend on the state of the smart window. The VT and SHGC are controlled by the applied voltage. The EC window is transparent in its initial state, but when applying a voltage it reaches a different state with lower VT and SHGC. The PDLC and SPD windows have the lowest SHGC and VT values in their initial state. When applying a voltage here, the VT and SHGC of both window technologies will increase.

Another variable in the model is the orientations of the facade. Four orientations of the facade are

considered, namely facing north, east, south and west. This is because the position of the Sun varies as a function of time and gives different values for the irradiance and illuminance for every orientation of the facade.

3.4. Climates

In the model different locations with different corresponding climates are considered. These climates are based on the Köppen-Geiger climate classification presented by [10]. The considered locations are Abu Dhabi in the United Arab Emirates, Bogota in Colombia, Delft in the Netherlands, Hong Kong and Reykjavik in Iceland. An overview of the characteristics of these locations are shown in table 3.3. These characteristics include the type of climate, the longitude, latitude and elevation with respect to sea level, the timezone with respect to Greenwich time and the average dry-bulb or ambient/outdoor temperature. A positive latitude angle indicates that a location is located above the equator and a positive longitude angle indicates that a location is located on the east with respect to Greenwich, England. The climate of Abu Dhabi is specified as a hot, dry and sunny desert climate with an average annual temperature of 27°C. The sky is expected to be clear throughout the year and the outdoor temperature as given in the weather file does not go below 5°C. Bogota is located 2548 m above sea level and has a subtropic highland climate. The average temperature is 13.6°C but the maximum and minimum temperatures throughout the year are similar. The latitude and longitude are respectively 4.7° and -74.1°. The low latitude indicates that Bogota is close to the equator which means that during a summer day the solar altitude is higher than for locations such as Delft and Reykjavik which have a relative higher latitude. Delft has a temperate oceanic climate and an average annual temperature of 10.8°C. During the summer the outdoor temperature in Delft can get higher than in Bogota while during winter the minimum temperature in Bogota appears to be higher. The average annual temperature of Reykjavik is significantly lower than the other considered locations, this is because of its high latitude. The climate of Reykjavik is a subpolar oceanic climate. The outdoor temperature during summer is larger than during winter which is similar to Delft. Hong Kong is characterised by a humid subtropical climate which means that is hot and humid during the summer. The hourly ambient temperature for all locations is plotted in figure 3.1. The latitude of Delft and Reykjavik are relatively high and this means that the number of solar hours during the summer will be higher than during the winter.

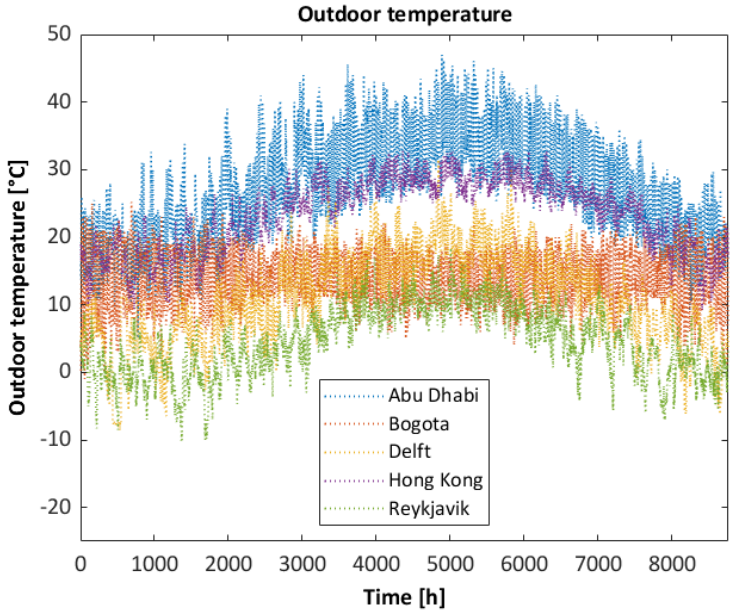

Figure 3.1: Outdoor temperature for different locations with difference climates.

Location	Abu Dhabi	Bogota	Delft	Hong Kong	Reykjavik
Climate	Hot desert	Subtropic highland	Temperate oceanic	Humid subtropical	Subpolar oceanic
Latitude [°]	24.5	4.7	52	22.32	64.13
Longitude [°]	54.4	-74.1	4.4	114.17	-21.9
Timezone [h]	+4	-5	+1	+8	0
Elevation [m]	27	2548	1	65	61
Average temperature [°C]	27.1	13.6	10.8	23.1	4.5

Table 3.3: The climates of the different locations investigated in the model taken from [68].

3.5. Solar position

In the model the solar position can be determined for any moment of the year (in hours, minutes or seconds) for given coordinates and corresponding timezone [87]. When creating two time point $t1$ and $t2$ in Matlab where $t1$ is the first time point of the period and $t2$ is the last time point of the period, by defining the year, month, day, hour, minute and second, these time points are then translated into a vector of julian date points JD where every data point represents a time step in either seconds, minutes or hours. A julian date point is defined as the number of days since 1 January 4713 BC according to the Julian calendar and this is convenient to determine the time D passed since Greenwich noon on 1 January 2000 in days. Note that $t1$ and $t2$ are also given for Greenwich time and to correct the julian date point which represents the local time, the timezone of the location should thus be subtracted from ”hour” input for the time point $t1$ and $t2$. For example if the local time in Hong Kong would be 9 PM, then $t1$ would be 1 PM since the time offset of Hong Kong is +8:00 with respect to Greenwich time.

When considering the case where the data points are in hours, JD is calculated in the Matlab model using

$$JD = juliandate(t1) : (1/24) : juliandate(t2), \tag{3.2}$$

which means that if $t1$ is defined as 1 January at 1 AM (Greenwich time) of a random year and $t2$ is defined as 1 January at 12 AM (Greenwich time) of the next year, JD is a vector consisting 8760 data points in this case. If the time steps would be in minutes, then the factor 1/1440 should be used instead of 1/24. To calculate the number of days D since 1 January 2000 noon (12 AM) the equation

$$D = JD - 2451545 \tag{3.3}$$

is used and this is used to determine the mean longitude q of the Sun and the mean anomaly of the Sun in degrees. The mean longitude of the Sun is calculated using

$$q = mod(280.459 + 0.98564736D, 360), \tag{3.4}$$

where mod is the modulus which makes sure the angle does not exceed 360°. A similar equation is for the mean anomaly of the Sun which is given by

$$g = mod(357.529 + 0.98560028D, 360). \tag{3.5}$$

With the mean longitude of the Sun and the mean anomaly of the Sun the ecliptic longitude of the Sun (λ_s) can be calculated. This accounts for ecliptic movement of the Earth around the Sun due to not being a perfect sphere. The ecliptic longitude of the Sun is calculated according to

$$\lambda_s = mod(q + 1.915 \sin g + 0.02 \sin 2g, 360). \tag{3.6}$$

The ecliptic longitude of the Sun can be translated into equatorial coordinates using an axial tilt e which is given by the equation

$$e = mod(23.429 - 0.00000036D, 360). \tag{3.7}$$

To determine the solar position the local mean sidereal time needs to be calculated and this depends on the Greenwich mean sidereal time (GMST) and the longitude of the location of the observer (λ_0). GMST is the time on the clock in the timezone of Greenwich in hours and this depends on the time according to

$$GMST = mod(18.697374558 + 24.06570982441908D + 0.000026((D/36525)^2), 24), \tag{3.8}$$

where D is again the number of days since 1 January 2000 noon (12 AM) Greenwich time which is corrected using the timezone to represent the local time. The longitude of the location of the observer is given in degrees and the local mean sidereal time can then be calculated according to

$$\theta_L = mod(15GMST + \lambda_0, 360). \tag{3.9}$$

Then finally with all these calculated values the solar azimuth (A_s) can be calculated in degrees according to

$$A_s = \arctan \frac{\nu_s}{\zeta_s}, \tag{3.10}$$

where

$$\nu_s = \sin\theta_L \cos\lambda_s + \cos\theta_L \cos e \sin\lambda_s \tag{3.11}$$

and

$$\zeta_s = -\sin\phi_0 \cos\theta_L \cos\lambda_s - (\sin\phi_0 \sin\theta_L \cos e - \cos\phi_0 \sin e) \sin\lambda_s. \tag{3.12}$$

The solar azimuth is a number between 0 and 360 thus if ζ_s is lower than 0, 180° is added to A_s and if ν_s is below 0, then 360° is added to A_s. The solar altitude or elevation (a_s) in degrees is calculated according to

$$a_s = \arcsin(\cos\phi_0 \cos\theta_L \cos\lambda_s + (\cos\phi_0 \sin\theta_L \cos e + \sin\phi_0 \sin e) \sin\lambda_s). \tag{3.13}$$

3.6. Solar irradiance

The solar irradiance has three components, direct irradiance, diffuse irradiance and ground irradiance and is given in the units W/m^2. Direct irradiance is irradiance which directly reaches the window without diffusing in the sky. Ground irradiance is direct irradiance which reaches the window after it is reflected by the ground with a specific albedo α. The albedo for a city is considered and this is considered to be 0.20. This is namely the default albedo used in EnergyPlus [68]. Besides the direct and ground irradiance which reaches a window, diffuse irradiance is also considered which is diffused in the sky before it reaches the window. The total solar irradiance on a surface is equal to

$$G_{tot} = G_{dir} + G_{diff} + G_{ground}. \tag{3.14}$$

3.6.1. Direct and ground irradiance

The direct irradiance is calculated using the direct normal irradiance (DNI) and the position of the Sun according to the model presented by Smets et al. [87]. The DNI is usually found in weather data files for various locations. The first step in calculating the direct irradiance G_{dir} is by determining the cosine of the angle of incidence (AOI) and multiplying this to the DNI according to

$$G_{dir} = DNI \cos(AOI), \tag{3.15}$$

which is assumed to be zero for negative values of G_{dir}, since negative values for irradiance have no physical interpretation. The cosine of the AOI depends on the orientation of the facade represented by A_m, the azimuth of the Sun A_s and the altitude of the Sun (a_s) according to

$$\cos(AOI) = \sin a_s \cos\theta_m + \sin\theta_m \cos a_s \cos(A_s - A_m). \tag{3.16}$$

As described in section 3.5 the A_s and a_s are used to calculate the AOI of sunlight directly facing on the facade. θ_m is the tilt angle of the surface with respect to the horizontal, thus the tilt angle of a vertical surface is 90°. The ground irradiance is calculated according to the equation

$$G_{ground} = \alpha GHI \frac{1 - \cos\theta_m}{2}. \tag{3.17}$$

3.6.2. Diffuse irradiance: Perez model

The diffuse irradiance component is less straight forward to determine, compared to the direct and ground irradiance components which are originated directly from the Sun. This is because diffuse irradiance originates from light which is scattered in the sky and which arrives at the window under

different angles of incidences. Several models have been proposed for the determination of the diffuse irradiance, these are distinguished between isotropic and anisotropic models. In the isotropic sky model presented by Liu and Jordan (1960) [57], the sky is considered to be isotropic which means that the diffuse irradiance is independent of the orientation of the window and only on the tilt angle. However it was found in later research that anisotropic sky models would improve the accuracy for tilted surfaces and be more representative of the reality. The diffuse irradiance model presented here is based on two anisotropic sky models, namely the Perez sky model [79] and the Hay-Davies model [44].

The Perez model is a model commonly used in simulation software such as Grasshopper, because it has been extensively been validated for different locations. This model was found to be one of the most accurate diffuse irradiance models among isotropic and anisotropic models, specially under clear sky conditions. In the Perez diffuse sky model a sky clearness ϵ is calculated which represents how clear the sky is and thus how much light is diffused in the sky. This is done according to

$$\epsilon = \frac{\frac{DHI+DNI}{DHI} + \kappa\theta_z^3}{1 + \kappa\theta_z^3}, \tag{3.18}$$

where DHI is the diffuse horizontal irradiance, DNI is the direct normal irradiance, θ_z is the zenith angle which is equal to 90-a_s in degrees and κ is a constant which is 5.535e-6 if θ_z is in given in degrees and 1.041 if θ_z would be given in radians. If ϵ is small an overcast sky is considered while if ϵ is large a clear sky is considered. The next step to calculate the diffuse irradiance involves calculating an air mass (AM) which characterizes the solar spectrum and the corresponding direct irradiance as a function of the a_s according to

$$AM = \frac{1}{\sin a_s + 0.50572(6.07995 + a_s)^{-1.6364}}. \tag{3.19}$$

$AM1.5$ is the standard air mass which is used to determine the efficiency of solar cells. The irradiance which corresponds to this air mass is around 1000 W/m^2 and this is a convenient round number. When calculating AM as a function of the position of the Sun, it is possible that there is still diffuse irradiance while the Sun is down. This is the case if θ_z exceeds 90° and the DHI is greater than zero. To consider the contribution of the DHI here, the AM is defined as 37 which corresponds to an a_s of 0°. Using the DHI and the extra-terrestrial irradiance I_{extra} which are given in the weather data and the AM, a variable Δ can be calculated according to

$$\Delta = DHI\frac{AM}{I_{extra}}. \tag{3.20}$$

Then parameters F1 and F2 are calculated using this Δ according to

$$F1 = max(0, f11 + \Delta f12 + \theta_z\frac{\pi}{180}f13), \tag{3.21}$$

and

$$F2 = f21 + \Delta f22 + \theta_z\frac{\pi}{180}f23, \tag{3.22}$$

where f11, f12, f13, f21, f22 and f23 are the Perez model coefficients as given in table 3.4 and θ_z is in degrees. The Perez model coefficients are parameters determined through measurements done by [79] and correspond to a range of the clearness indices. F1 and F2 depend on ϵ, if ϵ is between 1 and 1.065, then the coefficients of the first row which correspond to ϵ bin 1 are used. ϵ bins 2, 3, 4, 5, 6, 7 and 8 correspond to the ranges of ϵ of respectively 1.065-1.230, 1.230-1.500, 1.500-1.950, 1.950-2.800, 2.800-4.500, 4.500-6.200 and 6.200- above. Finally the diffuse irradiance component G_{diff} is calculated according to

$$G_{diff} = G_{iso} + G_{circum} + G_{hor}, \tag{3.23}$$

where G_{iso}, G_{circum} and G_{hor} are the isotropic, circumsolar and horizon brightening diffuse sky irradiance components respectively. The isotropic component represents the diffuse irradiance of an uniform sky and is equal to

$$G_{iso} = DHI[(1 - F1)\frac{1 + \cos\theta_m}{2}], \tag{3.24}$$

and this is taken from the Liu and Jordan isotropic sky model [57]. The circumsolar component represents the solar radiation that appears to come from the region around the Sun from the perspective of an observer on the ground and is given by

$$G_{circum} = DHI[F1\frac{\cos(AOI)}{\cos\theta_z}]. \tag{3.25}$$

To avoid dividing by zero, all values of $\cos(\theta_z)$ which are lower than $\cos(85)$ are assumed to be equal to $\cos(85)$.

The horizon brightening component accounts for solar irradiance near sunrise and sunset and is expressed by

$$G_{hor} = DHI[F2\sin\theta_m]. \tag{3.26}$$

The total irradiance G_{tot} is equal to the sum of G_{dir}, G_{diff} and G_{ground}.

ϵ bin	f11	f12	f13	f21	f22	f23
1	-0.008	0.588	-0.062	-0.06	0.072	-0.022
2	0.13	0.683	-0.151	-0.019	0.066	-0.029
3	0.33	0.487	-0.221	0.055	-0.064	-0.026
4	0.568	0.187	-0.295	0.109	-0.152	-0.014
5	0.873	-0.392	-0.362	0.226	-0.462	0.001
6	1.132	-1.237	-0.412	0.288	-0.823	0.056
7	1.06	-1.6	-0.359	0.264	-1.127	0.131
8	0.678	-0.327	-0.25	0.156	-1.377	0.251

Table 3.4: Perez coefficients for diffuse irradiance [79].

3.6.3. Diffuse irradiance: Hay-Davies model

According to [98], the Perez model overestimates the diffuse irradiance for high latitude locations and it was found that the Hay-Davies model [44] would give a better approximation of the diffuse irradiance for such locations. In this model it is proposed to use the Hay-Davies model to calculate the diffuse irradiance for locations which have a latitude higher than 40° with respect to either north or south. The diffuse irradiance is calculated according to

$$G_{diff} = DHI\left[(1+A_i)\left(\frac{1+\cos\theta_m}{2}\right)+r_bA_i\right], \tag{3.27}$$

where A_i is the anisotropic index which represents the direct irradiance transmittance through the atmosphere and this is equal to

$$A_i = \frac{DNI}{I_{extra}}. \tag{3.28}$$

I_{extra} is the extraterrestrial irradiance which is on average 1365 W/m2 depending on the distance between the Sun and the Earth. r_b is equal to the direct irradiance which reaches a tilted surface divided by the direct irradiance which reaches a horizontal surface and is calculated according to

$$r_b = \frac{max(\cos(AOI),0)}{max(\cos(\theta_z),\cos(89))}. \tag{3.29}$$

The denominator of the ratio has $\cos(89)$ as bottom limit, because for a zenith angle of zero r_b would be infinite and for zenith angles below zero the ratio would become negative. A negative r_b value could potentially give negative diffuse irradiance values which have no physical meaning.

3.7. Illuminance

To simulate the natural illuminance which reaches the window, the Perez diffuse sky model as explained in section 3.6.2 is used similarly to the diffuse irradiance calculation. However to calculate the illuminance the direct normal illuminance (DNI_{lux}), global horizontal illuminance (GHI_{lux}) and diffuse

	Normalized Transmittance				
	a	b	c	d	e
A 3mm clear	1.470E-02	1.486E+00	-3.852E+00	3.355E+00	-1.474E-03
B 3mm bronze	5.546E-01	3.563E-02	-2.416E+00	2.831E+00	-2.037E-03
C 6 mm bronze	7.709E-01	-6.383E-01	-1.576E+00	2.448E+00	-2.042E-03
D Single coated	3.462E-01	3.963E-01	-2.582E+00	2.845E+00	-2.804E-04
E Double clear 3mm	2.883E+00	-5.873E+00	2.489E+00	1.510E+00	-2.577E-03
F Double coated 3mm clear	3.025E+00	-6.366E+00	3.157E+00	1.213E+00	-1.367E-03
G Double 3mm tinted 3mm	3.229E+00	-6.844E+00	3.535E+00	1.088E+00	-2.891E-03
H Double glazing: coated - 6mm clear	3.334E+00	-7.131E+00	3.829E+00	9.766E-01	-2.952E-03
I Double glazing: 6 mm tinted-6mm clear	3.146E+00	-6.855E+00	3.931E+00	7.860E-01	-2.934E-03
J Triple coating 3mm clear-coated	3.744E+00	-8.836E+00	6.018E+00	8.407E-02	4.825E-04

Table 3.5: Fitting parameters for angular dependent SHGC and VT to determine transmitted solar heat and visible light as given by [5].

horizontal illuminance (DHI_{lux}) are used in equations (3.15), (3.17) and (3.23) instead of the irradiance components respectively. These values can be found in the same weather data files which contain of the DNI, DHI and GHI values. For the diffuse illuminance calculation, the equations (3.21) and (3.22) use the Perez model coefficients for illuminance as shown in table 3.6. To determine the indoor illuminance level, an average indoor illuminance L_{in} is calculated using an equation adapted from [56]. In the original method the average indoor illuminance is calculated according to

$$L_{in} = \frac{A_{window} L_{tot} VT}{A_{tot,in}(1 - R_{room})}, \tag{3.30}$$

where A_{window} is the area of the window, $A_{tot,in}$ is the total area of the interior walls, floor and ceiling, R_{room} is the total reflectance of the room and L_{tot} is the total illuminance which is equal to the sum of the direct, diffuse and ground illuminance components L_{dir}, L_{diff} and L_{gr}. Because the VT in this case is independent of the angle of incidence, the original method has been adjusted in this work. Equation (3.30) after adjustment becomes

$$L_{in} = (L_{dir} VT_{dir} + L_{diff} VT_{diff} + L_{gr} VT_{gr}) \frac{A_{window}}{A_{tot,in}(1 - R_{room})}, \tag{3.31}$$

where VT_{dir}, VT_{diff} and VT_{gr} are VT values corresponding to the direct, diffuse and ground illuminance and depend on the angle of incidence. The angle dependent VT corresponding to the direct illuminance component is calculated using

$$VT_{dir}(AOI) = VT[a(\cos(AOI))^4 + b(\cos(AOI))^3 + c(\cos(AOI))^2 + d\cos(AOI) + e]. \tag{3.32}$$

Here VT is the constant which is given for each window in the model and a, b, c, d and e are fitting parameters which were empirically determined by [5] and correspond to the U-value and SHGC of the windows as given in table 3.5. If the U-value of the window is larger than or equal to 4.5 $\frac{W}{m^2K}$ and the SHGC is larger than or equal to 0.65 the VT is described by the fitting parameter corresponding to window A from table 3.5, if the U-value is smaller than 4.5 $\frac{W}{m^2K}$ and the SHGC is larger than or equal to 0.45, the fitting parameters correspond to window E from table 3.5. If the U-value is larger than or equal to 4.5 $\frac{W}{m^2K}$ and the SHGC is between 0.45 and 0.65, then the VT is calculated using the fitting parameters corresponding to windows B, C and D from table 3.5 and are averaged. The same is done using the fitting parameters of windows F, G, H and I if the U-value is between 4.5 $\frac{W}{m^2K}$ and 1.7 $\frac{W}{m^2K}$ and the SHGC is between 0.3 and 0.45. For a SHGC smaller than 0.45 and U-value smaller than 1.7 $\frac{W}{m^2K}$, the fitting parameters of window J are used, For other SHGC and U-value properties the fitting parameters of windows F and H are used and the results are averaged. Because for the switchable glazing the SHGC changes, it is possible that the fitting parameters for the window in its transparent state are different than for the window in its opaque state and that the window in the two states is regarded as a different type of window. To determine the angle dependent VT corresponding to the diffuse and ground components, the VT is calculated according to equation (3.32) for each angle of

incidence from 0 up to 90°. An average VT is then determined for VT_{diff} and VT_{gr} according to

$$VT_{diff} = \frac{\sum_{i=1}^{90} VT(i) L_{diff} \cos(AOI, i)}{\sum_{i=1}^{90} L_{diff} \cos(AOI, i)} \tag{3.33}$$

and

$$VT_{gr} = \frac{\sum_{i=1}^{90} VT(i) L_{gr} \cos(90 - AOI, i)}{\sum_{i=1}^{90} L_{gr} \cos(90 - AOI, i)}. \tag{3.34}$$

For VT_{gr} the cosine of (90-AOI) is used because ground illuminance originates from the ground.

The total area of the interior walls, floor and ceiling is equal to

$$A_{tot,in} = A_{wall} + A_{floor} + A_{ceiling}, \tag{3.35}$$

where A_{wall} is equal to

$$A_{side,1} + A_{side,2} + A_{back,3} + (A_{facade} - A_{window}). \tag{3.36}$$

$A_{side,1}$ and $A_{side,2}$ are interior walls with the same dimensions and $A_{back,1}$ is the wall parallel to the facade. The reflectance of the room is calculated using the surface areas and reflectance R of the walls, floor, ceiling and window according to

$$R_{room} = \frac{R_{wall}A_{wall} + R_{ceiling}A_{ceiling} + R_{floor}A_{floor} + R_{window}A_{window}}{A_{tot,in}}. \tag{3.37}$$

The reflectance of the walls, floor and ceiling are respectively 0.5, 0.2 and 0.8 are retrieved from the reference office [82]. The reflectance of the window is assumed to be equal to 1-VT (thus not considering absorption). Here the VT for an angle of incidence of 0° is considered. The average indoor illuminance of the reference office should be between 500 lux and 2000 lux for optimal comfort conditions. If this is the case during a weekday between 8 AM and 6 PM, then the smart window needs to be in the transparent state. For the PDLC and SPD window, this means that a voltage needs to be applied while for the EC window no electricity loads are required since the EC window is transparent in its initial state. A PV system is designed to provide the required electricity which allows the windows to be in the transparent state or opaque state. The modelling of this PV system model is be discussed in section 3.9. If the average indoor illuminance is higher than 2000 or lower than 500 lux, then the PDLC and SPD windows will be in their opaque state which means that no voltage is applied. For the EC window a voltage is applied when 2000 lux is exceeded and the window needs to switch between different states. If the state is the same as for the previous time step then no electricity load is required. In the case that the indoor illuminance drops below 500 lux during the week and during 8 AM and 6 PM, the artificial lights will be turned on, which will consume electricity. In the model it is possible to choose between a light source which provides a constant amount of lighting when turned on and an adaptable light source where the power consumption depends on the indoor illuminance. It should be noted that the illuminance for high latitude locations is also determined using the Perez diffuse sky model because no articles were found in the literature where the Hay-Davies model is used to calculate the illuminance.

3.8. Thermal part of model

In the thermal part of the simulation model, the heating and cooling loads of an office room are determined. As mentioned in section 3.2, no heat is exchanged through the internal walls, floor and ceiling, because the temperature difference is assumed to be small between different rooms and floors of an office building. This means that the heat transfer through the facade only should be considered. The components which are considered in heat transfer are the solar heat gain, internal heat gains, infiltration heat gains and losses, ventilation heat gains and losses and conduction heat gains and losses. Solar heat gain is due to solar irradiance which is transmitted through the window and adds heat to the room. Internal heat gains are due to heat radiated by the lighting, equipment and the users of the room. The infiltration, ventilation and conduction heat transfer components are either positive or negative, depending on the difference between the indoor and outdoor temperature. If the temperature outside is

ϵ bin	f11	f12	f13	f21	f22	f23
1	0.011	0.57	-0.081	-0.095	0.158	-0.018
2	0.429	0.363	-0.307	0.05	0.008	-0.065
3	0.809	-0.054	-0.442	0.181	-0.169	-0.092
4	1.014	-0.252	-0.531	0.275	-0.35	-0.096
5	1.282	-0.42	-0.689	0.38	-0.559	-0.114
6	1.426	-0.653	-0.779	0.425	-0.785	-0.097
7	1.485	-1.214	-0.784	0.411	-0.629	-0.082
8	1.17	-0.3	-0.615	0.518	-1.892	-0.055

Table 3.6: Perez model solar illuminance coefficients [79].

greater than the indoor temperature, heat will be added to the room through ventilation, infiltration and conduction. However if the indoor temperature is greater than the outdoor temperature heat will be lost from the room. To determine the cooling and heating contribution, the sum of the heat gains and losses is calculated according to

$$Q_{tot} = Q_{solar} + Q_{internal} + Q_{infil} + Q_{vent} + Q_{cond}, \tag{3.38}$$

and this should be zero. This means that if the sum is negative, heating is required while if the sum is positive cooling loads are required. As mentioned earlier the surfaces except for the facade are adiabatic and this is because it is assumed that the office rooms have the same designed indoor temperature. That means that no heat is exchanged through the internal walls since this depends on temperature difference which is thus zero. A.C.van der Linden et al. (2006) [97] specified the acceptable indoor temperature limits for buildings in the Netherlands. For winter, spring/autumn, summer and hot summer are respectively 20.6-23 °C, 21.1-23.8 °C, 22-25.2 and 22.6-27 °C. In the proposed model the designed indoor temperature is fixed at 23 °C during the whole year, for all locations which are considered. This is also considered for time points outside of the working hours to keep the indoor temperature constant.

3.8.1. Solar heat gains

To calculate the solar heat gain Q_{solar} of the office, the irradiance outputs from sections 3.6 are required. In some models where the solar heat gain is calculated, the total irradiance on the window and the SHGC of the window are used and the solar heat gain is calculated here as

$$Q_{solar} = A_{window} G_{tot} SHGC. \tag{3.39}$$

A_{window} is the area of the window in m^2, G_{tot} is the total irradiance on the window surface in W/m^2 and the SHGC is the solar heat gain coefficient which is a number between 0 and 1. In another solar heat gain calculation proposed by [36], equation (3.39) is changed by splitting the total solar heat gain into the direct, diffuse and ground solar heat gain components and this method is adapted in this model because the same method is used to calculate the illuminance which is transmitted through the window. To determine the solar heat gain which is transmitted through the window, a solar transmittance τ is used instead of the SHGC, because the heat absorbed in the glass layers which is incorporated in the SHGC is not considered here. The solar heat gain is thus calculated according to

$$Q_{solar} = A_{window}(G_{dir}\tau_{dir} + G_{diff}\tau_{diff} + G_{ground}\tau_{ground}). \tag{3.40}$$

Researchers from the Lawrence Berkeley National Laboratory [5] presented a method to use the U-value, VT and SHGC to calculate τ from the SHGC. For U-values higher than 4.5 $\frac{W}{m^2K}$ which is the case for single glazed windows, τ is equal to

$$\tau = 0.939998SHGC^2 + 0.20332SHGC, \tag{3.41}$$

if the SHGC is lower than 0.7206 and equal to

$$\tau = 1.30415SHGC - 0.30515 \tag{3.42}$$

if the SHGC is higher than or equal to 0.7206. For U-values lower than 3.4 $\frac{W}{m^2K}$ which is the case for multiple pane windows, τ is equal to

$$\tau = 0.41040SHGC, \tag{3.43}$$

if the SHGC is lower than or equal to 0.15 and τ is equal to

$$\tau = 0.085775SHGC^2 + 0.963954SHGC - 0.084958. \tag{3.44}$$

In the presented model, the U-value of all considered window technologies is lower than 3.4 $\frac{W}{m^2K}$, but if window technologies with U-values between 3.4 and 4.5 $\frac{W}{m^2K}$ would be considered then linear interpolation between the results for single glazed and for the multiple glazing would be necessary. The solar transmittance values τ_{dir}, τ_{diff} and τ_{ground} which are used in equation (3.40) are calculated in the same way as done for VT_{dir}, VT_{diff} and VT_{gr} as discussed in section 3.7, but now VT is substituted by τ and the illuminance components are substituted by the irradiance components.

3.8.2. Internal heat gains

The internal heat gains include heat from lighting, equipment and the persons in the room. The internal loads only have a contribution during the week and only during 8 AM and 6 PM, holidays are not considered. It is assumed that the average heat contribution for a person doing seated computer work in a room is 120 W at 23°C [90], which is the indoor temperature. The equipment accounts for 8 W heat per m^2 floor area during working hours according to [82]. Regarding the lighting consumption, two types of light sources can be selected in the model. The first one is defined as $P_{l,constant}$ and here the lighting source has a constant power of 10.1 W per floor area which is also considered in the reference office [82]. The constant lighting power in the reference office is thus approximately 298 W when turned on. The other light source which can be selected depends on the illuminance and this is related to the luminous efficacy. This is defined as $l_{l,smart}$ and is equal to 172.1 lm/W [80] for commercially available LED light. This lighting source is considered in the model, because these are much more efficient and less heat emitting than traditional light bulbs as shown in table 3.7. It was found by [89] that a LED bulb only emits 0.08 W of heat per W electrical power.

Light source	Heat emission coefficient [W/W]	Luminous efficacy [lm/W]
LED bulb	0.08	172.1
Incandescent light bulb	0.95	12
Halogen bulb	0.82	16
Compact fluorescent lamp	0.31	56

Table 3.7: Heat emission coefficient and luminous efficacy of different light sources. Adapted from [89] using LED bulb luminous efficacy from [80].

The total internal heat gains in the room can be calculated using the constants given in table 3.2 according to

$$Q_{internal} = q_{light}P_{light} + q_{equip}A_{floor} + Q_{person}n_{person}, \tag{3.45}$$

where q_{light} is the heat emission in W per W power LED light and P_{light} in its ON state can be expressed according to either

$$P_{light} = P_{l,constant}A_{floor}, \tag{3.46}$$

for a constant light source or according to

$$P_{light} = A_{floor}(500 - L_{in})/l_{l,smart}, \tag{3.47}$$

for an adaptable/smart light source. Here L_{in} is the average indoor illuminance which is calculated in section 3.7. When using the equation (3.47), the lighting is controlled such that the indoor illuminance is 500 lux.

3.8.3. Infiltration gains and losses

The infiltration, conduction and ventilation heat gains and losses are calculated using simplified method described in [48]. The infiltration gains and losses depend on the difference between the outdoor or

ambient temperature T_{amb} and indoor temperature T_{in} and the infiltration rate of air through the exterior wall q_{infil} according to the equation

$$Q_{infil} = \rho C_{air} q_{infil} dT, \tag{3.48}$$

where

$$dT = T_{amb} - T_{in}. \tag{3.49}$$

The facade area is equal to the width of the room multiplied to the height of the room which are given in table 3.1. The infiltration rate is considered to be constant for every time point. The constants used in the infiltration heat transfer equation are given in table 3.2.

3.8.4. Ventilation gains and losses

The equations for ventilation are similar to those for infiltration, but the difference is that ventilation is used to supply fresh air to the room. The HVAC system is designed such that it refreshes the room during the working hours with an airflow which depends on the floor area and the number of persons in the office room during the working hours. It is assumed that the number of persons in the room is six during the working hours and zero otherwise. For simplicity it is also assumed that the occupants do not leave the room for lunch breaks. The heat gains and losses due to ventilation are calculated using

$$Q_{vent} = \rho C_{air} (q_{vent,pers} n_{persons} + q_{vent,floor} A_{floor}) dT. \tag{3.50}$$

Although buildings nowadays allow for heat recovery, this is not considered in the presented model.

3.8.5. Conductive heat gains and losses

The conductive heat transfer depends on the U-value of the exterior wall. In the simulation model it is assumed that the exterior wall consists of layers of brick, air, insulation and concrete with an overall U-value of 0.365 $\frac{W}{m^2 K}$. The U-value of some of the window technologies, which are discussed in chapter 2, is calculated according to

$$U = \frac{1}{R_{in} + R_{out} + \sum_1^i R_{layer,i}}, \tag{3.51}$$

where R_{in} and R_{out} are the interior and exterior surface thermal resistance respectively and $R_{layer,i}$ is the thermal resistance of layer i. For windows in the Netherlands, R_{in} and R_{out} are given by [50] to be 0.13 and 0.04 $\frac{m^2 K}{W}$ respectively. When calculating the U-value of a double glazed window, then $R_{layer,1}$ is the thermal resistance of the first glass pane, $R_{layer,2}$ is the thermal resistance of the cavity filling and $R_{layer,3}$ is the thermal resistance of the second glass pane. The thermal resistance of each layer can be calculated using the thermal conductivity k and thickness t of a material according to

$$R_{layer} = \frac{t}{k}. \tag{3.52}$$

The heat gains and losses due to conduction through the wall and window in the facade can be calculated using

$$Q_{cond} = U A_{surface,material} dT. \tag{3.53}$$

Here $A_{surface,material}$ is the surface area of the material through which heat is transferred such as the window or the exterior wall.

3.9. Energy generation

The amount of solar cells needed to power the active smart window depends on the consumption loads of the smart window, on the characteristics of the solar panels and on the solar irradiance available during the year. A string of PV cells is called a PV module and a string of PV modules is called a PV array. In this model the loads profiles of three smart window are calculated per hour for a full year. The consumption loads depend on the applied voltage and the current density of the time point and these are given in table 3.2. Because the Sun does not constantly provide electricity, a battery should be installed as well. The battery model and the argumentation on why it is needed are discussed in section 3.9.2. For the generation of energy, the usage of a maximum power point tracker (MPPT),

a charge controller and an inverter with their efficiencies are also considered and these components together with the batteries are called the balance of system. The MPPT makes sure that the PV cells function at their maximum power point and thus maximize their performance. The charge controller assures that the output voltage of the PV cells does not exceed the input voltage of the inverter which could damage the inverter. The inverter transforms the DC generated energy by the solar cells into AC power. For the power generation it is assumed that there is no shading, thus that no PV cells are blocked. The DC power output of the solar cells depends on the efficiency of the PV cells. The efficiency of the PV cells depends on the PV cell temperature and the PV cell temperature depends on the outdoor temperature and irradiance. In section 3.9.4 it will be explained how to simulate the PV cell temperature and section 3.9.5 will discuss how this affects the efficiency of a PV cell. In the model different sizes of rectangular PV cells are considered to power the smart window. This will affect the current and voltage which can be generated and thus also the amount of cells required and the total area of PV needed. This will be discussed in section 3.9.3.

3.9.1. Charge controller and inverter

When selecting the power components for the PV system such as the charge controller and inverter, it is important that the input and output voltage of all components match and currents are within the minimum and maximum allowed limits. For the solar powered PDLC window which was build by [75], an inverter [1] was selected which converts the DC voltage output of the charge controller into AC voltages from 35 V up to 75 V. The input voltage of this inverter is in the range of DC voltages between 10 V and 32 V and its nominal voltage is 12 V. It is assumed that this inverter can supply 5, 10, 15 and 20 V AC as well, because the states of the PDLC window for these applied voltages are considered in the model.

To power the SPD window, a different inverter is required which can supply 100 V AC as discussed in chapter 2. A solar powered SPD window was build by [38] and here an inverter was used with a nominal voltage of 12 V and an efficiency of 90%. These are the same nominal voltage and efficiency as for the inverter used by [75]. The nominal voltage implies that a charge controller with a DC output voltage of 12 V is suitable for both the PDLC and the SPD window. The charge controller which was used by [75] to power the PDLC window can supply this voltage and is therefore selected in this work. The output current of this charge controller is between 2 and 5 A, which is lower than the maximum allowed input current of the inverter of 16 A. The input voltage of the charge controller is the equal to the DC output voltage of the PV cells and the battery system. This should be between 8 and 28 V since these are the minimum and maximum voltage limits of the charge controller [8]. The minimum input current of the charge controller is 3 mA in order to function and the maximum current which is allowed to run through the wires is fixed at 10 A. This is because higher currents will give higher energy losses and at 16 A the wires will even melt. Currents up to 10 A are not expected for smart window applications. The rated efficiency of the charge controller as given in [8] is 93%.

Although its output DC voltage is between 5 V and 26 V, it is assumed that the charge controller does allow for 1 V and 3 V DC voltage outputs. These voltages are namely used in the model to switch the transparency of the EC window from its most transparent state to an opaque state or back. The maximum input voltage of the charge controller is 28 V and the maximum allowed current is 10 A. To make sure that these limits are not exceeded, the maximum battery capacity which is allowed in the PV system is equal to 280 Wh. Note here that if more than 280 W of power would be required to power the window, then the selected charge controller and inverter would not be suitable. With all these given requirements, it is possible to determine the minimal battery capacity and number of PV cells in series and in parallel which are required to power the smart window. The output power in AC of the inverter is equal to

$$P_{ac} = \eta_{inv} P_{dc}, \tag{3.54}$$

where η_{inv} is the efficiency of the inverter which is given to be 90% in [1].

3.9.2. Battery model

In order to power a PDLC or SPD smart window when it is cloudy and the availability of the Sun is low but when the window should still be transparent, it is proposed to add a battery to the system. This way the window functions autonomously and does not rely on power from the grid. For the EC window a battery system is also designed. The sizing of the battery depends on the mismatch between the

energy production and the energy consumption of the window. The energy production depends on the number of solar cells installed and on the weather conditions. The consumption of the smart window is determined using the illuminance L_{out} that reaches the window which is calculated in section 3.7. If the illuminance is between 500 and 2000 lux during a week day and during the working hours, the smart window will be in transparent mode. In the case of the PDLC or SPD window a load $P_{smartwindow}$ is required. For the EC window energy is consumed to switch between the transparent and opaque states, but here no constant load is required. Using the PV power generation model which will be discussed in sections 3.9.3, 3.9.4 and 3.9.5, the energy generation defined as P_{PV} can be determined and this depends on the number of PV cells in series.

The battery model is based on [13] and calculates the state of charge (SOC) for every data point throughout the year. The type of battery considered for the system is a lithium battery, because these are available in small sizes and are thus lightweight, recharging of lithium batteries is more quickly compared to other rechargeable battery types, and the energy density is higher than other rechargeable battery types. The bottom SOC limit of the battery is fixed at 10% while the top SOC limit is fixed at 95%. These limits are set because completely discharging the battery to 0% or charging to 100% would decrease the battery lifetime. To size the battery capacity, an iterative calculation is done using an initial number of PV cells connected in series and where in each step this number is increased. There are some requirements when sizing the battery capacity. One of them is

$$\sum_{t}^{8760} P_{in,t} \geqslant \sum_{t}^{8760} P_{smartwindow,t} SF, \tag{3.55}$$

where SF is a sizing factor here assumed to be 1.1 and $P_{in,t}$ is the input power of the smart window which is equal to $P_{DC,t}$ or $P_{AC,t}$ depending on the smart window load requirements. $P_{DC,t}$ is calculated according to

$$P_{DC,t} = P_{pv,t} \eta_{MPPT} \eta_{CC}, \tag{3.56}$$

were t is the hourly time step, η_{MPPT} is the efficiency of the MPPT tracker which is assumed to be 95%, η_{CC} is the efficiency of the charge controller which is given in the datasheet to be 93% and P_{DC} is the DC power output of the charge controller. $P_{AC,t}$ is calculated according equation 3.54 using $P_{DC,t}$. If the requirement of equation (3.55) is not met, the number of PV cells should be increased. If the first requirement is met, then for every time step the current, initial battery capacity and SOC is determined. The charging/discharging current for a single time step, when assuming a 100% charge/discharge efficiency, is calculated using

$$I_{batt} = \frac{P_{in} - P_{smartwindow}}{V_{nom}}, \tag{3.57}$$

where V_{nom} is the nominal voltage of 12 V. Then the initial battery capacity is determined using

$$E_{batt,t} = E_{batt,t-1} + P_{in} - P_{smartwindow} - R_{batt} I_{batt}^2 - D_{self} E_{batt,t-1}, \tag{3.58}$$

where $E_{batt,t}$ is the initial battery capacity of a time step, $E_{batt,t-1}$ is the initial battery capacity of the previous time step, R_{batt} is the resistance of the battery during either charging or recharging and D_{self} is the self-discharge factor. The SOC is calculated according to

$$SOC, t = 100\% \frac{E_{batt,t}}{E_{batt,tot}}, \tag{3.59}$$

where $E_{batt,tot}$ is the total battery capacity. To determine $E_{batt,1}$ which is the first time point, $E_{batt,0}$ is defined as 5.12 Wh which is equal to the capacity of four Li-ion batteries of 3.2 x 0.4 = 1.28 Wh. This is used because the nominal voltage is 12 V and at least four Li-ion batteries are required to reach this voltage. The self-discharge factor accounts for the yearly capacity lost due to self-discharging and is taken from [13]. Here it was given that 20% of the capacity was lost per year and this was divided over 8760 hourly time steps to estimate the hourly capacity loss which is equal to 0.0023%/hr. Note that this is a simplistic approximation of the self-discharge factor because in reality this depends heavily on the temperature. D_{self} plays a role for all data points except for the first time point. If at the end of the year or even before the battery capacity goes below the bottom limit, the battery capacity is not high enough. The capacity of a single Li-ion battery is then added and the calculation is repeated from the first data

point. If the required capacity exceeds 280 Wh, then the battery capacity is too high for the PV system due to the charge controller limits. This indicates that the number of PV cells should be increased or that a location and orientation are not suitable for an autonomously functioning smart window in this case.

3.9.3. Determining PV area and maximum PV power output

The first step of the PV energy generation model is to determine the total PV area A_{PV} and the power at maximum power point ($P_{mpp,stc}$) under standard test conditions (STC). The total active PV area is calculated using

$$A_{PV} = n_s n_p A_{PV,cell}, \tag{3.60}$$

Where n_s is the number of PV cells which are connected in series per string, n_p is the number of parallel strings and $A_{PV,cell}$ is the area of one PV cell with a with W_{PV} which is the width of the cell and L_{PV} which is the length of the cell. The power of a custom PV cell at maximum power point ($P_{mpp,stc}$) under STC can be derived from the open circuit voltage (V_{oc}), short circuit current (I_{sc}), voltage at maximum power point (V_{mpp}), current at maximum power point (I_{mpp}) and fill factor FF. The width and length of a standard cell is 15.675 cm x 15.675 cm and the corresponding I-V characteristics are given in the datasheet [21]. According to [87], the voltage is linearly dependent on the number of cells in a string which are connected in series and the current over all cells is equal to the current of the cell with the lowest current. When applying the model for the PV cell with custom sizes, it is assumed that all PV cells in the model have the exact same properties and that the current of a string of cells in series is equal to the current of a single cell. The I_{sc} of a custom PV cell is determined according to a relation given by [87] and verified by [60], namely

$$I_{sc} = I_{sc0} \frac{A_{PV,cell}}{A_{PV0}}, \tag{3.61}$$

where I_{sc0} is the short circuit current of the standard cell, $A_{PV,cell}$ is the area of the custom PV cell and A_{PV0} is the area of the standard PV cell from which $A_{PV,cell}$ was obtained. $A_{PV,cell}$ cannot be larger than A_{PV0}. The equation to determine I_{sc} of a custom PV cell was verified by cutting standard c-Si PV cells into different sizes using a laser cutter. The investigated PV cells were respectively a full cell (15.675 cm x 15.675 cm), half a cell, a quarter cell, and cells with areas of respectively 20 cm^2, 9 cm^2 and 5.2 cm^2. It was found that the V_{oc} of a single PV cell with different sizes was relatively similar to the V_{oc} of the original cell. The V_{oc} and V_{mpp} of a custom PV cell are therefore estimated to be equal to the V_{oc} and V_{mpp} values of a standard PV cell in this work. The fill factor is assumed to be a constant and is calculated using the properties of the standard PV cell under STC according to

$$FF = \frac{P_{mpp,stc0}}{I_{sc,stc0} V_{oc,stc0}}, \tag{3.62}$$

where

$$P_{mpp,stc0} = I_{mpp,stc0} V_{mpp,stc0}. \tag{3.63}$$

With FF, the $I_{mpp,stc}$ can be determined according to

$$I_{mpp,stc} = I_{sc,stc} FF \frac{V_{oc,stc}}{V_{mpp,stc}}. \tag{3.64}$$

Then finally using equation (3.63) with the $I_{mpp,stc}$ and $V_{mpp,stc}$ for the custom PV cell, the $P_{mpp,stc}$ can be determined. Note that $P_{mpp_{stc}}$ could have been done without calculating the $I_{mpp,stc}$ using only the FF, $V_{oc,stc}$ and $I_{sc,stc}$, but the variable $I_{mpp,stc}$ needs to be considered since it is the input current of the charge controller. If the input current of the charge controller is lower than 3 mA [8] then the charge controller cannot function. In the same research group, R. Weegink [100] measured the I-V curves and power conversion efficiency for unlaminated PV cells and laminated PV modules which he made by cutting standard c-Si PV cells into cells of 3.9 cm x 3.9 cm using the same laser cutter which was used by [60]. When applying the above mentioned equations to a single PV cell of 3.9 cm x 3.9 cm, the expected V_{oc}, I_{sc}, V_{mpp}, I_{mpp}, P_{mpp}, FF and efficiency values are close to the actual measured values as shown in table 3.8. From these measurements, it can be assumed that it is possible to cut standard c-Si PV cells to custom sizes using a laser cutter without decreasing the efficiency significantly.

	V_{oc} [V]	I_{sc} [A]	V_{mpp} [V]	I_{mpp} [A]	P_{mpp} [W]	FF [-]	η [%]
Calculated	0.66	0.57	0.56	0.56	0.31	0.80	20.6
Measured	0.66	0.59	0.54	0.55	0.30	0.77	19.5

Table 3.8: Calculated and measured solar cell properties by [100].

After lamination the efficiency of the PV modules was also measured to be around 19.5%. This was calculated for the active PV area and indicates that the lamination process does not significantly affect the efficiency. For the PV modules which are required to power a smart window in this work, it will thus be assumed that these are laminated and have an efficiency of 19.5%. An assumption made here is that the active area of the laminated module is equal to the total PV area.

3.9.4. PV cell temperature

In the second step of the energy generation model, the surface temperature of the PV cells is determined using the photovoltaic array performance model which is presented by [49]. The surface temperature is of the PV cells directly affects the electrical properties of a PV cell. The higher the surface temperature the lower the efficiency. The module surface temperature T_M is equal to

$$T_M = G_{tot} e^{(a+bW)} + T_{amb}, \tag{3.65}$$

where G_{tot} is the total irradiance on the surface as calculated in section 3.6, W is the wind speed in m/s and T_{amb} is the outdoor temperature in °C. The factors a and b are empirically-determined coefficients which have been determined for different types of modules as shown in table 3.9. The factor a represents the upper limit of the module temperature at low wind speeds under high solar irradiance and b represents the decrease of the module temperature when the wind speed increases. From the PV module surface temperature, the PV cell surface temperature T_C can be calculated using

$$T_C = T_M + \Delta T \frac{G_{tot}}{G_{stc}}, \tag{3.66}$$

where ΔT is the temperature difference between the module and the cell, and G_{stc} is the solar irradiance under STC G_{stc} which is equal to 1000 W/m^2. To determine the PV cell surface temperature for a PV module integrated in the window, the case of a "Glass/cell/glass" module in open rack is considered in this model.

Module	Type Mount	a	b	ΔT [°C]
Glass/cell/glass	Open Rack	-3.47	-0.0594	3
Glass/cell/glass	Close roof mount	-2.98	-0.471	1
Glass/cell/polymer sheet	Open Rack	-3.56	0.0750	3
Glass/cell/polymer sheet	Insulated Back	-2.81	-0.455	0
Polymer/thin-film/steel	Open Rack	-3.58	-0.113	3
22X Linear Concentrator	Tracker	-3.23	-0.130	13

Table 3.9: Empirically determined coefficients a and b [49].

3.9.5. PV cell efficiency

The PV power generation P_{pv} which is needed as an input for the battery model as presented in section 3.9.2, depends on the efficiency of the PV cells. The efficiency is affected by the PV cell temperature which is calculated in section 3.9.4 and by the solar irradiance on the facade which is calculated in section 3.6 [87]. The dependence of the efficiency on temperature is represented by the temperature coefficient. This is defined here as κ_{temp} and is found in datasheets or in literature for different PV technologies. The efficiency is also affected by the irradiance dependent $P_{mpp,G}$, which is the power output at maximum power point. To calculate $P_{mpp,G}$ for a single solar cell, an irradiance dependent $V_{oc,G}$ and $I_{sc,G}$ are calculated. When calculating these for a module the number of cells in series and in parallel should be considered. $V_{oc,G}$ is calculated using

$$V_{oc,G} = V_{oc,stc} + 0.0385 \ln\left(\frac{G_{tot}}{G_{stc}}\right), \tag{3.67}$$

where G_{tot} is the result of section 3.6. $I_{sc,G}$ is determined according to

$$I_{sc,G} = I_{sc,stc}\frac{G_{tot}}{G_{stc}}. \tag{3.68}$$

Using the FF for STC which is assumed to be a constant, the $P_{mpp,G}$ is determined according to

$$P_{mpp,G} = FFV_{oc,G}I_{sc,G}. \tag{3.69}$$

The irradiance dependent PV cell efficiency η_G is then calculated using

$$\eta_G = \frac{P_{mpp,G}}{G_{tot}A_{PV}}. \tag{3.70}$$

The final irradiance and temperature PV cell efficiency is then equal to

$$\eta_{PV} = \eta_G(1 + \kappa_{temp}(T_C - T_{stc})). \tag{3.71}$$

For most PV technologies κ_{temp} is negative thus a for higher cell temperatures, the efficiency η_{PV} will be lower than for lower cell temperatures under the same irradiance conditions. In this case the power output is thus lower at higher temperatures. An increasing irradiance will increase the voltage and current outputs of a PV cell for the same cell temperature.

3.9.6. PV window modelling

When calculating the energy performance of semitransparent PV windows, the energy generation yield of the window is considered when calculating the potential savings. In literature and in datasheets the electrical properties of semitransparent PV modules or PV cells are given and these are shown in table 2.4. When scaling the size of the PV module or PV cell to the window area, the V_{oc} and V_{mpp} of these modules or cells are assumed to remain constant while the I_{sc} is linearly dependent to the area of the window. No shading is considered in the energy yield calculation of the PV windows. The maximum input voltage limit of the charge controller is raised to 600 V. This is because the charge controller which is selected to power smart windows is designed for small systems and thus unsuitable for relatively high power outputs. The value of 600 V was found for commercially available c-Si power windows [88].

4

Concept design

In this chapter the concept design of a solar powered smart window is discussed. The properties of a PV cell with custom sizes is discussed and the method to find the optimal number of PV cells connected in series and in parallel and the corresponding battery capacity is explained.

4.1. Earlier designs

The design for the smart window is based on earlier work done within the Photovoltaic Modules and Devices (PVMD) research group of Delft. [75] made self-adhesive PDLC windows and integrated different PV cells in the glass or added to the glass and with different shapes and different backsheets for aesthetic analysis. These backsheets were either white or black. The reason why self-adhesive PDLC was used, was due to incompatibility of EVA with non-adhesive PDLC. The EVA which was available in the laboratory in Delft namely needed a higher temperature in the lamination process than PDLC. The actual build prototype is shown in figure 2.17 in chapter 2. Although in this project no actual smart window was built, a concept design is proposed. The smart window is a double glazed window with argon gas as cavity fill. In the outside facing glass, c-Si PV cells are laminated on the bottom of the window and a black backsheet is considered. The inside facing glass consists of laminated smart window technology. The PV technology which is considered is non-transparent monocrystalline silicon, because this technology currently has the highest efficiency among the commercially available PV technologies [11]. [100] created PV modules using cells of 3.9 cm by 3.9 cm which were cut from standard c-Si solar cells of 15.6 cm by 15.6 cm using a laser cutter. From a single standard solar cell which were used, 12 identical mini solar cells could be cut which have a front and rear contact centered in the middle. After laminating the PV module power conversion efficiency was measured to be 19.5% which is higher than the module efficiency of 15% found in semitransparent c-Si as discussed in section 2.3. The dimensions of the PV cells which were used by [100] are also used in the simulation model, because the smart windows require small currents to switch transparency which means that the area of single PV cells can be decreased. The V_{oc} and I_{sc} of the custom sized cell can be calculated using the equations from the section 3.9.3 and these are calculated to be 0.66 V and the 0.57 A respectively. In order to provide enough electricity to power the smart window, a number of PV cells should be connected in series and number of PV strings should be connected in parallel.

4.2. Properties of PV cell

The PV cells which are used to make the PV module is based on c-Si and its corresponding V_{oc}, V_{mpp}, I_{sc} and I_{mpp} are given in the table 3.8. Here the calculated values are considered. The output voltage of the PV cells should match the rated voltage of the battery system which is set at 12 V. As discussed in section 3.9.3 when changing the sizes of a PV cell in a tailored made design the output voltage per PV cell will not vary significantly from the voltage of PV cell with standard sizes. However the short circuit current is proportional to the area of the PV cell and will thus be smaller for cells smaller than the standard sizes. The fill factor is assumed to be constant.

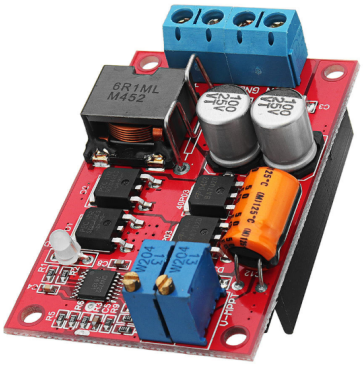

(a) Charge controller from [8]

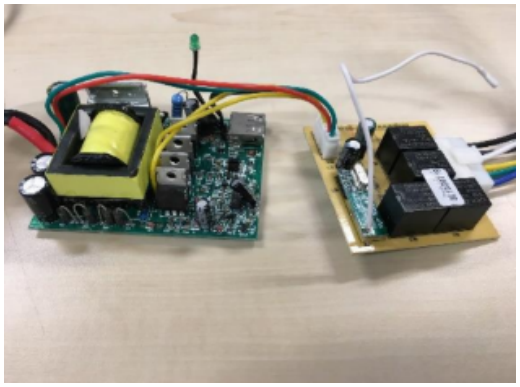

(b) Inverter from [1]

Figure 4.1: PV components.

4.3. Design PV system based on lowest costs

The PV system which powers the smart window consists of PV cells which form a PV module, a battery, a charge controller, and inverter in the case of a PDLC or SPD window. The PV cells produce DC power which needs to be converted to AC using an inverter for a smart window which requires AC input. In the case when an EC window is used, then a DC load input is required. The inverter which is chosen has a rated DC voltage of 12 V which means that the input voltage should be constantly 12 V. Because the PV cells have no constant voltage output, a charge controller is required to keep the input voltage of the inverter at 12 V and to prevent damage because of voltage fluctuations. When the energy production is low while the window should be transparent, energy should be supplied from the battery system. The battery system is composed of rechargeable Li-ion batteries with each 3.2 V and 0.4 Ah capacity. To reach a rated voltage of 12 V, at least 4 batteries should be connected in parallel. Depending on the sizes of a single PV cell, the current changes proportional to the area. The maximum number of parallel PV array strings thus depends the current through a single PV cell and on the maximal input current of the charge controller which is set to 10 A. This is because for higher currents the resistance becomes more significant and the wires heat up and can eventually be burned which decreases the lifespan and would increase maintenance work. The minimal and maximal number of PV cells which are connected in series depend on the minimal and maximal DC voltage input of the charge controller. As mentioned in section 3.9.1 the input voltage limits are between 8 and 28 V.

Inputs for the model are the number of PV cells which are connected in series n_s and the number of PV array strings which are connected in parallel (n_p). No initial guess needs to be filled in if the charge controller properties are described in the model. The model namely calculates the battery capacity for every n_s and n_p for which the voltage and current limits of the charge controller are not exceeded. The minimal and maximum number of PV cells in series are calculated according to

$$n_{s,min} = ceil(\frac{V_{cc,min}}{V_{oc,stc0}}), \tag{4.1}$$

and

$$n_{s,max} = floor(\frac{V_{cc,max}}{V_{oc,stc0}}). \tag{4.2}$$

In these equations the term ”ceil” is used to round the ratio to the nearest integer larger than or equal to the ratio and ”floor” is used to round the ratio to the nearest integer less than or equal to the ratio. For example if the ratio $\frac{V_{cc,max}}{V_{oc,stc0}}$ would be equal to 5.2, then because of ”floor” this becomes 5. If the ratio $\frac{V_{cc,min}}{V_{oc,stc0}}$ would be equal to 5.2, then it becomes 6 because of ”ceil”. These terms are used because if the number of PV cells in series n_s is lower than $n_{s,min}$, then the minimal voltage input of the charge controller cannot be met and if n_s is higher than $n_{s,max}$ then the upper voltage limit for the charge controller is exceeded. The same principle is applied for the number of PV strings n_p based on the minimum and maximum currents for the charge controllers. For each n_s and n_p for which the charge controller limits are met the battery capacity is calculated. Then for each n_s and n_p the total system

costs are calculated which includes the costs for low iron toughened glass (6 mm), busbars, PV cells or modules, batteries, labor costs, charge controller and inverter (only in case of AC based load). The total costs for PV area, glass area, busbars, batteries are the variables. It is estimated that any tailor made PV system requires three full work days of 8 hours for completion, which is equal to a total of 24 hours. An overview of the costs of a custom made PV design excluding the smart window itself is given in table 4.1. Here the costs per inverter was given to be €150.41 by [1] after converting from US dollar to Euros using an exchange rate between the US dollar and Euro of 0.89. The costs per charge controller were found in [8] to be €9.04 after converting from US dollar. The costs of glass was calculated to be €128.76 per PV area [95], after converting from GBP using an exchange rate between GBP and Euro of 1.11 and after multiplying by 2. The factor 2 is because two glass layers are required in the lamination process. To connect PV cells to produce a PV module, busbars are soldered on the front and rear sides of each PV cell. The costs of busbars were estimated using the properties of soldering tin for which a density of 8885 kg/m^3 given by [91] and costs of €4.29 per 100 g were found in [4]. The volume of soldering tin required per standard PV cell was estimated by considering wire with a diameter of 0.6 mm and assuming that 1 m of soldering tin is required for one single standard PV cell. The cross section area of the wire is then calculated to be $\frac{1}{4}\pi(0.6)^2 = 0.28mm^2$. The amount of soldering tin required per PV area is then calculated using $8885 * 42.9 * 1 * 0.28e-6 = €4.39$.. The hourly salary of a PV module producer is assumed to be €13. The tailor made PV cells are cut from standard c-Si PV cells of 15.675 cm by 15.675 cm which are estimated to be €0.10 per piece. In the model the sizes of a custom PV cell can be made smaller and in this case the number of PV cells which can be cut from a single PV cell with standard sizes is defined as $n_{custom,standard}$ and is calculated according to

$$n_{custom,standard} = floor(A_{PV,standard}/A_{PV,custom}). \tag{4.3}$$

Here $A_{PV,standard}$ is the area of the standard PV cell and $A_{PV,custom}$ is the area of the custom PV cell. The costs of the PV cells C_{PV} is calculated according to

$$C_{PV} = C_{PV0}A_{PV,standard}ceil(\frac{n_{custom,total}}{n_{custom,standard}}), \tag{4.4}$$

where C_{PV0} is the costs per standard PV cell and $n_{custom,total}$ is the total number of custom PV cells required to fill the total PV area. This is calculated according to

$$n_{custom,total} = ceil(\frac{A_{PV,tot}}{A_{PV_{custom}}}). \tag{4.5}$$

$A_{PV,tot}$ is the total PV area which depends on n_s and n_p. The costs for the batteries are taken from [26] where the costs are given for small batteries with a voltage of 3.2 V and capacity of 0.4 Ah. These costs are €2.73/Wh which are relatively higher than for Li-ion based battery systems which are on the market and used in residential PV systems. In [13] it was found that the costs per battery capacity could be as low as €1.13/Wh, however in this case the battery capacity was 1638 Wh.

Type of costs	Cost
PV cell [€/piece]	0.10
Batteries [€/Wh]	2.73
Inverter [€/piece]	150.41
Charge controller [€/piece]	9.04
Glass [$€/m2$ PV area]	128.76
Busbars [$€/m2$ PV area]	4.39
Labor [€]	312

Table 4.1: Costs of PV system components.

5 Simulation results

This chapter discusses the validation of the simulation model and the simulated energy performance of buildings when considering different types of window technologies.

5.1. Overview used models

The equations used in the model which is presented in this report are based on equations used in different simulation models and books. To determine the solar position with respect to the surface the equations presented in the book by A. Smets et al (2016) [87]. Also the calculations for the direct and ground irradiance components are based on this book. The diffuse irradiance component is derived from the Perez model [79]. In a model presented by Waide and Norton [98] a different method of calculating the diffuse irradiance component is used which is based on the Hay-Davies model [44]. This method is adopted instead of the Perez model for high latitude locations, because in the article it is claimed that for high latitude locations this model has been found to be more accurate in predicting the irradiance compared to the Perez model [98]. Because high latitude locations have not been explicitly defined in literature, these are defined here for latitudes higher than 40° north or south. For illuminance reaching the window the same approach as for the irradiance is used based on the equations presented by [87] and [79] but now using the direct normal illuminance instead of the direct normal irradiance, and the diffuse and global horizontal illuminance instead of the diffuse and global irradiance. This is used instead of the ray-tracing method which simulation tools such as DIVA and Radiance use and which is also used in the case for the reference office room [82]. The method used to calculate the visible light and solar heat transmittance factors through a window is based on equations presented by EnergyPlus [68]. Here at first a solar transmittance factor is derived from the SHGC at normal incidence. Next the solar and visible light transmittance factors are determined as a function of the AOI using fitting parameters which correspond to types of windows depending on the SHGC and U-value. Using these angle dependent VT and SHGC factors the solar heat gain and indoor illuminance can be calculated using the method presented in [36]. To determine the HVAC requirements for heating and cooling, the infiltration, ventilation and conduction through the exterior wall are calculated using simplified equations presented by [48].

The internal heat gains depend on the equipment loads, occupancy and lighting consumption. The PV energy generation calculations are based on methods presented by [87] and [52]. The calculations for the battery system design are adapted from [13].

5.2. Validation model

To validate the proposed model, the calculated solar position and irradiance and the heat transfer through the facade are compared to a model which is made in Grasshopper in Rhino with EnergyPlus, Honeybee and Ladybug plug-ins. This is done for offices located in respectively Amsterdam, Bogota and Hong Kong with four orientations of the facade. Grasshopper is one of the many simulation tools which is available for architects to design buildings. The irradiance and solar position are validated using Grasshopper and simulation tools from Sandia National Laboratories [52] and System Advisor Model (SAM) [69] which is developed by the National Renewable Energy Laboratory in collaboration

with Sandia National Laboratories. The plug-in EnergyPlus which is available in Grasshopper is used for validation of heat transfer related simulations. There are some differences between the reference office room based on [82] and the office room used in Grasshopper model. The first difference is that in the validation model in Grasshopper the conduction heat transfer through the exterior wall is not equal to 0.365 $\frac{W}{m2K}$ but is calculated to be 0.215305 $\frac{W}{m2K}$. Also in Grasshopper it is assumed that the internal heat gains from lighting are equal to the lighting consumption and that the lights are always on during working hours. Besides the dimensions of the validation model in Grasshopper are 9 m x 9 m x 2.8 m instead of 3.6 m x 8.2 m x 2.8 m. At last the Hay-Davies model for diffuse irradiance calculations of high latitude locations is not considered in the validation model. The presented model is adjusted for these changes to compare the outputs of Grasshopper to the presented model.

5.2.1. Validation angle of incidence

The solar position is expressed by the azimuth A_s and altitude a_s angles and with these the angle of incidence (AOI) of direct sunlight on a window is calculated using equation (3.16). The AOI outputs of the presented model are compared to Sandia, Grasshopper and SAM for Amsterdam, Bogota and Hong Kong. Because it is based on the equations used in Sandia, it is expected that the AOI outputs of Sandia and the presented model are the same. The AOI for Amsterdam with a facade facing north is plotted in figure 5.1b for 8760 time points.

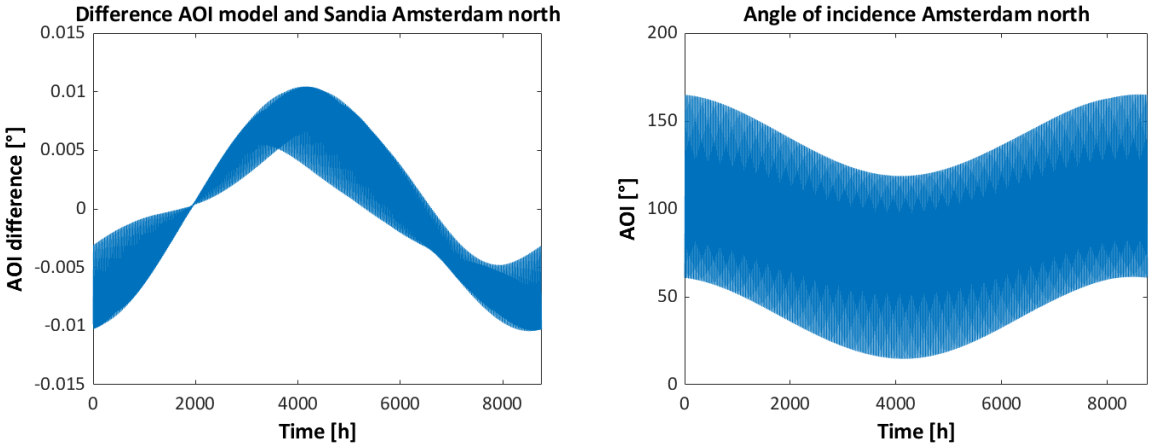

(a) AOI output of presented model minus Sandia output values.

(b) The angle of incidence as calculated by presented model.

Figure 5.1: Angle of incidence for north facing facade in Amsterdam.

The differences between the AOI calculated in the model and in Sandia are shown in figure 5.1a when considering the same year. The differences are determined by subtracting the output values of the Sandia model from those of the presented model and are found to be in the order of 0.01° while the values itself are between 15 and 165°. This indicates that the solar position calculations are almost perfectly adopted.

In figures 5.2a and 5.2b and the differences between the model AOI outputs with respect to the SAM model outputs are plotted. It can be observed in figure 5.2a that there are differences between the outputs of the model and SAM because in SAM the AOI is set to zero before sunrise and after sunset [69]. When setting the output values of the presented model to zero where the output values of SAM are zero and subtracting the output values of SAM from these of the presented model, the result is plotted in figure 5.2b.

According to the reference document of SAM [69], SAM uses a ”typical meteorological year” which is given in the weather file to calculate the solar position while in the presented model this is calculated for the year 2017. The difference here is that in SAM the weather data for days and hours in January can for example correspond to the year 1995 while the weather data for February can correspond to the year 2003. This can give a difference between the AOI calculated in the presented model and found using SAM for the same time point. In the reference document of SAM the method to calculate the solar position is also found to be different from the method used in the Sandia model. These differences are shown in figure 5.3 where the output values of SAM are subtracted from the output values of Sandia.

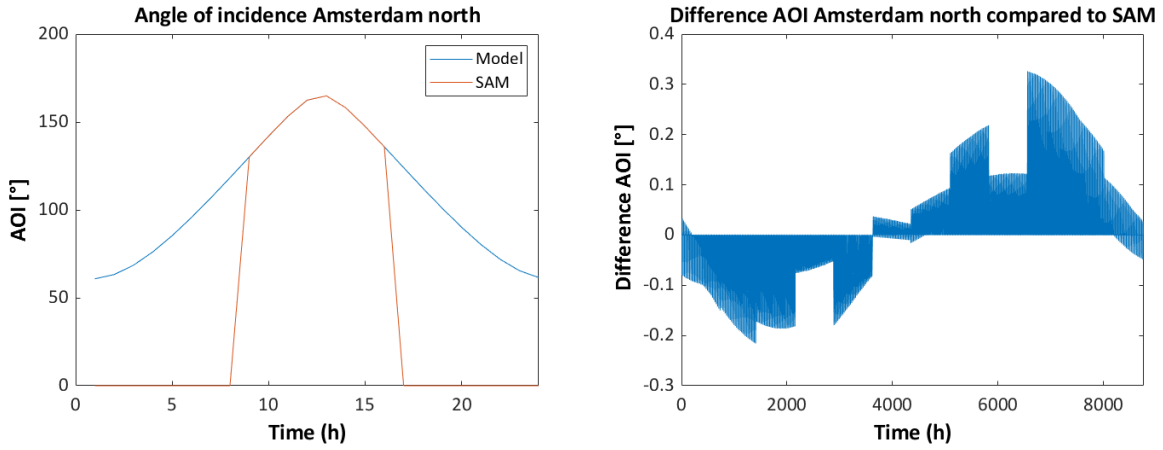

(a) The AOI of presented model and SAM plotted for one day.

(b) The differences in AOI between presented model and SAM.

Figure 5.2: Comparison angle of incidence between model and SAM for a north facing facade in Amsterdam.

Here the same year from the .epw weather file is taken in both models. The differences between the Sandia model and SAM model to calculate the solar position are not significant.

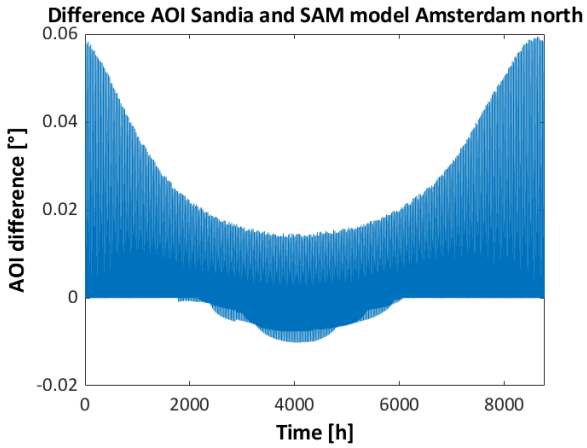

Figure 5.3: Difference between Sandia model and SAM model for facade facing north in Amsterdam.

The AOI outputs of Grasshopper are not directly available and are therefore calculated from the direct irradiance output of Grasshopper by reversing equation (3.15) to get

$$AOI = \arccos(\frac{G_{dir}}{DNI}). \tag{5.1}$$

To avoid dividing by zero only DNI values larger than zero are considered thus the AOI is set to zero for time points where the DNI is zero. The AOI output of Grasshopper is shown in figure 5.4b where it is indicated in orange while the AOI output of Matlab is indicated in blue. It can be observed that these are not similar. In figure 5.4a the AOI of the presented model is plotted which is now calculated using equation (5.1), the same DNI values but with the G_{dir} output calculated in Matlab. Here it can be observed that the trends are similar but that there are differences and this indicates that the solar position is calculated differently in Grasshopper. In [68] the method to calculate the solar position is given and this is calculated for a typical year where the solar position depends on the hour of a year and is independent of the actual considered year. A fractional year γ which depends on the day of the year (DOY) is calculated according to

$$\gamma = \frac{2\pi}{366}(DOY), \tag{5.2}$$

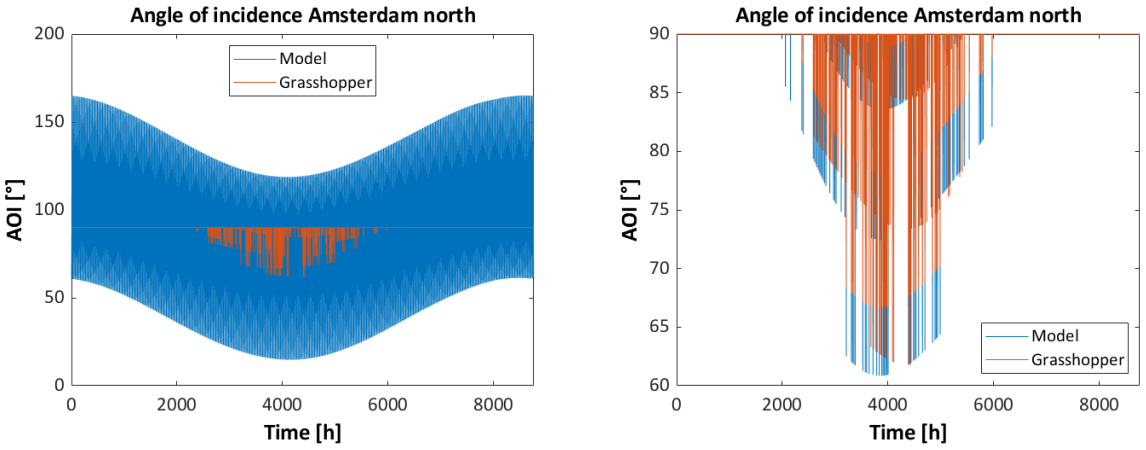

(a) AOI is plotted for Grasshopper outputs calculated from direct irradiance and AOI output from presented model.

(b) AOI is plotted for Grasshopper and model outputs when both are calculated from direct irradiance.

Figure 5.4: Angle of incidence plotted for presented model and Grasshopper for a north facing facade in Amsterdam.

and an apparent solar time H is calculated according to

$$H = (15(12 - (TimeValue + EquationOfTime)) + (TimeZoneMeridian - Longitude)). \quad (5.3)$$

Here $TimeValue$ is the hourly time value γ when considering DOY as 8760 time points, $TimeZoneMeridian$ is the timezone of the location and $EquationOfTime$ gives the difference between the apparent solar time and the mean solar time. This can be expressed as

$$EquationOfTime = [q(D) - \alpha_s(D)]\frac{1}{15}\frac{hour}{deg}, \quad (5.4)$$

where q is the mean longitude of the Sun as calculated in equation (3.4), D is the number of days as calculated in (3.3) and α_s is a so-called right ascension term which is related to the ecliptic longitude of the Sun λ_s, calculated in equation (3.6) and the axial tilt e calculated in equation (3.7) according to

$$\alpha_s = \cos e \tan \lambda_s. \quad (5.5)$$

Using the AOI, the solar irradiance and solar illuminance on the window can be calculated. In the next section the irradiance outputs of the presented model which are based on Sandia are compared to the outputs of Grasshopper and SAM. The direct and ground irradiance are calculated using the straightforward equations (3.15) and (3.17). The diffuse irradiance is calculated using the Perez model and this method is also available in the Grasshopper and SAM. The ground irradiance is not validated using the simulation models, because in Grasshopper this component appeared to not be considered in the total irradiance calculation and in SAM the same straightforward equation was used where the GHI is the variable which is taken from the same weather data file used in the presented model.

5.2.2. Validation direct irradiance

The difference between the direct irradiance outputs of the presented model and Sandia are represented in figure 5.5a, where the outputs of the Sandia model are subtracted from the outputs of the presented model. In this graph it can be observed that there are no significant differences, since the irradiance difference is lower than 0.06 W/m^2 while the irradiance itself is in the order of up to 90 W/m^2 for Amsterdam with a facade facing north. Similar differences are found for different orientations and for Bogota and Hong Kong and these plots are therefore not shown here. The differences compared to SAM are also small because the differences in the AOI outputs were determined to be small in the previous section. These differences are not plotted as well.

To compare the direct irradiance output of the model to Grasshopper, the direct irradiance outputs from Grasshopper, but also the direct irradiance outputs calculated using the a_s and A_s outputs from Grasshopper are considered. The direct irradiance here is calculated using equations (3.15) and (3.16).

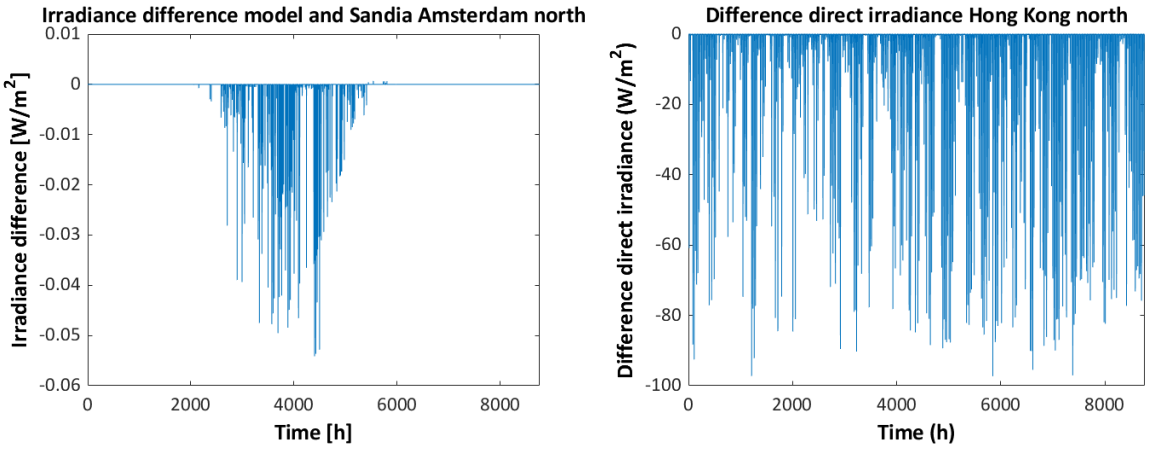

(a) Output values presented model minus the output values of Sandia model for a north facing facade in Amsterdam.

(b) Output values of presented model minus the output values of Grasshopper model for a west facing facade in Hong Kong.

Figure 5.5: Difference in direct irradiance compared to Sandia and Grasshopper.

When comparing the direct irradiance of the model to the direct irradiance calculated using the solar position outputs from Grasshopper, it can be found that these are very similar except for some rare offset peaks with a maximum deviation of 4 W/m^2. However when comparing the direct irradiance output of the model to the direct irradiance output of Grasshopper, the highest differences can be up to 100 W/m^2 as shown in figure 5.5b for Hong Kong with a facade facing west. From this it can be concluded that the direct irradiance output of Grasshopper is different from the direct irradiance which is calculated using the solar position outputs of Grasshopper. This also implies that the AOI which is used in Grasshopper is significantly different than the one calculated in the presented model. The equation to determine the direct irradiance is namely straightforward. The difference in the AOI has a significant impact on energy calculations.

5.2.3. Validation diffuse irradiance

Regarding the diffuse irradiance the method of the presented model is also used by Sandia. As shown in figure 5.6a the graphs for the presented model and Sandia overlap which indicate that the method is adopted correctly.

When comparing the diffuse irradiance to SAM and Grasshopper, it is found that SAM and Grasshopper predict a higher diffuse irradiance than the presented model and Sandia. To determine the origins of these differences, the equations given in the reference document are compared. It is found that in SAM the diffuse irradiance is equal to the isotropic diffuse irradiance component only for zenith angles between 87.5° and 90° while in the presented model and Sandia model the circumsolar and horizontal brightening components are also contributing. Besides SAM uses a different equation to calculate the air mass compared to the presented model. While in the presented model equation (3.19) is used, in SAM the equation

$$AM = \frac{1}{\cos(b) + 0.15(93.9 - \theta_z)^{-1.253}}, \tag{5.6}$$

with

$$b = max(\cos(85), \cos(\theta_z)). \tag{5.7}$$

The simulation tools from Sandia allow for both equations (5.6) and (3.19) to be used to calculate the diffuse irradiance and the differences are shown in figure 5.6b. Here the diffuse irradiance calculated using the AM calculated according to equation (3.19) and from this is subtracted the diffuse irradiance calculated when using equation (5.6). In the figure it can be observed that using a different method to calculate can change the outcome by up to 10 W/m^2. However when comparing the outcomes of the diffuse irradiance when using equation (5.6) to the outputs of SAM, these are still different from SAM. In all cases it appears that SAM overestimates the diffuse irradiance compared to Sandia.

Between the presented model and the Sandia model there is a small difference as well. When using equation (3.19) to calculate AM in both models, the outcomes are slightly different. This difference is

because in Sandia only zenith angles between 0° and 90° are considered to calculate the relative air mass. All angles above 90° are considered as "not-a-number" (NaN) while in the proposed model these zenith angles are considered for further calculations. In both diffuse irradiance calculations based on the Perez model zenith angles larger than 90° are considered. For these time points where the zenith angles are larger than 90°, if the DHI value for that time point is larger than zero the AM is defined as 37 which corresponds to the zenith angle of 90°. In the model of Sandia however the AM for zenith angles above 90° are defined as NaN thus has no contribution in equations (3.20), (3.21) and (3.22). This thus explains the differences in the diffuse irradiance between the presented model and Sandia which are based on the same Perez model.

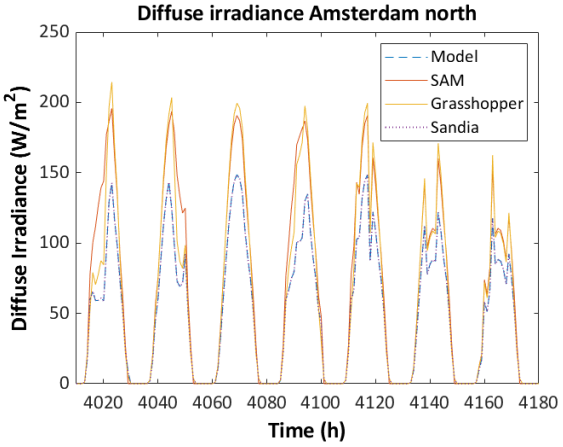

(a) Diffuse irradiance outputs for different models for a north facing facade in Amsterdam during a week period.

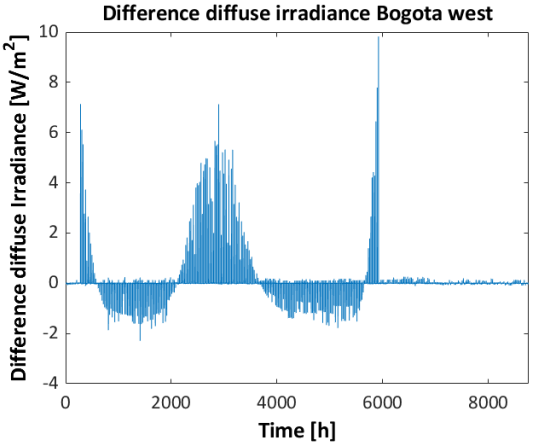

(b) Difference in diffuse irradiance calculated using Sandia for different air mass equations for facade facing west in Bogota.

Figure 5.6: Diffuse irradiance outputs plotted for different models and for Sandia model when using different air mass.

Regarding the diffuse irradiance output of Grasshopper, differences are found in the outputs compared to the model outputs. However the method to calculate the diffuse irradiance using the Perez diffuse sky model is similar to the method presented in this work. It appears that the outputs are close to the outputs of the SAM model. It is therefore likely that the differences are due to the different methods to calculate the solar position since the AOI affects the diffuse irradiance calculation.

5.2.4. Validation HVAC loads

The HVAC loads part of the presented model is validated using the EnergyPlus plug-in in Grasshopper. When comparing these outputs to the validation model, the validation model will be referred to as "EnergyPlus" instead of "Grasshopper". The internal heat gains of a building are due to electrical devices or equipment, human heat radiation and lighting. Besides there are heat gains and losses due to infiltration and conduction heat transfer through the facade, ventilation heat transfer and solar heat gains which are considered in HVAC load calculation or energy balance. EnergyPlus has multiple outputs regarding heating and cooling, namely latent, sensible, total and supply air. When comparing the results of the model in Matlab to EnergyPlus, the supply air component is the most relevant component because this represents how much energy is added to or removed from the room which is what is calculated using the energy balance. In the next sections the heat transfer components are discussed.

Validation internal heat gains

As mentioned in section 3.2, the year 2017 is considered in the presented model to validate the outputs and this is because in Grasshopper/EnergyPlus a typical year is represented. Here the first day of the year always falls on a Sunday by default which means that the workday starts 24 hours later. If for example 1 January 2020 at 12 AM would be considered as first time point, then this would be a Wednesday and this would change the schedule for the internal heat gains and thus the yearly energy consumption. While in the presented model the lighting requirements can be controlled, in the validation model it is considered to be always on during working hours independent of the illuminance level. The internal heat gains are due to equipment, lighting and occupants in the room and in figure 5.7 the total internal heat gain is shown for a week starting on Sunday. This schedule is repeated for every week of

the year and is exactly the same for both the presented model and EnergyPlus. This is the case for all considered locations and orientations.

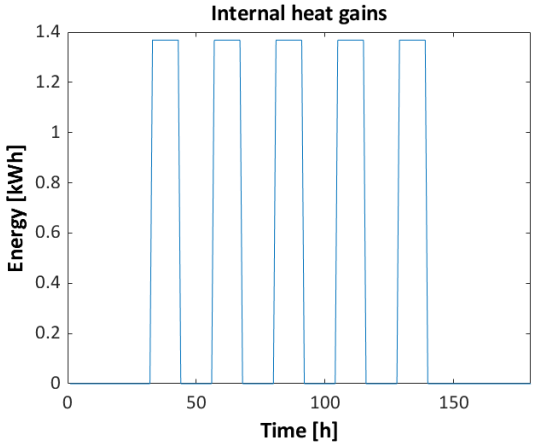

Figure 5.7: The hourly internal heat gains given during a week starting on Sunday.

Validation infiltration heat gains and losses

The infiltration outputs of the model in Matlab and in EnergyPlus are shown in figures 5.8a and 5.8b for Amsterdam and Hong Kong with a facade facing north respectively. It can be observed that the trends are similar in both cases but that there are differences between the peaks. It appears that the heat gains and losses as calculated in Matlab are underestimating in both cases. A measure to determine the average difference is by using the normalized root mean square error (NRMSE) method. For this first the root mean square error (RMSE) is determined according to

$$RMSE = \sqrt{\frac{\sum_{i=1}^{n}(x_i^m - x_i^s)^2}{n}}, \tag{5.8}$$

where i is each time point, x_i^m and x_i^s are the simulated output values of the model in Matlab and EnergyPlus at time points i respectively and n is the number of time points. For example when considering a full year divided in hours, then n is 8760. The NRMSE is calculated using

$$NRMSE = \frac{RMSE}{max(x_i^m) - min(x_i^m)} 100\%. \tag{5.9}$$

The RMSE and NRMSE for infiltration is determined for three locations (Amsterdam, Bogota and Hong Kong) and for four orientations (north, east, south and west). The results are given in table 5.1 together with the results for conduction, ventilation and solar heat gain which will be discussed later in this chapter. For Amsterdam and Bogota the maximum NRMSE regarding the infiltration heat transfer is 11% and 9.3% respectively, however for Hong Kong this is 34.9%. The differences are likely because the density and specific heat capacity of air are considered for dry air at 20 °C and 1 atmospheric pressure in the presented work. In EnergyPlus the air density depends on the average temperature of the indoor and outdoor space. Besides it depends on the air humidity which also affects the specific heat capacity of the air. Water vapor namely has a higher specific heat capacity than air [94]. In section 3.4 it was mentioned that the climate in Hong Kong is humid during the summer and this could explain why the differences between the presented model and EnergyPlus are higher during the summer.

Validation ventilation heat gains and losses

In figures 5.9a and 5.9b the heat gains and losses are shown for Amsterdam and Hong Kong with a facade facing north respectively. In both figures the ventilation heat gains and losses determined in the model follow the same trend as the EnergyPlus outputs but appear to be underestimated compared to the validation model. In table 5.1 the NRMSE is given for ventilation. For Amsterdam and Bogota the maximum NRMSE is 5.5% and 9.1% respectively, while for Hong Kong this is 22.5%. The differences are similar to the differences between the infiltration heat transfer outputs.

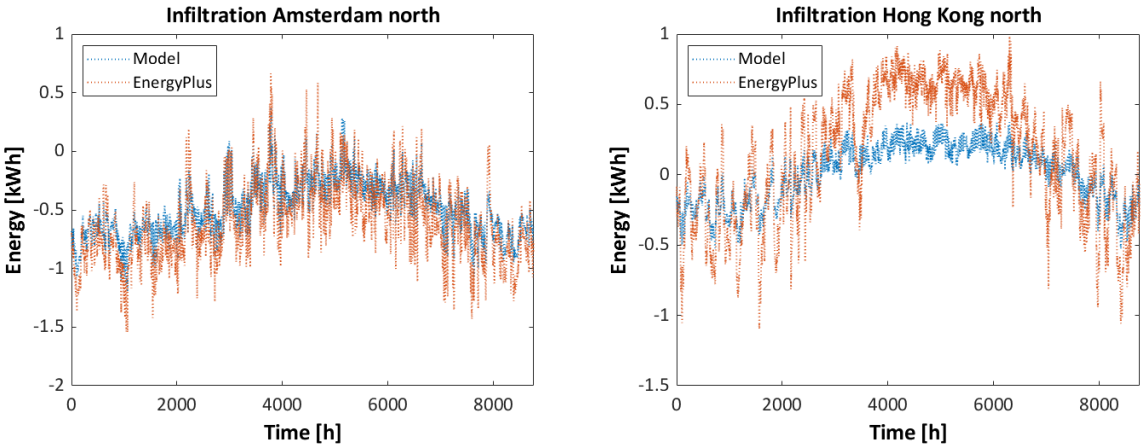

(a) North facing facade in Amsterdam.

(b) North facing facade in Hong Kong.

Figure 5.8: The hourly infiltration heat gains and losses.

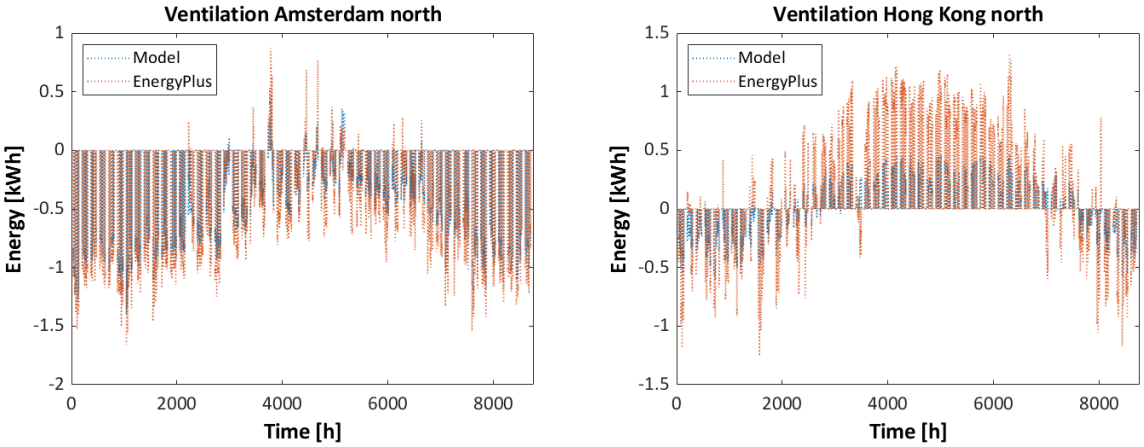

(a) North facing facade in Amsterdam.

(b) North facing facade in Hong Kong.

Figure 5.9: The hourly ventilation heat gains and losses.

Validation solar heat gains

In order to determine the potential HVAC savings of different window technologies, the solar heat gain is one of the most important factors to consider, because the infiltration, ventilation, and conduction heat transfer through the wall are considered to be the same independent of the type of window technology used. In figures 5.10a and 5.10b the hourly solar heat gain throughout the year is compared for the model in Matlab and in EnergyPlus. The figure indicates that the shape of the graphs is very similar and this is the case for all investigated locations and facade orientations. Table 5.1 has summarized the RMSE and NRMSE values for the different scenarios. The largest NRMSE values for Amsterdam, Bogota and Hong Kong are respectively 3.9%, 5.8% and 3.8% which indicate that the differences between the solar heat gain calculation are small. The solar heat gain was also calculated using the Grasshopper irradiance outputs, but when determining the NRMSE in this case, this would be higher for all locations and orientations. This indicates that the method to calculate the solar heat gain in EnergyPlus is slightly different from the method in the presented model, but also that the method and inputs used in Matlab give a good approximate of the values expected from EnergyPlus.

For the validation of the conduction heat transfer, the contributions of the conduction through the window and exterior wall only are considered in the presented model. In EnergyPlus while considering the internal walls, floor and ceiling to be adiabatic however, there still appear to be heat gains and losses through these surfaces. These are found in the EnergyPlus output called ”Surface Average Face Conduction Heat Transfer Energy”. Figures 5.11a and 5.12a give the hourly outputs for conduction heat transfer through the window and wall respectively for a facade facing north in Amsterdam and figures

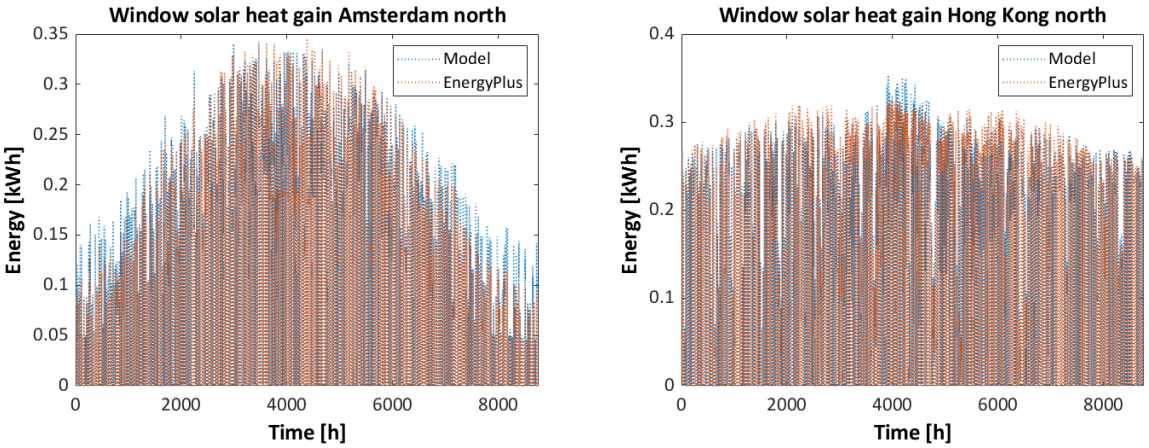

(a) North facing facade in Amsterdam.

(b) North facing facade in Hong Kong.

Figure 5.10: The hourly solar heat gains.

5.11b and 5.12b give these hourly outputs for a facade facing north in Hong Kong.

Validation conduction heat gains and losses

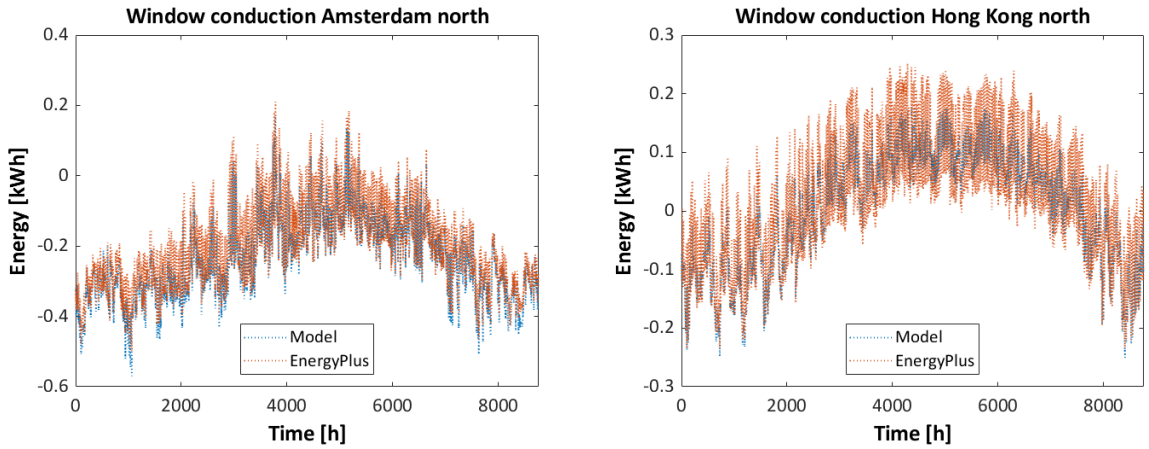

(a) North facing facade in Amsterdam

(b) North facing facade in Hong Kong

Figure 5.11: The hourly conduction heat gains and losses through window.

Although for the conduction heat transfer through the window the graphs for both the presented and EnergyPlus model show a similar behavior, this is not the case for the exterior wall as shown in figure 5.12a. The conduction heat transfer through the exterior wall and window in the presented model is calculated using equation (3.51) which is a straightforward equation. Here no contributions from heat storage due to thermal mass, or convection and radiative heat transfer are considered. These contributions however are considered in EnergyPlus where the inside and outside facing surface heat balance equations are solved in iterative calculations [68]. The convection heat transfer depends on the temperature of the wall surface and on the convective heat transfer coefficient which depends on the wind speed. The radiative heat transfer determines how much heat is radiated by a surface and depends on the surface temperature which is affected by the absorbed irradiance. The effect of irradiance and wind speed is illustrated in figures 5.13a and 5.13b where the total irradiance G_{tot}, wind speed W and ambient temperature or outdoor temperature T_{amb} are plotted for the same time points as the conduction heat transfer for a facade facing north in respectively Amsterdam and Hong Kong. It can be observed that in figure 5.13a between time points 105 and 115 (on the x-axis) the ambient temperature shows an increasing trend and the Matlab outputs as well, while the EnergyPlus output show a trend similar to that wind speed and irradiance. Between time points 130 and 135 the ambient temperature and the

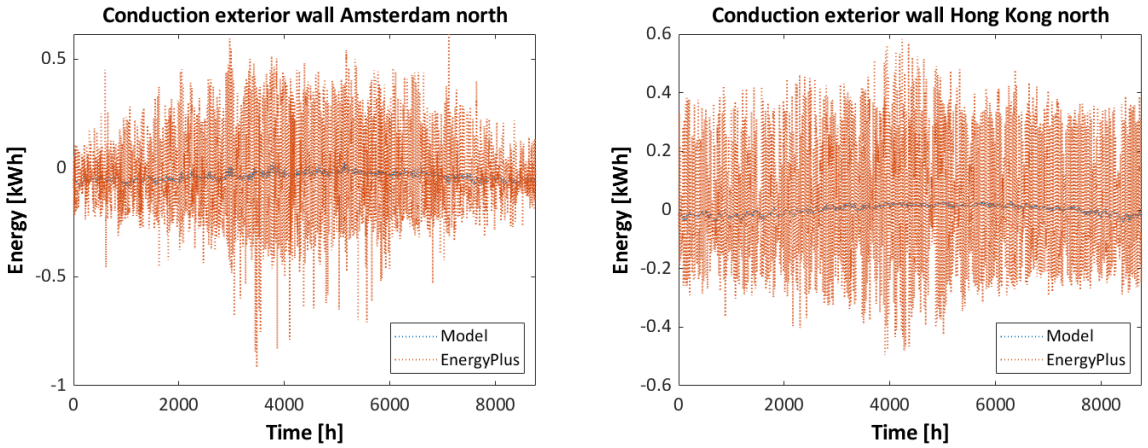

(a) North facing facade in Amsterdam.

(b) North facing facade in Hong Kong

Figure 5.12: The hourly conduction heat gains and losses through the exterior wall.

Matlab model outputs show again an increasing trend while the EnergyPlus outputs now show a trend similar to these of the irradiance outputs. Between these time points the wind speed now shows a decreasing trend. In figure 5.13b between time points 115 and 125 the ambient temperature decreases while the conduction heat transfer output of EnergyPlus for these values increases. The closer the ambient temperature gets to the indoor room temperature, the smaller the difference between the indoor and outdoor temperature becomes and one would thus expect less heat to be lost when the ambient temperature becomes less negative. This is however not always the case in EnergyPlus because of the effects of the wind speed and irradiance. It should also be noted that although EnergyPlus appears to include heat storage in the heat balance equation, this is not shown in the conduction heat transfer as this variable fluctuates more frequently compared to the outputs of the Matlab model.

Regarding the conduction heat transfer through the window, it appears that the Matlab model outputs are similar to the outputs of the EnergyPlus model for a north facing facade in Amsterdam and in Hong Kong, which indicate that the method used in Matlab gives a good approximate of the window heat conduction heat transfer in these cases. The maximum NRMSE values for the locations Amsterdam, Bogota and Hong Kong when also considering different orientations are determined to be 18.7% for Amsterdam facing south, 29.4% for Bogota facing east and 23.9% Hong Kong facing south. These relatively high NRMSE values are found to be due to the irradiance dependence.

	Infiltration		Conduction through window		Ventilation		Solar heat gain	
Location (orientation)	RMSE [W]	NRMSE [%]	RMSE [W]	NRMSE [%]	RMSE [W]	NRMSE [%]	RMSE [W]	NRMSE [%]
Amsterdam (N)	172.3	11	41.0	5.5	104.1	5.6	13.4	3.9
Amsterdam (E)	169.5	10.8	92.1	12.4	103.5	5.6	48.8	3.2
Amsterdam (S)	167.8	10.7	139.2	18.7	102.3	5.5	45.3	2.6
Amsterdam (W)	170.0	10.9	98.1	13.2	103.0	5.5	46.2	3.7
Bogota (N)	91.6	9.2	56.7	11.9	72.3	8.9	34.4	5.8
Bogota (E)	92.8	9.3	140.0	29.4	73.1	9.1	76.7	5.7
Bogota (S)	91.0	9.1	63.3	13.3	72.8	9.0	36.3	4.0
Bogota (W)	91.8	9.2	126.1	26.5	72.5	9.0	95.2	5.4
Hong Kong (N)	307.7	34.2	41.0	9.6	232.2	21.8	20.1	5.0
Hong Kong (E)	311.4	34.6	87.1	20.3	235.3	22.1	47.6	3.7
Hong Kong (S)	313.6	34.9	102.3	23.9	237.4	22.2	27.9	1.9
Hong Kong (W)	316.5	35.2	97.3	22.7	239.4	22.5	63.2	3.8

Table 5.1: RMSE and NRMSE values for different locations and orientations.

Validation energy balance

An energy balance is created by adding up the hourly internal heat gains, infiltration heat transfer, conduction through the window, conduction through the exterior wall, ventilation and solar heat gains. In the presented model this is set to zero which is reached by heating or cooling. When calculating the energy balance using both the outputs of the model and of EnergyPlus, the shapes of both energy balances are found to have a similar behavior. This is plotted for a facade facing north in Amsterdam

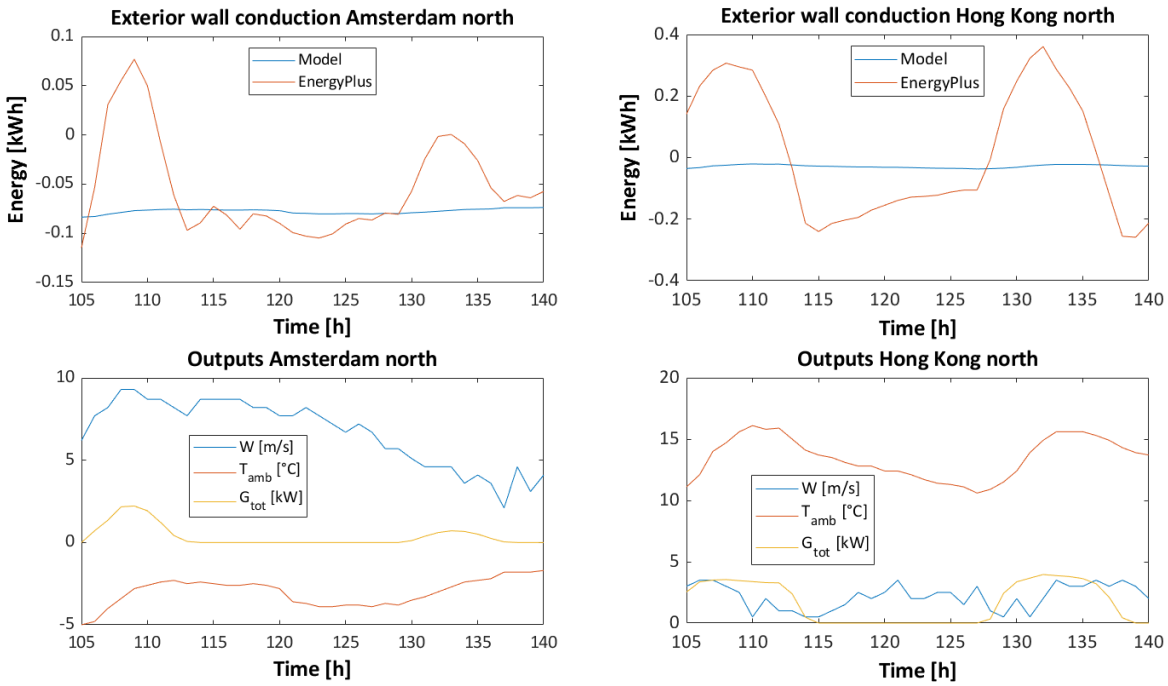

(a) North facing facade in Amsterdam.

(b) North facing facade in Hong Kong.

Figure 5.13: The hourly conduction heat transfer through the wall, wind speed, irradiance and ambient temperature are plotted for a range of time points.

and in Hong Kong as shown in figures 5.14a and 5.14b. The NRMSE for Amsterdam and Hong Kong for a facade facing north are respectively 5.2% and 11.7%. The NRMSE values for other orientations as well as for Bogota are given in table 5.2.

Location	Amsterdam				Bogota				Hong Kong			
Orientation	north	east	south	west	north	east	south	west	north	east	south	west
NRMSE [%]	5.2	6.2	6.7	5.1	6.9	10.6	7.5	7.2	11.7	11.8	11.9	10.5

Table 5.2: NRMSE calculated for energy balance.

In figure 5.15a, the energy balance when adding up the heat transfer components using the EnergyPlus output is plotted together with the supply air cooling and heating loads. In the energy balance for EnergyPlus the contributions of the heat exchange through the floor, ceiling and interior walls are considered. The negative heating loads are plotted because these should be equal to the negative values of the energy balance since negative energy heat transfer indicate heat losses which should be compensated. It can be observed in the figure that heating and cooling load outputs do not exactly overlap the energy balance outputs which indicates that the EnergyPlus energy balance is not nullified by heating and cooling. In figure 5.15b the same energy balance is considered but now the heating and cooling loads as calculated in the Matlab model are plotted. These outputs appear to be closer to outputs of the EnergyPlus energy balance compared to EnergyPlus heating and cooling load outputs. Because it was found in section 5.2.4 that the exterior conduction heat transfer outputs of EnergyPlus and Matlab were significantly different, in figure 5.16 the energy balance is plotted where the EnergyPlus wall conduction heat transfer output is substituted by the Matlab output. When comparing the energy balance in this case to the heating and cooling loads calculated in Matlab these appear to be more similar. This indicates that the differences between the energy balances for Amsterdam for a facade facing north are mainly due to the wall conduction heat transfer.

In figures 5.17a and 5.17b the EnergyPlus heat balance output is plotted for a facade facing north in Hong Kong and compared to the heating and cooling load outputs from EnergyPlus and Matlab. Here it can be observed that the EnergyPlus energy balance output is not nullified by the EnergyPlus heating

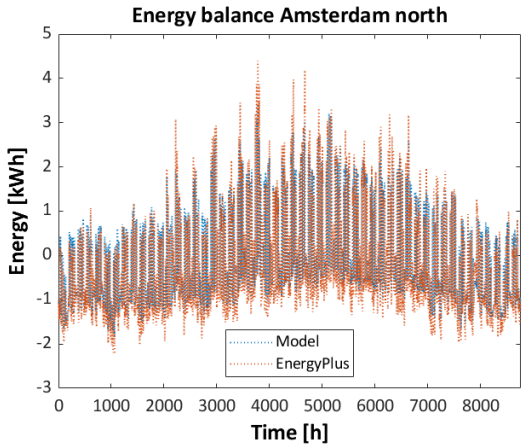

(a) North facing facade in Amsterdam.

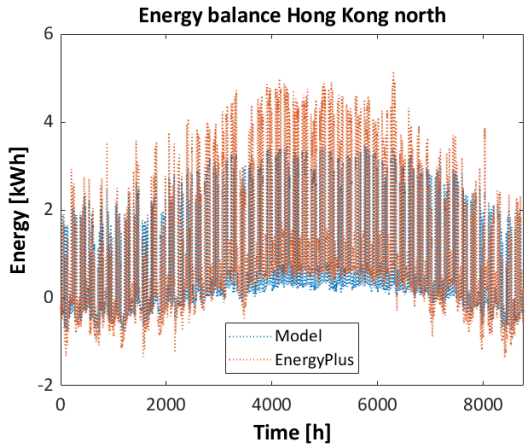

(b) North facing facade in Hong Kong.

Figure 5.14: Energy balance when adding up conduction, infiltration, ventilation, solar heat gain and internal heat gain contributions.

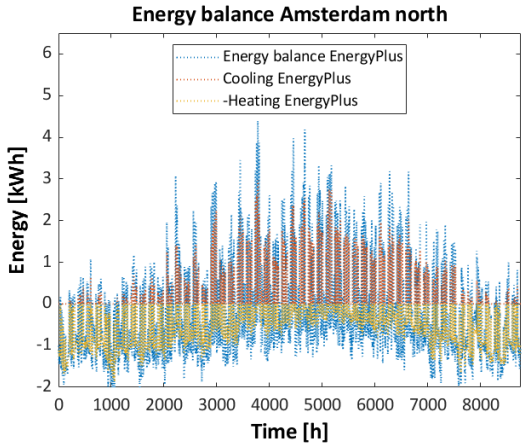

(a) EnergyPlus heating and cooling loads.

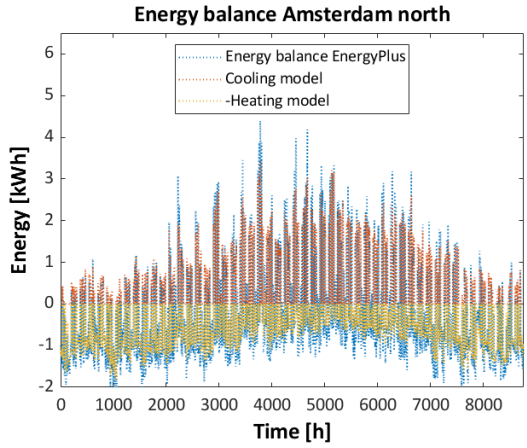

(b) Matlab heating and cooling loads.

Figure 5.15: EnergyPlus energy balance output plotted together with heating and cooling load outputs from EnergyPlus and Matlab for facade facing north in Amsterdam.

and cooling outputs which was also found for Amsterdam. It can also be observed that the Matlab heating and cooling loads are again closer to the EnergyPlus energy balance outputs. In figure 5.18 the EnergyPlus energy balance is plotted where the EnergyPlus exterior wall conduction heat transfer is replaced by that of the Matlab output. However when comparing this energy balance to the Matlab heating and cooling load outputs there are still significant differences between the graphs. These are likely because of the differences found in the ventilation and infiltration heat transfer components which were discussed in sections 5.2.4 and 5.2.4.

In figure 5.19a the yearly heat gains and losses are given for the different components for a north facing facade in Amsterdam. These are calculated by taking the sum over the hourly values and can be negative if throughout the year there are more hourly heat losses than heat gains. The heat losses are only due to the ventilation, conduction and infiltration components because these depend on the temperature difference which can be negative. It can be observed in the figure that throughout the year there are more heat losses than gains for these components for a north facing facade in Amsterdam. The calculated annual values of the model are relatively close to the outputs of EnergyPlus but the infiltration heat losses appear to be underestimated. In figure 5.20a the yearly heating, cooling and lighting loads corresponding to the same north facing facade in Amsterdam are shown and in figure 5.20b these loads are given per floor area. The yearly heating and lighting loads are similar as shown in figure 5.20a, while the cooling loads are overestimated compared to the EnergyPlus model. For

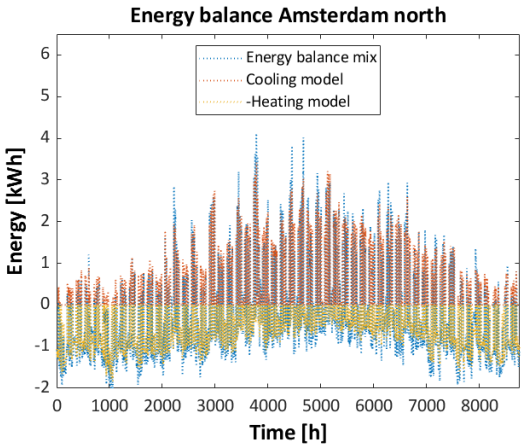

Figure 5.16: Energy balance of EnergyPlus outputs but with wall conduction output from Matlab plotted with Matlab heating and cooling outputs

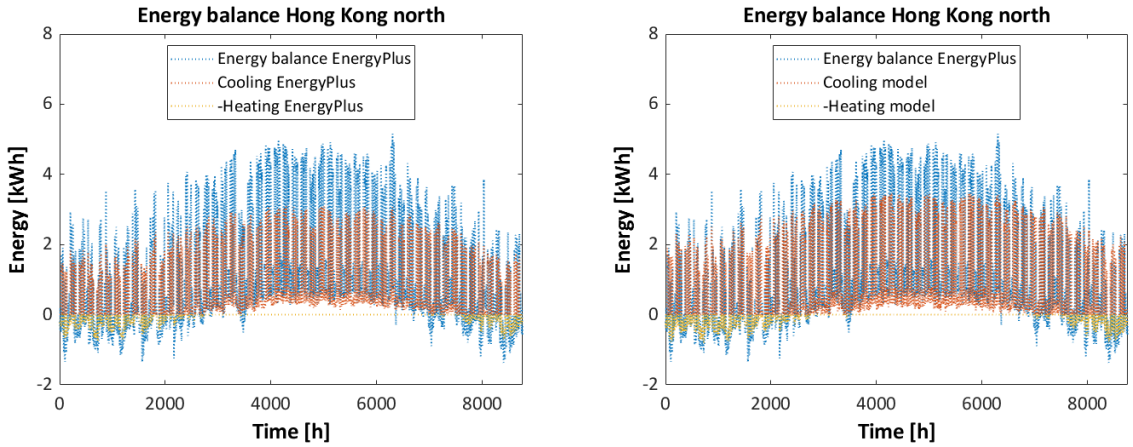

(a) EnergyPlus heating and cooling loads.

(b) Matlab heating and cooling loads.

Figure 5.17: EnergyPlus energy balance output plotted together with heating and cooling load outputs from EnergyPlus and Matlab for facade facing north in Amsterdam.

Amsterdam the annual heating loads are higher than the annual cooling loads which can be expected since the yearly ventilation, conduction and infiltration heat losses are larger than the solar heat gain and internal heat gains. In figure 5.19b the yearly heat gains and losses are given for a north facing facade in Hong Kong. Here it can be observed that regarding ventilation, conduction and infiltration heat transfer throughout the year the annual values are all positive and are small compared to Amsterdam. It can thus be expected that in Hong Kong more cooling loads is required and this is indeed the case as shown in figures 5.21a and 5.21b where the yearly heating, cooling and lighting consumption loads are plotted. The annual heat gains calculated in the model which are due to ventilation and infiltration appear to be underestimated compared to EnergyPlus.

Summary validation results

To summarize this validation section, the presented model outputs regarding heat transfer and irradiance were compared to the outputs of validation models in Grasshopper, SAM, Sandia and EnergyPlus. It was found that the solar position is calculated differently in Grasshopper and in SAM which affects the calculations of the irradiance. It was also found that the heat transfer components which are calculated in Matlab using simplified methods show a behavior similar to the EnergyPlus results. However there are differences between the conduction heat transfer outputs. These are due to a different and more complex method which is used to calculate this component in EnergyPlus. Here the irradiance and wind speed are involved which are not considered for the conduction heat transfer in the presented model. Regarding ventilation and infiltration heat transfer, it was found that in EnergyPlus the air density and

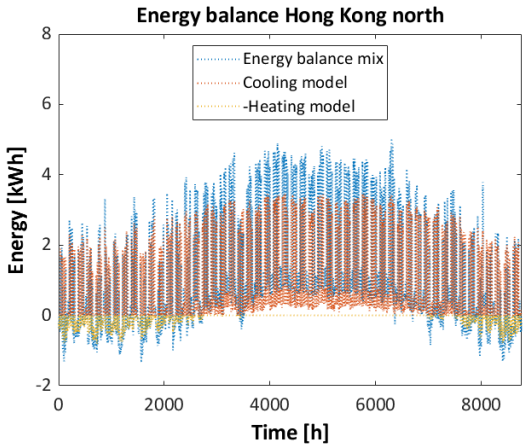

Figure 5.18: Energy balance of EnergyPlus outputs but with wall conduction output from Matlab plotted with Matlab heating and cooling outputs

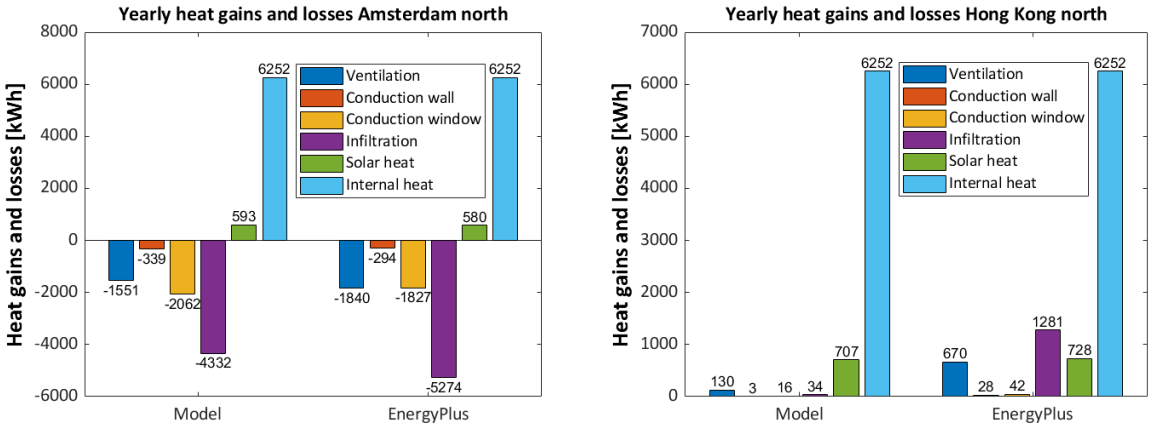

(a) Amsterdam with a facade facing north.

(b) Hong Kong with a facade facing north.

Figure 5.19: Yearly heat gains and losses for model and EnergyPlus.

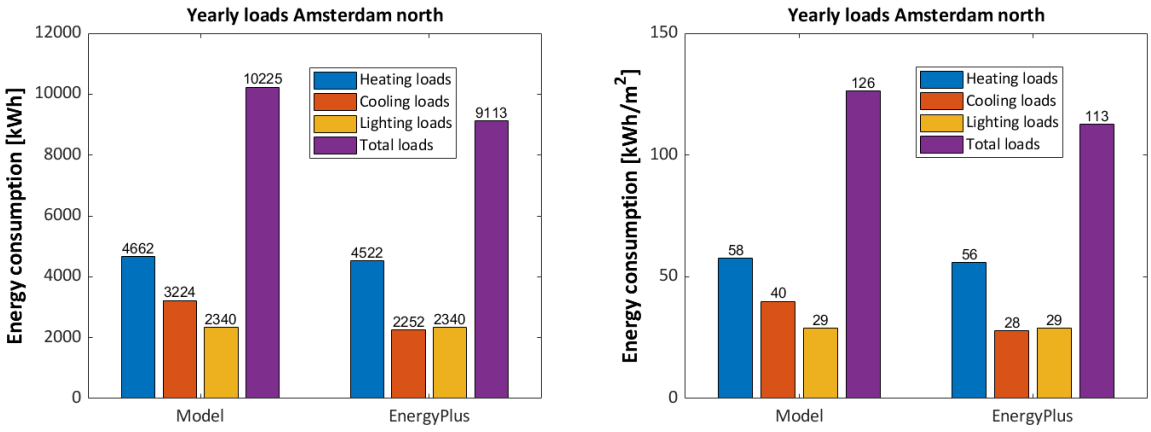

(a) Yearly energy consumption loads

(b) Yearly energy consumption loads per floor area

Figure 5.20: Yearly consumption loads for north facing facade in Amsterdam.

specific heat capacity depend on the average indoor and outdoor temperature and on the humidity of air. Furthermore it was found that when calculating an energy balance using the EnergyPlus outputs

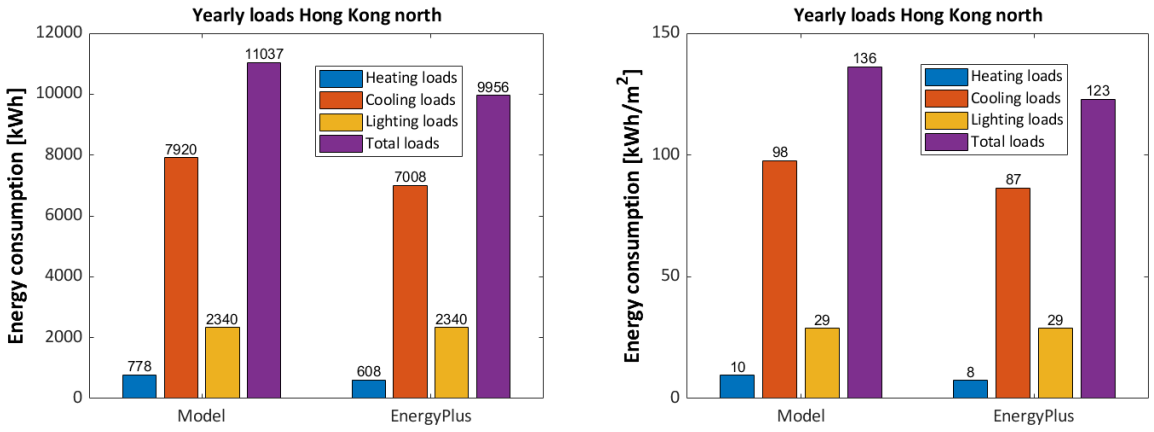

(a) Yearly energy consumption loads

(b) Yearly energy consumption loads per floor area

Figure 5.21: Yearly consumption loads for north facing facade in Hong Kong.

and comparing these to the EnergyPlus heating and cooling loads, that these outputs were not overlapping. This indicates that the energy balance is not nullified by heating and cooling but that EnergyPlus considers heat storage in thermal mass which is not considered in the Matlab model.

5.3. Energy performance of window technologies

In this section the energy performance of different window technologies will be compared for five different locations. These locations are Abu Dhabi (hot/dry climate), Bogota (subtropical highland/temperate climate) , Delft (temperate oceanic climate), Hong Kong (humid subtropical climate/temperate) and Reykjavik (subpolar oceanic/cold climate). For the simulations the parameters regarding the office room and window as described in chapter 3 are used while the parameters for the PV system design part are based on chapter 4. The building energy consumption depends on the heating, cooling and lighting consumption. Four different scenarios are considered with a different optimization strategy for the smart windows and a different light source. In the first scenario the building energy consumption is determined when considering a constant light source and here the energy consumption of the smart windows is optimized for the lowest building energy consumption. A constant light source means that when turned on the lighting power consumption is always the same. In the second scenario again a constant light source is considered but now the building energy consumption of the smart windows is optimized for the lowest building energy consumption while considering the optimal indoor illuminance limits. This means that for example for the EC window which has multiple opaque states, it is first determined whether or not the average indoor illuminance level is within the illuminance limits for all states. Then from the states which meet the requirement, a state is selected which corresponds to the lowest total energy consumption. This way the usage of natural daylight is optimized. The third and the fourth scenarios are similar to the first and second scenario but now a light source with adjustable lighting power consumption is considered such that when turned on the average indoor illuminance level reaches the minimum limit of 500 lux. In all scenarios the HVAC system is designed for a single optimal indoor temperature.

5.3.1. Potential energy savings when optimizing for lowest energy consumption

The total energy building consumption is the sum of heating, cooling and lighting demands. To determine the potential savings of different window technologies in terms of heating and cooling, first the potential savings of using an adjustable light source instead of a constant light source are determined. In figure 5.22 the yearly energy consumption and generation is plotted for different window technologies for a south facing facade in Abu Dhabi. In figure 5.22a a constant light source is considered while in figure 5.22b an adjustable light source is considered. The values which are given on the left side of the bar graph corresponding to the PV windows represent the yearly energy generation potential. The values given on the right side of the bar graphs correspond to the sum of the yearly heating, cooling and lighting consumption demand of the office room for the window technologies. When comparing

the energy consumption of an office room with reference window and constant light source to that of the same scenario but with an adjustable light source, it can be observed that using a controlled light source can save 3.6% of the total energy building consumption in this case. When considering a south facing facade in Reykjavik, the savings of using an adjustable light source instead of a constant light source can be 9.0%. These results are plotted in figure 5.23. The results for a south facing facade in Bogota, Delft and Hong Kong are shown in figures 5.24, 5.25 and 5.26 and the savings of using an adjustable light source here are calculated to be respectively 5.2%, 8.4% and 13.0%. When comparing the lighting load savings for other window technologies, it can be observed that windows with a low VT value such as a-Si and OPV show higher savings in lighting consumption when considering an adjusting light source instead of a constant light source. This can be explained because the probability of the average indoor illuminance to be lower than 500 lux is higher for a lower VT. Each time this is the case, the artificial lighting is turned on. The number of hours for which the artificial lighting is turned on is thus high if the VT of a window is low. The difference between using an adjustable light source instead of a constant lighting load would be more significant than the case of a window with with high VT.

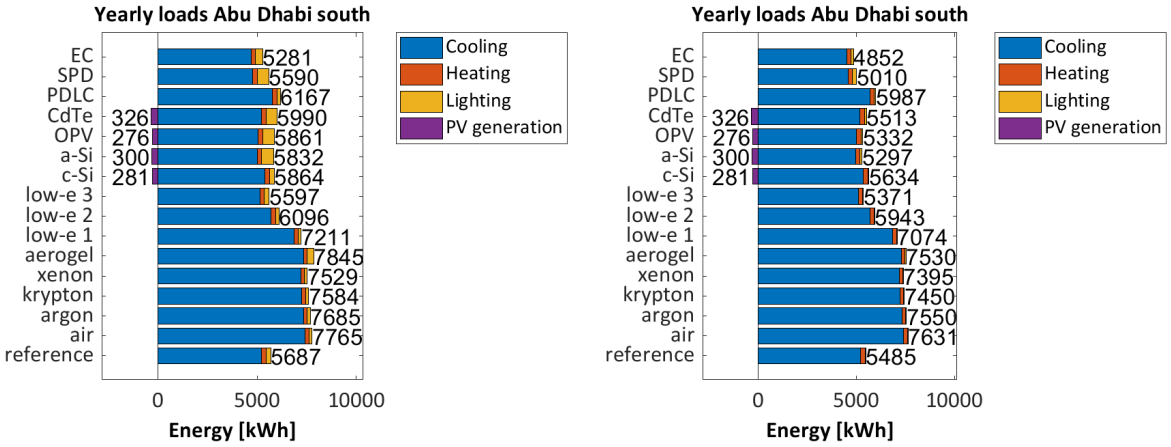

(a) Constant light source.

(b) Adjustable light source.

Figure 5.22: The yearly cooling, heating and lighting loads and energy generated for an office room in Abu Dhabi with an orientation towards south. The active PV area of the semitransparent c-Si window covers a third of the window area.

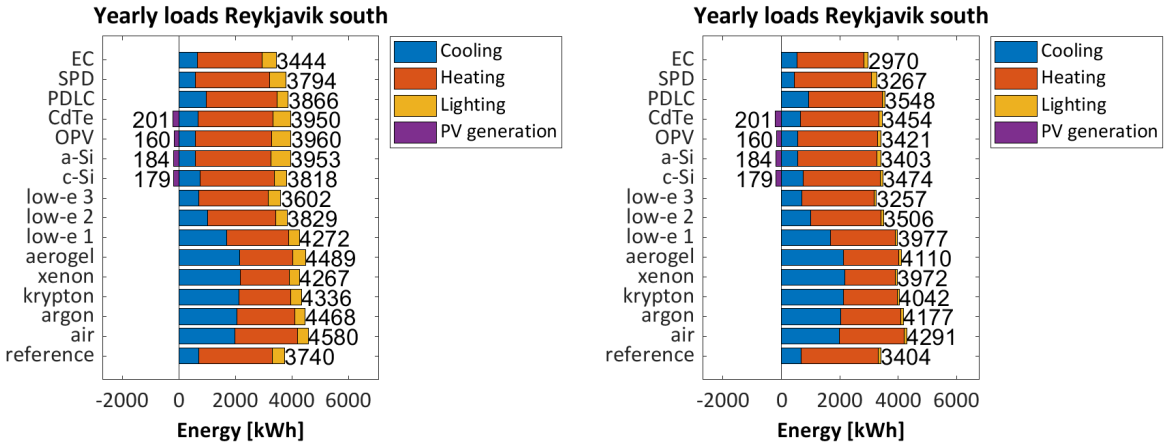

(a) Constant light source.

(b) Adjustable light source.

Figure 5.23: The yearly cooling, heating and lighting loads and energy generated for an office room in Reykjavik with an orientation towards south. The active PV area of the semitransparent c-Si window covers a third of the window area.

Abu Dhabi has a hot climate and for this location the cooling loads are significantly higher than the heating loads. Reykjavik on the other hand has a cold climate and here the heating loads are more

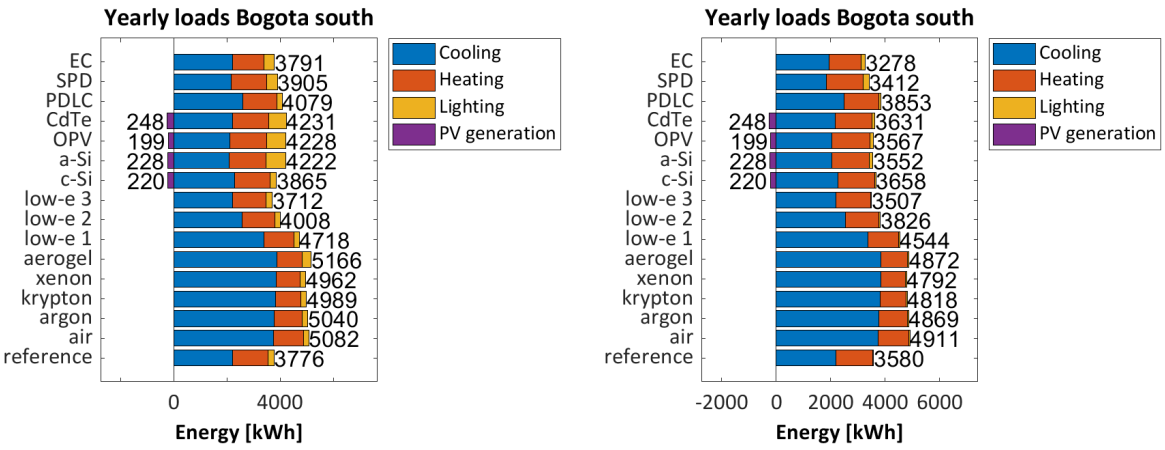

(a) Constant light source.

(b) Adjustable light source.

Figure 5.24: The yearly cooling, heating and lighting loads and energy generated for an office room in Bogota with an orientation towards south. The active PV area of the semitransparent c-Si window covers a third of the window area.

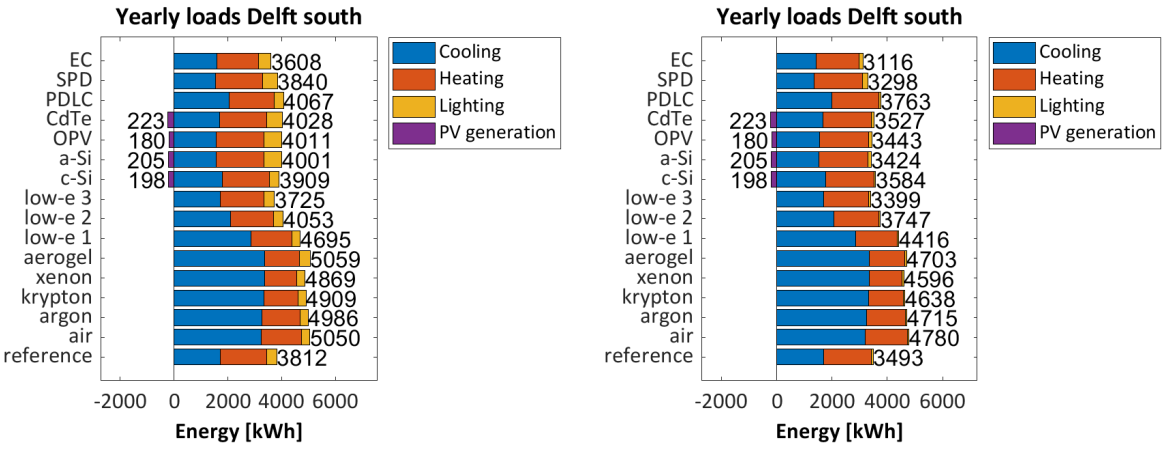

(a) Constant light source.

(b) Adjustable light source.

Figure 5.25: The yearly cooling, heating and lighting loads and energy generated for an office room in Delft with an orientation towards south. The active PV area of the semitransparent c-Si window covers a third of the window area.

contributing to the overall building energy consumption for most window technologies. For Bogota and Hong Kong which have a subtropic climate, the cooling loads are also higher than the heating loads. For Delft which has a temperate oceanic climate the heating and cooling loads are similar for some window technologies. In all figures the total energy consumption in terms of heating, cooling and lighting are shown on the right side of the bar graphs while the solar energy generation in the cases of PV windows is given on the left side of the bar graph. The window types ”low-e 1”, ”low-e 2” and ”low-e 3” represent double glazed windows with a low-e coating and with high SHGC, moderate SHGC and low SHGC respectively.

It can be observed in all figures where the annual energy loads and generation are shown, that the annual cooling loads for window technologies with respect to the reference window increase while the heating loads decrease if the SHGC value of the window technology is higher than for the reference window. For Reykjavik however it appears that the annual increase of cooling loads is larger than the decrease of heating loads for window technologies with high SHGC values which makes them more energy consuming than the reference window. This is not what is expected from table 2.1 where SHGC values above 0.60 are recommended for cold climates to reduce heating loads during winter. The simulations indicate that windows with a high SHGC reduce the heating loads during summer but significantly increase the cooling loads during summer. This can be explained because the internal heat gains during the working hours have a significant positive contribution to the energy balance and

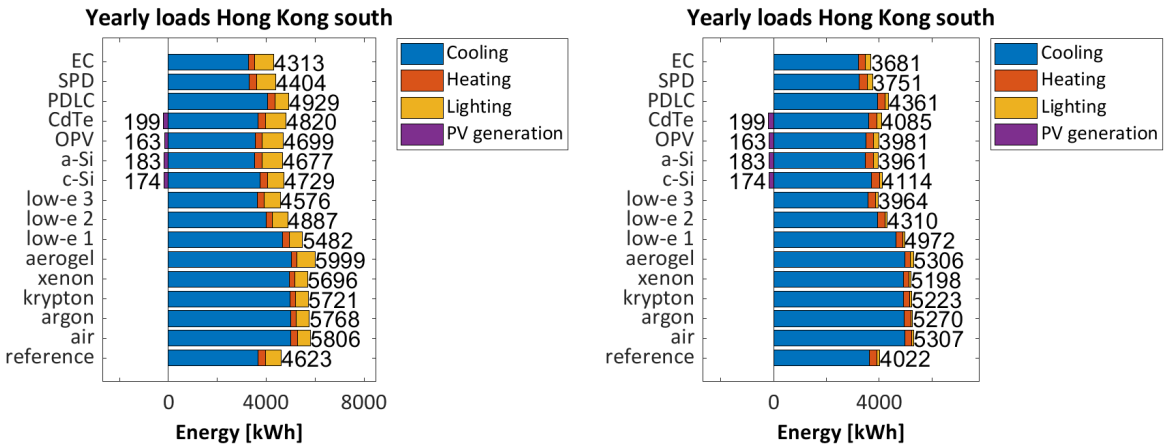

(a) Constant light source.

(b) Adjustable light source.

Figure 5.26: The yearly cooling, heating and lighting loads and energy generated for an office room in Hong Kong with an orientation towards south. The active PV area of the semitransparent c-Si window covers a third of the window area.

windows with relatively high insulating properties are considered. This means that more heat can be added to the internal space than dissipated through the window during the summer which leads to higher cooling loads. The sum of the heating and cooling loads thus tends to decrease for a lower SHGC.

Among the semitransparent PV windows, semitransparent CdTe shows the highest potential in terms of energy generation for all locations and orientations. For Abu Dhabi 326 kWh could be generated for semitransparent CdTe while for semitransparent OPV, a-Si and c-Si this is 276, 300 and 281 kWh respectively. The window area is 4.536 m^2 thus the yearly energy generation per window area is equal to 71.9, 60.8, 66.1 and 61.9 kWh/m^2. It should be mentioned that the energy yield of a semitransparent c-Si is lower than for a semitransparent a-Si or CdTe because of the lower power conversion efficiency which is considered as explained in section 2.3.1. For a south facing facade in Hong Kong the annual energy generation potential is shown in figure 5.26 to be 199, 163, 183 and 174 kWh for the semitransparent CdTe, OPV, a-Si and c-Si PV windows respectively. These results correspond to an energy yield per window area of 43.9, 35.9, 40.3 and 38.4 kWh/m^2. In [101] the energy generation potential of an a-Si PV window with a width of 3.81 m and a height of 1.25 m and the same electrical properties as considered in this model was determined to be 120 kWh. This window consisted of six a-Si PV windows with a width and height of respectively 0.635 m and 1.245 m. When considering the PV area, the yearly energy generation potential was calculated to be 25.2 kWh/m^2, while in the presented model it was calculated to be 40.3 kWh/m^2. In the reference article the simulation tool EnergyPlus was used to simulate the energy performance of the room and the equivalent one-diode model in this program was selected to calculate the energy yield of the window.

The energy yield is also calculated using SAM and here it is equal to 40.4 kWh/m^2 which is similar to the value calculated in the presented model. This indicates that there is a difference between the solar power generation calculations which are used in EnergyPlus and in SAM.

The yearly energy loads and generation of the locations with different orientations is shown in appendix A and here it can be observed that the energy generation potential of PV windows in Abu Dhabi and Hong Kong is higher for a west oriented facade compared to a south facing facade. For Bogota this is the case for both the east and west facing facade. The higher potential of the west facing facade can be explained because Abu Dhabi, Hong Kong and Bogota are close to the equator where the solar altitude is higher during summer which reduces the DNI contribution to the irradiance calculation. For Reykjavik and Delft the highest energy potential is for the south facing facade.

To calculate the annual energy savings, the net building energy consumption is determine and this is equal to the total building energy consumption minus the PV energy generated. The savings are then calculated according to

$$\eta_{saving} = \frac{E_{net,ref} - E_{net,window}}{E_{net,ref}} 100\%, \tag{5.10}$$

where $E_{net,ref}$ and $E_{net,window}$ are the net building energy consumption for the reference window and other window technologies respectively. The potential energy savings are given in figures 5.27, 5.28, 5.30, 5.31 and 5.29 for locations with an orientation towards south. In appendix B the graphs for different orientations are given. For the south oriented facade, it is observed that for some locations the overall savings of window technologies with respect to the reference window are negative and this indicates that the energy performance is worse than that of the reference window.

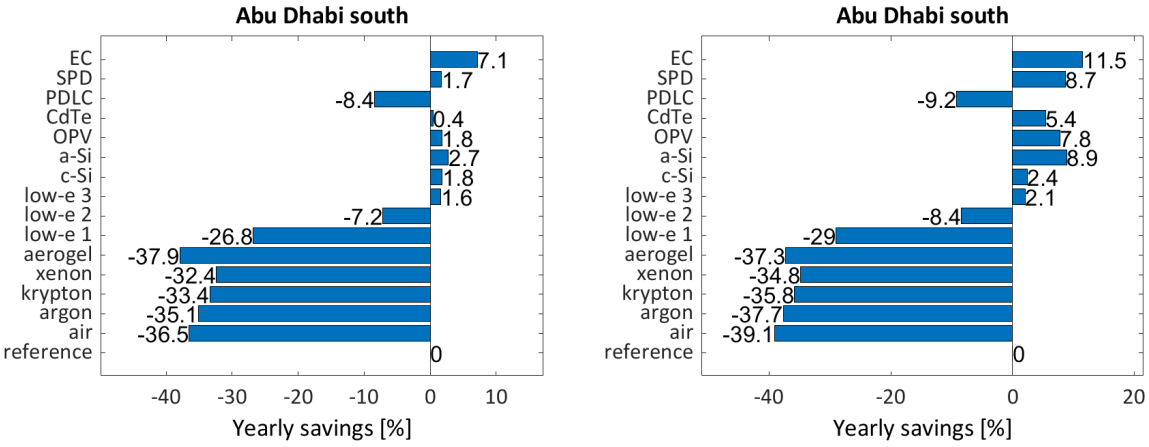

(a) Constant light source.

(b) Adjustable light source.

Figure 5.27: The yearly potential energy savings for an office room in Abu Dhabi with an orientation towards south.

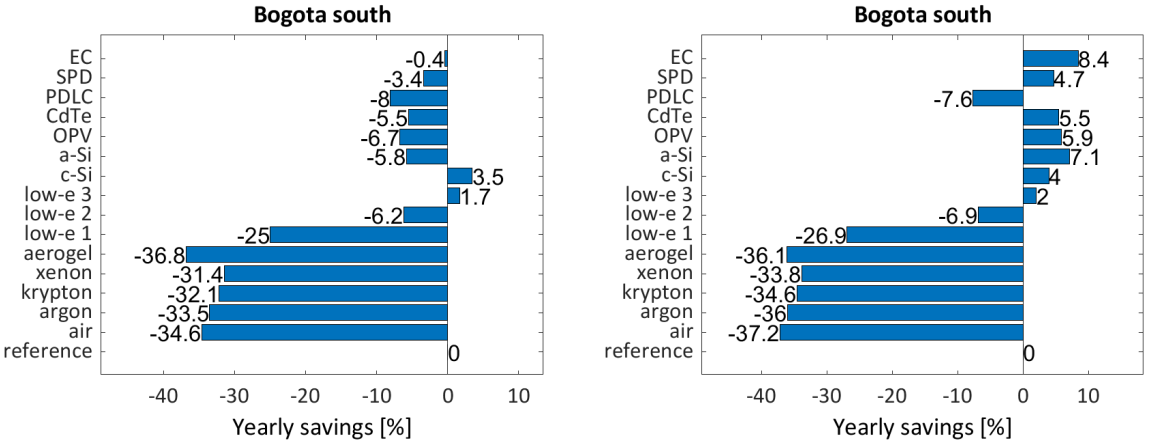

(a) Constant light source.

(b) Adjustable light source.

Figure 5.28: The yearly potential energy savings for an office room in Bogota with an orientation towards south.

Among the different window technologies, the highest potential savings appear to be for the EC window. The savings when using this window instead of the reference window could save up to 12% of the total energy consumption. The PV windows also show relatively high potential savings when considering the office room with an adjustable light source. However these savings are mainly achieved due to the subtraction of the energy generation from the total energy consumption loads rather than from the savings in terms of heating, cooling or lighting loads. This can be observed in the figures for the yearly heating, cooling and lighting loads and the energy generation. Here total yearly energy consumption of most PV windows appears to be similar or even higher than for the reference window. In cases where the yearly energy consumption is lower compared to the reference window, the difference between the energy consumption outputs is significantly smaller than the yearly energy yield.

SPD and low-e 3, which is a double glazed window with low-e coating and low SHGC, also show the energy savings compared to the reference for locations with a relatively warmer climate. Although it is expected that windows with a high SHGC would decrease the yearly energy consumption compared to

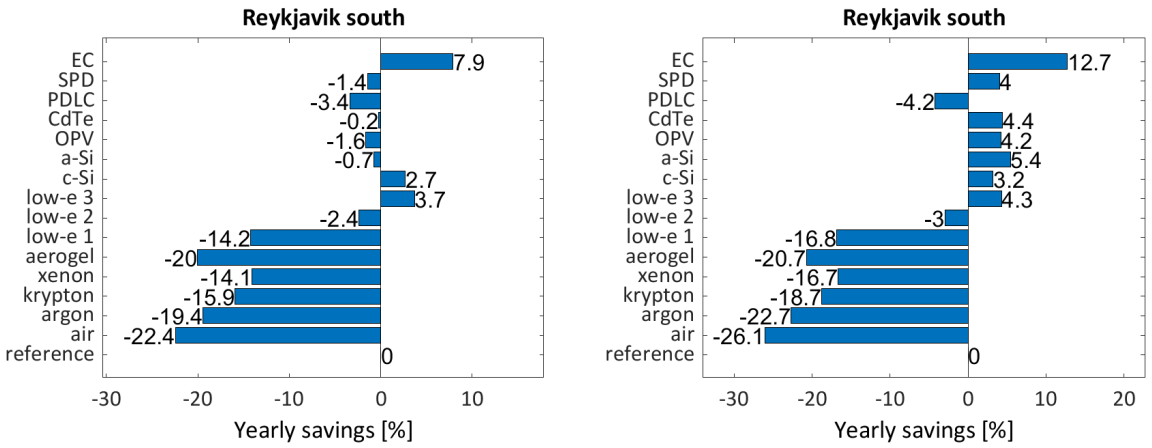

(a) Constant light source.

(b) Adjustable light source.

Figure 5.29: The yearly potential energy savings for an office room in Reykjavik with an orientation towards south.

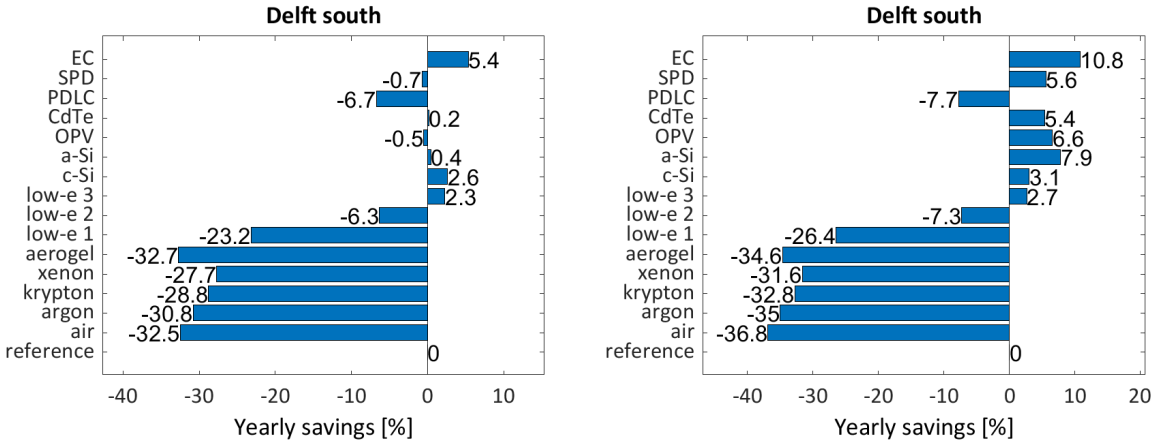

(a) Constant light source.

(b) Adjustable light source.

Figure 5.30: The yearly potential energy savings for an office room in Delft with an orientation towards south.

a reference window for a cold climate such as Reykjavik, it is found that for these windows the cooling loads increase more than the heating loads decrease. In general window types with a lower SHGC tend to decrease the building energy consumption with respect to the reference window. Among the switchable windows EC appears to have the highest potential savings with respect to the reference window which can be because the SHGC can range between 0.05 and 0.40 while for PDLC 0.39 is the lowest possible SHGC and because for the SPD window only one opaque and one transparent state are considered. The PDLC window shows no energy savings for any location and this is due to the relatively high SHGC. This indicates that the PDLC window is not suitable for controlling solar heat.

5.3.2. Potential energy savings when optimizing for indoor illuminance

In section 5.3.1 the energy performance of smart windows was optimized such that these were in the opaque or transparent state which corresponded to the lowest building energy consumption. During summer in warmer climates, these windows would thus be expected to be mainly in their opaque state to block solar heat while the average indoor illuminance could be between 500 and 2000 lux. In this section the energy performance of smart windows is determined when optimized for the lowest energy consumption while considering the indoor illuminance limits during the working hours. Here again a scenario with constant light source and adjustable light source are considered. The calculated savings are shown in table 5.3 and are less than for the scenario where the switchable windows are designed for the lowest energy consumption only. When considering the adjustable light source, the SPD and EC windows show energy savings for different locations with an orientation towards south when optimized

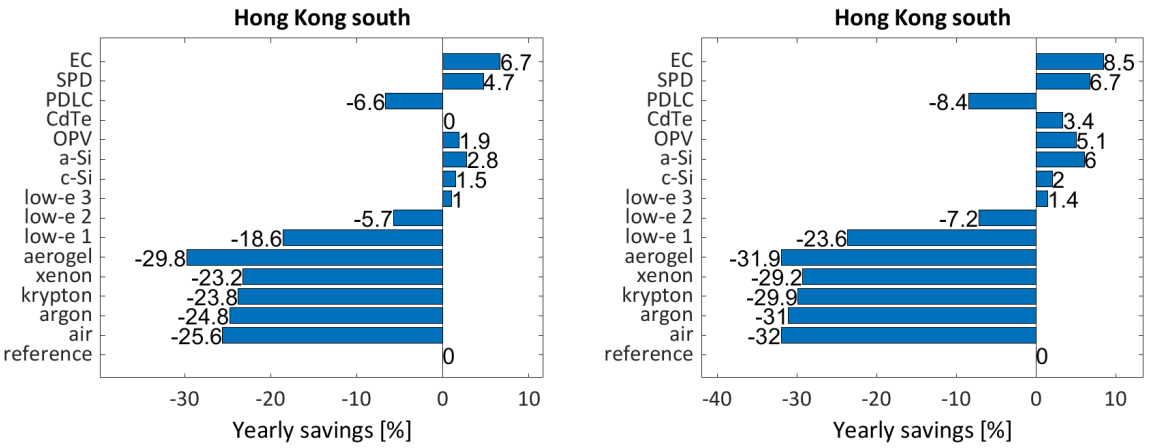

(a) Constant light source.

(b) Adjustable light source.

Figure 5.31: The yearly cooling, heating and lighting loads and energy generated for an office room in Hong Kong with an orientation towards south.

for the lowest energy consumption. However when also optimized for the illuminance, the potential savings of the SPD window with respect to the reference window are negative for Bogota, Delft and Reykjavik. Similarly to the previous section, it is found that the highest potential savings appear to be for the EC window. These can be up to 8.2% when optimizing for the lowest energy consumption while considering the indoor illuminance limits.

	Abu Dhabi South			Bogota South			Delft South			Hong Kong South			Reykjavik South		
	PDLC	SPD	EC	PDLC	SPD	EC	PDLC	SPD	EC	PDLC	SPD	EC	PDLC	SPD	EC
Savings (constant) [%]	-8.4	1.2	6.8	-8	-3.8	-1.3	-6.7	-1.5	4.8	-6.6	3.9	5.1	-3.4	-1.9	7.5
Savings (adjustable) [%]	-10.1	4.7	7.5	-9.3	-2.5	-1.1	-8.5	-0.6	4.8	-10.4	4.5	4.7	-4.8	-0.4	8.2

Table 5.3: Potential energy savings of smart windows when optimized for lowest energy consumption while considering the indoor illuminance limits for visible light transmittance.

5.3.3. Visual comfort

Some of the window technologies allow for energy savings with respect to the reference due to the low SHGC value. However in these cases the VT is also relatively lower which means that the amount of transmitted natural daylight is not optimized for these window technology. In these cases more artificial lighting is consumed than for windows with a high VT or with varying VT. In this section the percentage of the working hours for which the average indoor illuminance meets the limits is determined for all considered window types. This percentage is defined as ”visual comfort occurrence” in the plots. The number of time points corresponding to the working hours is equal to 2860.

The occurrence of visual comfort is plotted for a facade facing south for Abu Dhabi, Bogota, Delft, Hong Kong and Reykjavik respectively. Here the scenario is considered with adaptable light source where the switchable glazing types are optimized for the lowest energy consumption while considering the indoor illuminance limits during the working hours. In the bar graphs where the visual comfort occurrence is plotted for different locations, it can be observed that the highest occurrence of visual comfort is reached for the PDLC window for most of the locations. It should be noted that this is an average of the room and that the intensity of light close to the window is higher and could thus still cause discomfort glare. For EC the occurrence of visual comfort is higher than for the reference window for Abu Dhabi, Delft, and Reykjavik but lower for Bogota and Hong Kong. For SPD the visual comfort occurrence is lower compared to the reference window.

The visual comfort graphs indicate that the PDLC window is preferred over SPD or EC window when designing for the average indoor illuminance limits. However in the previous section it was also determined that EC showed potential savings when optimized for indoor illuminance thus this window type can both reduce the building energy load while improving the visual comfort conditions for users. For the SPD window the visual performance is worse than for the reference window and which is likely

because only two states are considered. It would be expected that if more states with corresponding VT and SHGC values would be considered in between the current values used for SPD that both the thermal as visual performance of this window would be improved. Regarding the PV window types a-Si, OPV and CdTe perform worse than the c-Si PV window which is due to the relatively low VT value of these window types compared to the VT of the c-Si window which is similar to the VT value of the reference window. In this section the visual comfort occurrence is not plotted for the scenario where the switchable glazing types are optimized for the lowest energy consumption only. However it can be noted that for almost all locations and orientations, the visual comfort occurrence for smart windows in this scenario would be significantly lower compared to the reference window.

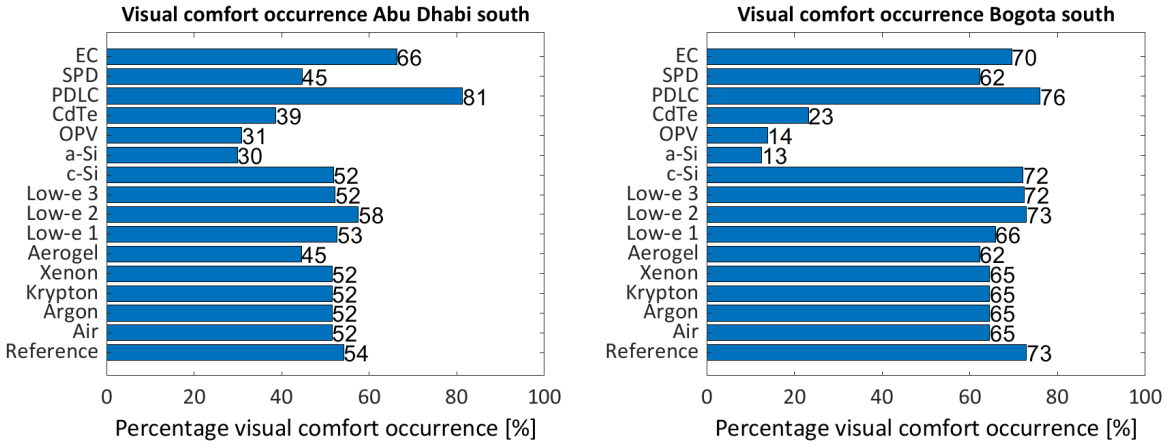

(a) Facade facing south in Abu Dhabi.

(b) Facade facing south in Bogota.

Figure 5.32: Visual comfort occurrence.

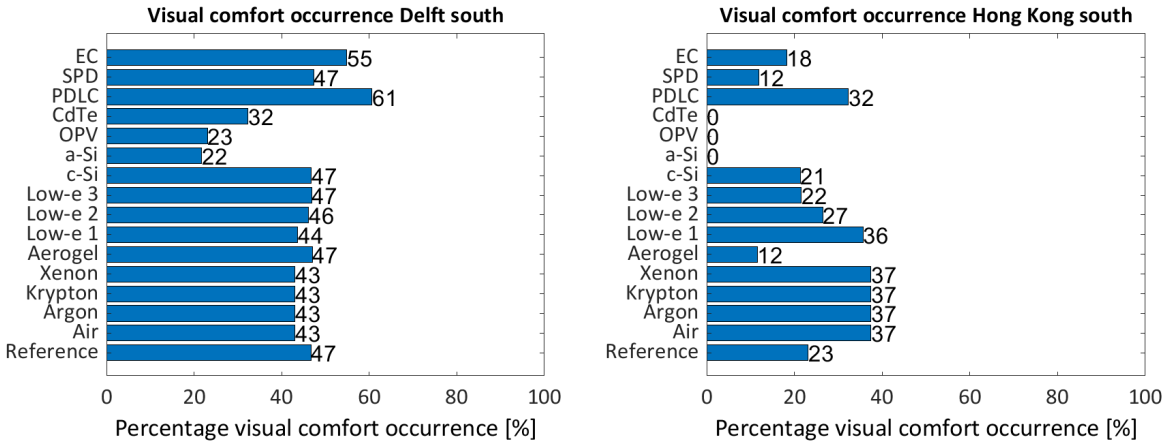

(a) Facade facing south in Delft.

(b) Facade facing south in Hong Kong.

Figure 5.33: Visual comfort occurrence.

5.3.4. Smart window load profile

In the previous sections, it was found that the EC window showed the highest potential for energy savings while SPD, PV windows and a window with low-e coating and low SHGC also showed potential energy savings in some cases. Besides it was found that the usage of natural daylight was optimized when using the PDLC window in most cases and when using the EC window in some of the cases. In this section the load profile for the smart windows is discussed when designing for the lowest energy consumption while considering the indoor illuminance limits. Because the highest savings were found for an adjustable light source, the smart window load profiles for this light source only are discussed. Table 5.4 shows that the yearly consumption load for the SPD window is the highest among the smart

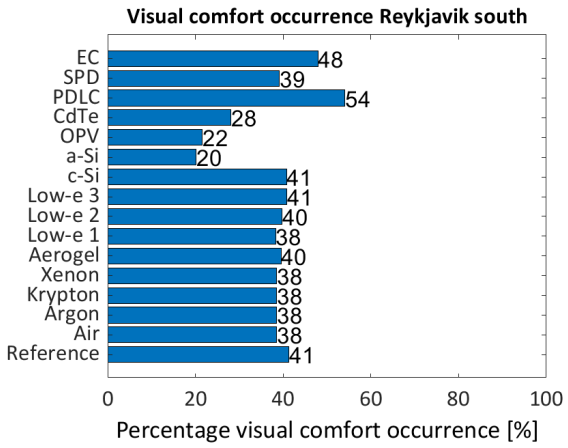

Figure 5.34: Visual comfort occurrence for facade facing south in Reykjavik.

windows, followed by PDLC for all locations and orientations. The lowest yearly loads are required for the EC window. This can be explained because no continuous power consumption is required here as it is only required to switch between states. Among the considered locations, the highest yearly energy requirements for the PDLC and SPD are found for Reykjavik while the requirements for EC for this location are the lowest. This indicates that in Reykjavik the smart windows are in the transparent state more often throughout the year than for other locations. For Hong Kong and Abu Dhabi the consumption requirements for EC are higher than for Bogota, Delft and Reykjavik. This indicates that the EC window for Hong Kong and Abu Dhabi switches the most between opaque and transparent states. A weekly load profile for each switchable window type is plotted for a week during summer and during winter for Abu Dhabi, Bogota, Delft, Hong Kong and Reykjavik. Again the orientation of the facade towards south is taken. The transparency of the smart window depends on the ambient temperature, solar heat gain and illuminance which are calculated using weather data. The load profile can thus be different per day. If the indoor illuminance is not between 500 and 2000 lux for any of the states during the working hours, then the state which gives the lowest total energy consumption is selected. This heavily depends on the solar heat gain and lighting loads which are calculated for each state of the smart window. When comparing the summer load profile of the windows for Abu Dhabi and Hong Kong to the winter load profile, it can be observed that during the winter week the PDLC and SPD window consume energy during some time points in the weekend which is not the case for the summer week. This is likely because during summer the heat gains are higher than the heat losses. If a smart window is its most opaque state, the solar heat gain is minimized which decreases the cooling demand. The EC window appears to consume energy at sunrise and sunset during the weekend in summer for Abu Dhabi and Hong Kong. For these time points the EC window is thus also in an opaque state similarly to the PDLC and SPD window.

For Bogota during the winter week, the PDLC window appears to be in its most opaque state around the afternoon. During the morning and afternoon it appears to be in a more transparent state. This is because the irradiance and illuminance are higher during the day than at sunrise or sunset. For the PDLC in its most opaque state during winter the average indoor illuminance is between 500 and 2000 lux in Bogota. This means however that the window is not see through. The irradiance and illuminance which reach the south oriented facade in Bogota are higher during winter than during summer. This explains why the PDLC window is in a more transparent state during the summer day compared to the winter day. The SPD window appears to be more in its transparent state than in its opaque state compared to the PDLC window in Bogota. This indicates that here the state with the highest transparency leads to the lowest total energy consumption during winter.

When comparing the summer and winter weeks of Delft and Reykjavik, it can be observed that total energy consumption of the PDLC and SPD windows during summer is higher than during winter. This is because the days are longer during the summer than in the winter and during the night there is no power consumption.

Yearly smart window energy consumption [Wh]						
Window technology	Location/ orientation	Abu Dhabi	Bogota	Delft	Hong Kong	Reykjavik
PDLC	N	7768	8421	13837	5433	18498
	E	5688	6631	11699	4885	16815
	S	4428	7893	10652	6189	14264
	W	4652	6533	11854	4649	16058
SPD	N	4698	17944	13894	6296	17663
	E	6167	17214	15487	7657	19958
	S	8915	17707	18965	7938	21238
	W	6928	17113	16772	9515	20336
EC	N	277	79	84	242	41
	E	250	104	81	323	42
	S	277	89	105	244	70
	W	354	130	115	283	45

Table 5.4: Yearly power requirements smart windows in Wh.

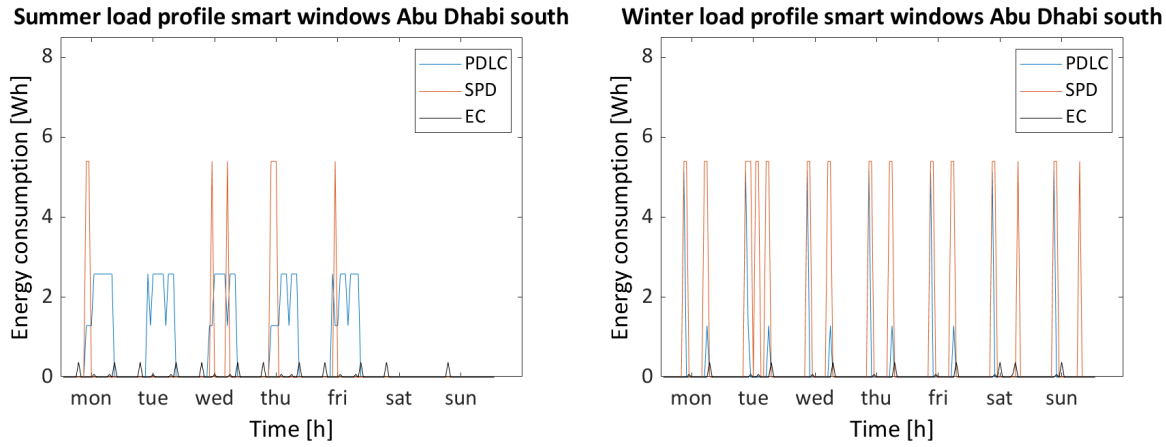

(a) Load profile during week in summer.

(b) Load profile during week in winter.

Figure 5.35: Load profile of smart windows for office room in Abu Dhabi with orientation facing south.

5.3.5. PV system design for smart window

The energy which is required to power the smart windows is generated by opaque c-Si PV cells which are laminated in the window. In this section it is determined how much of the total window area will be covered by the total PV area. When calculating the optimal PV system for each location and orientation, it is found that an autonomous solar powered PDLC or SPD window is not feasible for Reykjavik for any of the considered orientations. This is because the combination of power generated and battery capacity available here is insufficient to supply these smart windows for every time point where power is required throughout the year. The number of PV cells connected in series and in parallel depends on the minimum and maximum voltage and current inputs of the charge controller and it would thus be possible to increase the installed PV or battery capacity when selecting a charge controller with higher maximum voltage and current limits. However the objective is to minimize the PV area and battery capacity required to power a smart window, because PV modules are integrated in the window. A different charge controller is thus not considered here.

In figures 5.40 and 5.41 the SOC of the battery system is plotted throughout the year for Abu Dhabi, Bogota, Delft and Hong Kong. Here it can be observed that the SOC for PDLC and SPD in Abu Dhabi, Delft and Hong Kong is relatively high but drops for some time points where too little solar energy is available. In table 5.5 the optimal PV area and the corresponding battery capacity, total PV system costs and window coverage are given. Here it can be found that for the PV systems to power the PDLC and SPD windows in Hong Kong and Delft, the PV area is relatively large and would cover 22.5% of the

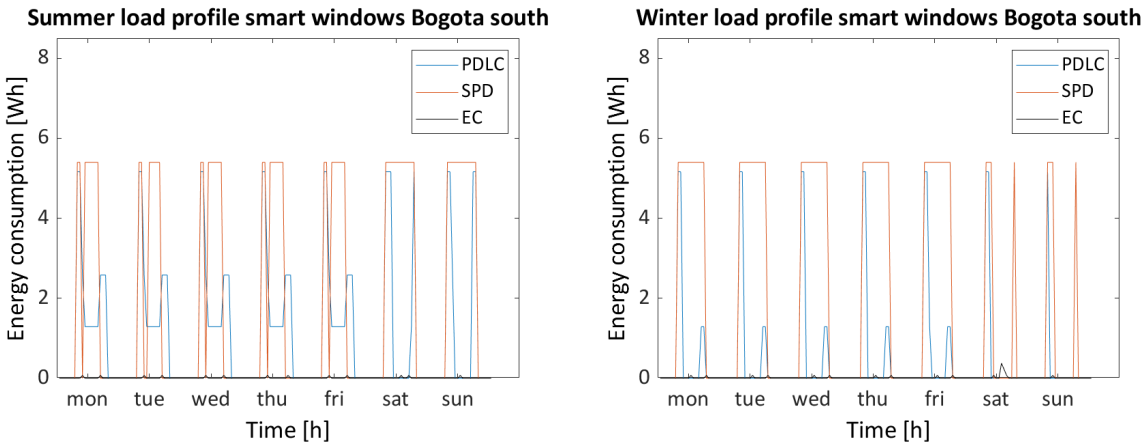

(a) Load profile during week in summer.

(b) Load profile during week in winter.

Figure 5.36: Load profile of smart windows for office room in Bogota with orientation facing south.

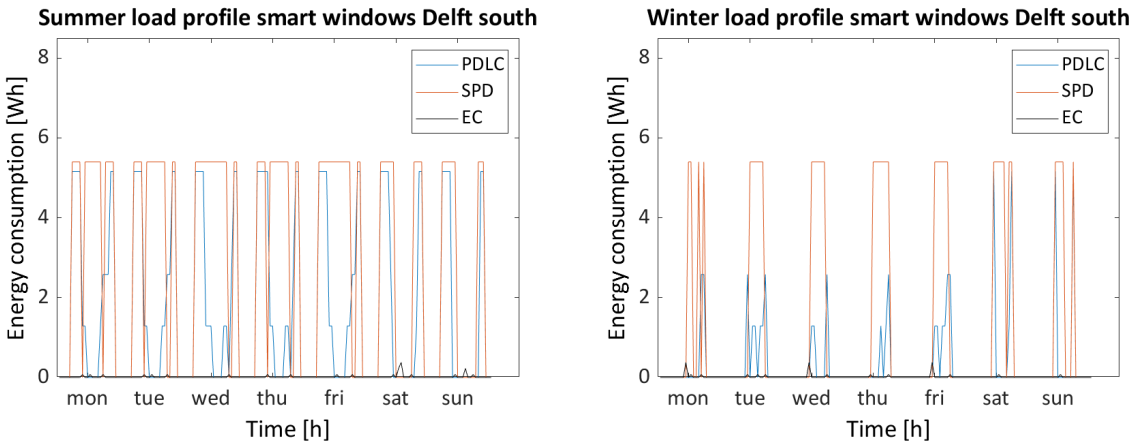

(a) Load profile during week in summer.

(b) Load profile during week in winter.

Figure 5.37: Load profile of smart windows for office room in Delft with orientation facing south.

window. This is found because the optimal PV system was found for the lowest costs and the costs to scale up the PV cells is significantly lower than the costs to scale up the battery capacity. The system with the lowest battery capacity is therefore selected. The optimal PV system to power a PDLC or SPD window was investigated while including an additional constraint such that the PV area cannot cover more than 10% of the window. For Delft it is found that the optimal system to power a PDLC window would include a battery capacity of 190.72 Wh and a total PV area of 0.45 m^2. For SPD no optimum was found however when considering the additional constraint. For Hong Kong the optimal PV area and corresponding battery capacity when considering the maximum of 10% of window area covered by PV, were determined to be respectively 0.45 m^2 and 94.72 Wh to power the PDLC window and 0.45 m^2 and 134.4 Wh for the SPD window.

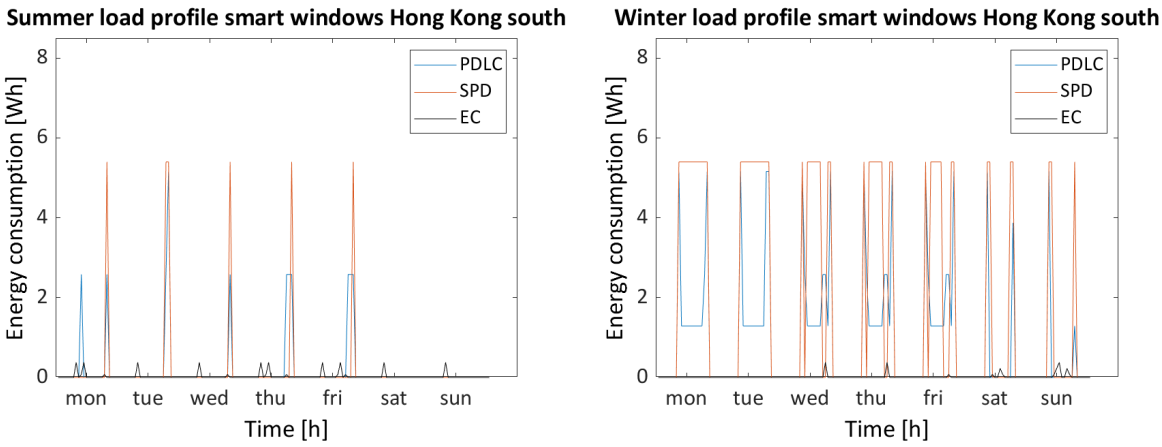

(a) Load profile during week in summer.

(b) Load profile during week in winter.

Figure 5.38: Load profile of smart windows for office room in Hong Kong with orientation facing south.

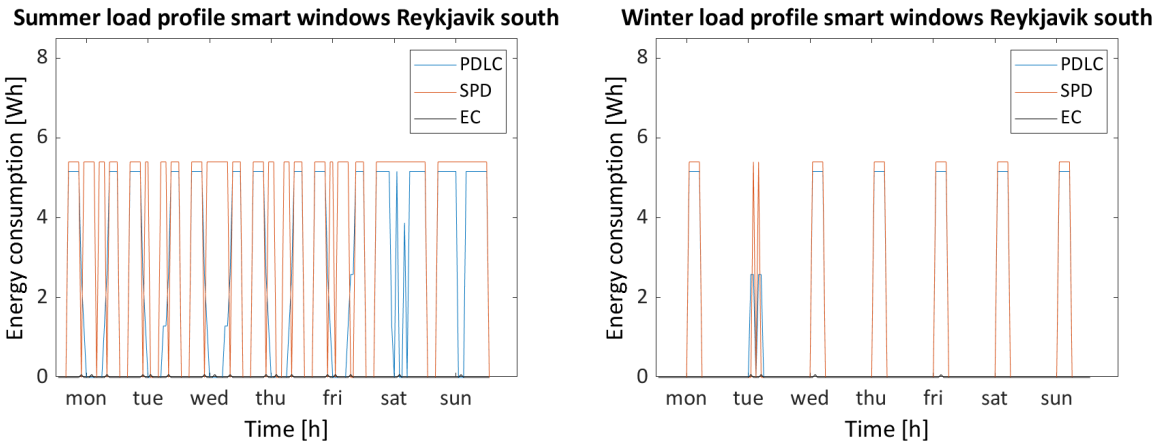

(a) Load profile during week in summer.

(b) Load profile during week in winter.

Figure 5.39: Load profile of smart windows for office room in Reykjavik with orientation facing south.

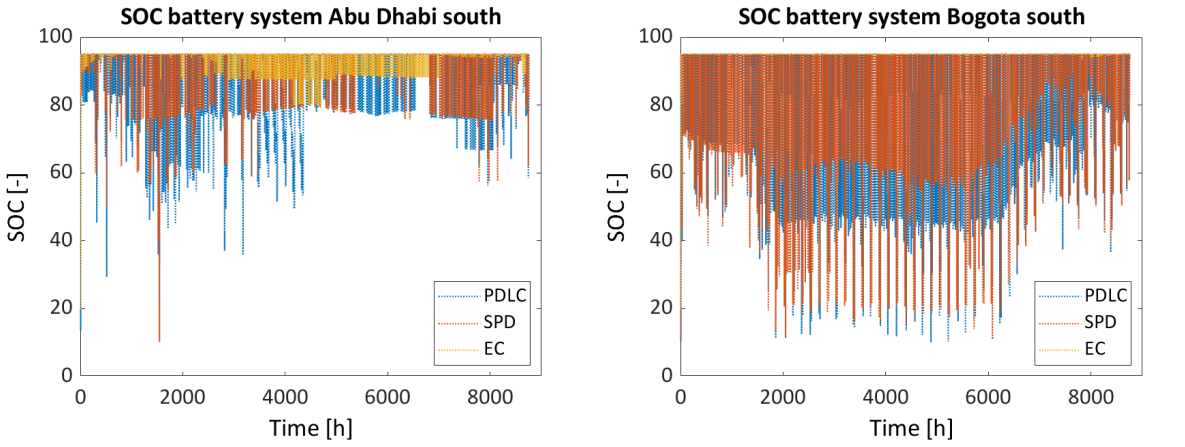

(a) SOC for PV systems to power smart windows in Abu Dhabi.

(b) SOC for PV systems to power smart windows in Bogota.

Figure 5.40: SOC for PV systems to power smart windows in Abu Dhabi and Bogota with facade facing south.

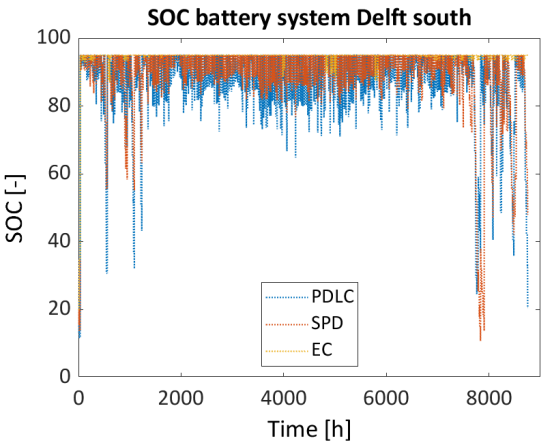

(a) SOC for PV systems to power smart windows in Delft.

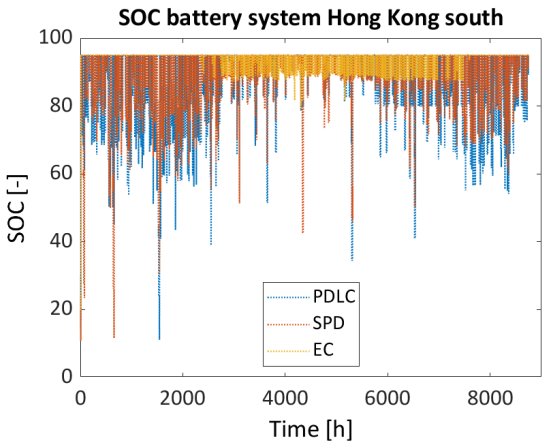

(b) SOC for PV systems to power smart windows in Hong Kong.

Figure 5.41: SOC for PV systems to power smart windows in Delft and Hong Kong with facade facing south.

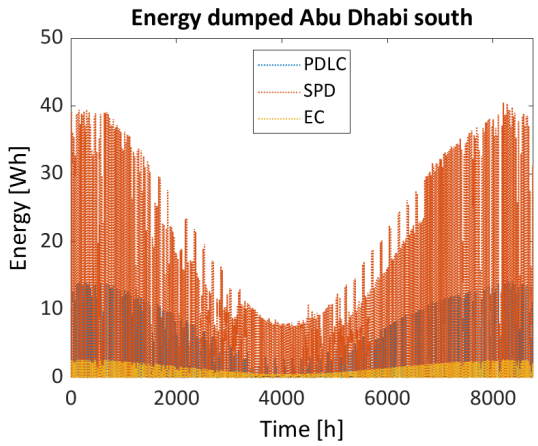

(a) PV energy dumped by PV system Abu Dhabi.

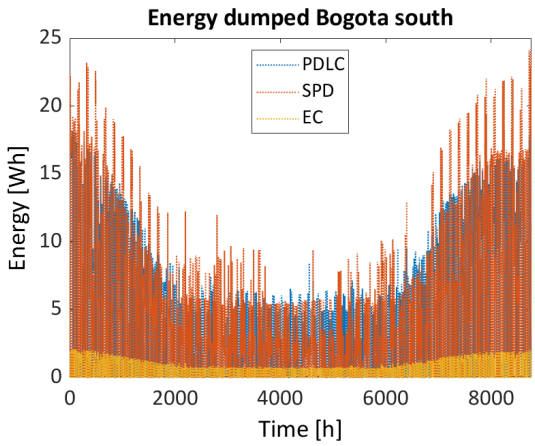

(b) PV energy dumped by PV system Bogota.

Figure 5.42: PV energy dumped by PV system in Abu Dhabi and Bogota with facade facing south.

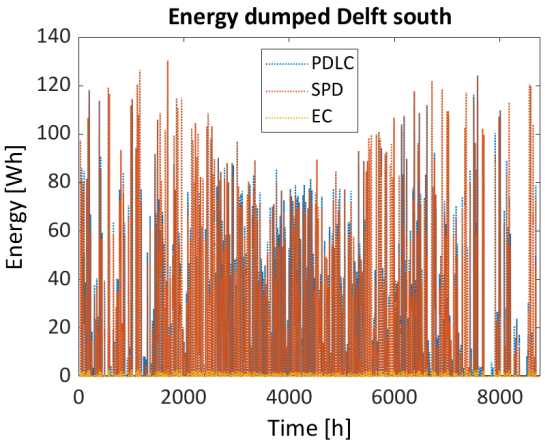

(a) PV energy dumped by PV system Delft.

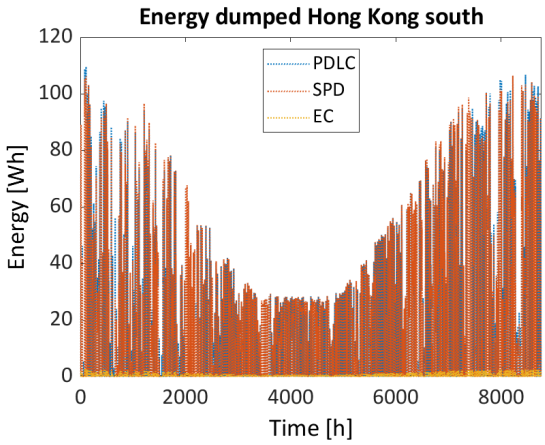

(b) PV energy dumped by PV system in Hong Kong.

Figure 5.43: PV energy dumped by PV system in Delft and Hong Kong with facade facing south.

Location	Orientation	PV area [m^2]	Battery capacity [Wh]	Total costs [€]	Window coverage [%]
Abu Dhabi	PDLC	0.12	26.88	561.16	7.5
	SPD	0.34	29.44	595.13	2.6
	EC	0.02	5.12	337.69	0.44
Bogota	PDLC	0.19	17.92	546.48	4.2
	SPD	0.26	16.64	552.39	5.7
	EC	0.02	5.12	337.69	0.44
Delft	PDLC	1.0	67.84	797.15	22.5
	SPD	1.0	120.32	758.65	22.5
	EC	0.02	5.12	337.69	0.44
Hong Kong	PDLC	1.0	34.56	706.15	22.5
	SPD	1.0	53.76	758.65	22.5
	EC	0.02	5.12	337.69	0.44
Reykjavik	EC	0.02	5.12	337.69	0.44

Table 5.5: PV system design outputs to power smart windows in different locations for facade facing south. The window coverage is the percentage of the total window area which is covered opaque c-Si PV cells.

6

Discussion

In the previous chapter, the heat transfer component outputs of the model were compared to the outputs of EnergyPlus. Here the solar heat gain outputs were similar in both models and the internal heat gains were identical. Differences were found however when comparing the heat transfer outputs of ventilation, infiltration and conduction. For ventilation and infiltration, the differences could be explained because in the presented model the air density and specific heat capacity of air are considered to be constant and for dry air. In EnergyPlus these are variables which depend on the average between the indoor and outdoor temperature and on the humidity of air. Regarding conduction, differences were found because in EnergyPlus convection, radiative and thermal mass contributions are considered to determine this component. Besides the heat balance equations for inside and outside facing surfaces were solved in an iterative calculation. This is not the case in the presented model. An energy balance was calculated by adding the hourly infiltration, ventilation and conduction heat gains and losses, the solar heat gain and internal heat gains. The heating and the cooling outputs of both models were compared to the energy balance which was calculated using the heat transfer outputs of EnergyPlus. It appeared that the heating and cooling outputs of the presented model were more similar to values of this energy balance than the cooling and heating outputs of EnergyPlus.
In chapter 5, the hourly energy consumption and generation for different window technologies was determined. It was found in the simulation results that the EC switchable window shows the highest potential in lowering the net energy building consumption. When considering the scenario where the smart windows were optimized for the lowest total energy consumption, the savings of EC could be up to 12%. When optimizing for the lowest total energy consumption while considering the indoor illuminance limits, the savings could be up to 8%.
To power the EC window for any of the considered locations, a minimal PV area of 0.02 m^2 and a battery capacity of 5.12 Wh are required. This is also the case for different orientations. The PV cells are opaque and the PV area covers only 0.44% of the window area. It can thus be argued that EC windows are suitable for energy performing facades. A disadvantage of the EC however is that the switching time from transparent to opaque or the other way around is relatively long. Because the hourly time points are considered in this work, the switching time is thus no problem.
The PDLC window is suitable for maximizing the usage of natural daylight in a building. The visual comfort occurrence during working hours is the highest for this smart window type for most locations. Another advantage of PDLC is that is has a fast switching time. However it appears that the total energy consumption of an office room with such window is higher than with a reference window. As mentioned earlier, the PDLC in its initial state is fully opaque and thus not see through. It can thus be concluded that PDLC would be more suitable for privacy applications. The SPD window shows potential energy savings for Abu Dhabi of 8.7% when optimizing for the lowest energy consumption only and 4.7% when also considering the average indoor illuminance limits. The PV area and battery capacity required to power the SPD window in Abu Dhabi are 0.34 m^2 and 29.44 Wh. The window coverage by PV is 2.6%. For Hong Kong this window type showed potential energy savings of 6.7% when optimized for the lowest energy consumption only and 4.5% when also considering the illuminance limits. The PV area and battery capacity in this case are determined to be 1.0 m^2 and 53.76 Wh. Because the window coverage by PV area in this case would be 22.5%, it was investigated what would be the minimal battery

capacity when limiting the window coverage at 10%. In this case the PV area would be 0.45 m^2 and the battery capacity would be 134.4 Wh. For PDLC and SPD windows, it is not possible to design a typical minimal PV system which does not depend on the location or orientation of the facade. This is due to the relatively higher energy demand when compared to the EC window. The energy generation potential of a location and orientation is thus more important when designing a PV system for the PDLC and SPD windows than for an EC window.
The simulations were done for a WWR of 45%, however it would be expected that the savings for EC and PV windows would increase when increasing the WWR to for example 60%. In this case the window area would namely increase and more natural daylight can pass through the window which could lower the artificial lighting consumption demand but increases the solar heat gain contribution. Controlling the incoming solar heat and daylight would be expected to be more important for larger window areas and thus higher WWR values.

6.1. Further research opportunities

For the scope of this research project, monocrystalline silicon solar cells were considered to power the smart window, since these have the highest efficiency among the commercially available PV technologies. Besides current semitransparent thin film PV technologies which are available on the market have a relatively low VT value and are colored. These PV technologies are thus less suitable to control the incoming light and to optimize the usage of natural day light.

In chapter 2 different types of semitransparent PV technologies were discussed, but not all of them are assessed in this report. For the EC window it was found that the annual energy consumption load is relatively low, namely lower than 0.4 kWh. In chapter 2 it was mentioned that a LSC window with CIGS in the window edge and with a high visible light transmittance could potentially produce up to 1.4 kWh per year for 1 m^2. It could thus be interesting to investigate the feasibility of integrating this with an EC smart window which appears to be the most promising in terms of building energy consumption savings. A concept design would then be a double glazed window with CIGS in the edge of the outside facing glass pane or in the window frame, an EC window integrated in the indoor facing glass and a high insulating cavity filling such as argon or krypton. Because mainly visible light is then transmitted through the first glass pane and IR is used by the CIGS to produce electricity, it would be expected that the EC would then absorb less IR and heats up less. This also means however that this EC glazing cannot control the same amount of much solar heat that enters the indoor space compared to a normal EC glazing where more IR irradiation reaches the EC glazing. The same can be stated for a neutral colored perovskite PV glazing type which has been proven to transmit visible light while absorbing IR for energy generation. According to [16] the potential energy yield for such PV window would be between 10 and 30 kWh/m^2 in Italy and this is higher than the calculated yearly energy demand for the PDLC and SPD windows. This indicates that perovskite could thus be integrated in both PDLC, SPD and EC. However the disadvantages of perovskite currently include a relatively low stability which indicates a short lifespan and the challenge to increase the size without compromising the power conversion efficiency.

It could be interesting to investigate how to integrate smart window technologies and selective PV technologies which only absorb light in the UV region for energy generation. This could namely give the possibility to produce a self-sustaining smart window which controls both the visible light transmittance and the solar heat gain. Depending on the state of the smart window light in the visible and IR region would be transmitted or reflected.

The potential savings of smart windows for different climates have been investigated, but for further research it could be investigated for different designed indoor temperatures. Besides different window-to-wall ratios and different sizes of rooms could be investigated. It would be expected that for higher WWR values controlling the solar heat and visible light will be more beneficial with respect to a reference window. The effect of the angle of incidence and weather conditions on the SHGC for a transparent and opaque smart window needs to be measured and validated under different temperatures and applied voltages. Also it could be investigated for an open office with multiple windows if it would be feasible to connect these to a central inverter with a shared control unit. Another possibility is to investigate the use of a rooftop PV system designed to power an entire building with smart windows. In the model the SOC of the battery is set to be between 10 and 95% but it could be investigated what is the required battery capacity when the SOC limits would be for example between 20% and 80%.

Regarding the calculation of the diffuse irradiance, this could be calculated using Perez coefficients which have been calibrated by [64] for vertical surfaces in Eindhoven. Here it was found that the currently used Perez coefficients overestimate the incident solar irradiance on vertical surfaces facing south. Also in the model the minimal window coverage by PV is calculated to power smart windows, but the effect of the presence of these PV modules in the glazing is not included in the HVAC calculation.

The model used simplifications for the HVAC calculation which gave different results compared to EnergyPlus. Therefore the model could be made more sophisticated by calculating the heat gains and losses when solving the heat balance equations. However this would increase the simulation time. In the presented model it takes approximately 7 minutes in total to simulate the energy performance of an office room for 16 window technologies, 5 locations and 4 orientations, while in EnergyPlus it takes around 1 minute for a single location, orientation and window technology.

In this work the flow rates for ventilation and infiltration have been considered as a constant, but could instead be changing as a function of the wind speed. Also in the model an average indoor illuminance was calculated and could be investigated for different positions in the office. This way the optimal state of smart windows can be determined such that it maximizes the indoor comfort conditions for all of these positions. At last the PV double skin facade was mentioned in chapter 2 but not modelled in this model. In further research it could be investigated what the potential energy savings would be when implementing a smart window in a double skin facade with highly transparent PV integrated in the outer glass layer.

Bibliography

[1] St1230-75pm dc-smart tint mobile module adapter, 2020. URL https://shop.smarttint.com/ST1230-75PM-DC-Smart-Tint-Mobile-Module-Adapter_p_3256.html. Accessed on 18-03-2020.

[2] PBL Netherlands Environmental Assessment Agency. Assessment of the dutch human environment 2014 – the future is now. 2014. URL https://www.pbl.nl/sites/default/files/downloads/pbl-2014-Assessment-of-the-dutch-human-environment-1597.pdf. Accessed on 10-03-2020.

[3] AKD and JLL. Manage your edc risk. the upcoming rpc regulation for buildings in the netherlands. 2018. URL http://www.jll.nl/netherlands/nl-nl/Research/Manage%20Your%20EPC%20Risk.pdf. Accessed on 13-03-2020.

[4] Allekabels. Soldeertin. URL https://www.allekabels.nl/solderen/102/7717/soldeertin.html. Accessed on 27-06-2020.

[5] D. Arasteh, C. Kohler, and B. Griffith. Modeling windows in energy plus with simple performance indices. 2009. URL https://eta-publications.lbl.gov/sites/default/files/2804e.pdf. Accessed on 26-05-2020.

[6] ASHRAE. Ventilation for acceptable indoor air quality, 2015. URL https://www.ashrae.org/File%20Library/Technical%20Resources/Standards%20and%20Guidelines/Standards%20Addenda/62_1_2013_p_20150707.pdf. Accessed on 19-03-2020.

[7] R. Baetens, B. P. Jelle, and A. Gustavsen. Properties, requirements and possibilities of smart windows for dynamic daylight and solar energy control in buildings: A state-of-the-art review. 2010. URL https://www.sciencedirect.com/science/article/pii/S0927024809002992. Accessed on 02-06-2020.

[8] Banggood. Mppt 5a zonnepaneelregelaar controller batterij opladen 9v 12v 24v automatische schakelaar. URL https://nl.banggood.com/MPPT-5A-Solar-Panel-Regulator-Controller-Battery-Charging-9V-12V-24V-Automatic-Switc
html. Accessed on 02-04-2020.

[9] S. Barman, A. Chowdhury, S. Mathur, and J. Mathur. Assessment of the efficiency of window integrated cdte based semi-transparent photovoltaic module. 2018. URL https://www.sciencedirect.com/science/article/abs/pii/S2210670717308041. Accessed on 21-06-2020.

[10] H. E. Beck, N. E. Zimmermann, T. R. McVicar, N. Vergopolan, A. Berg, and E. F. Wood. Present and future köppen-geiger climate classification maps at 1-km resolution. 2018. URL https://www.nature.com/articles/sdata2018214. Accessed on 10-06-2020.

[11] B.Joseph, T. Pogrebnaya, and B. Kichonge. Semitransparent building-integrated photovoltaic: Review on energy performance, challenges, and future potential. 2019. URL http://downloads.hindawi.com/journals/ijp/2019/5214150.pdf. Accessed on 10-06-2020.

[12] A. Gustavsen D. Arasteh H. Goudey R. Hart B.P. Jelle, A. Hynd. Fenestration of today and tomorrow: A state-of-the-art review and future research opportunities. 2012. URL https://www.sciencedirect.com/science/article/pii/S0927024811004685. Accessed on 28-05-2020.

[13] A. Calcabrini. Integration of pv systems in urban environments. 2017. URL http://resolver.tudelft.nl/uuid:095299ff-8987-47f1-b17f-e9e3d6d9d229. Accessed on 19-03-2020.

[14] A. Cannavale and F. Martellotta. Smart perovskite-based technologies for building integration: a cross-disciplinary approach. 2019. URL https://www.sciencedirect.com/science/article/pii/B9780081026410000190. Accessed on 17-07-2020.

[15] A. Cannavale, G.E. Eperon, P. Cossari, A. Abate, H.J. Snaith, and G. Gigli. Perovskite photovoltachromic cells for building integration. 2015. URL https://doi.org/10.1039/C5EE00896D. Accessed on 17-07-2020.

[16] A. Cannavale, M. Hörantner, G.E. Eperon, H.J. Snaith, F. Fiorito, U. Ayr, and F. Martellotta. Building integration of semitransparent perovskite-based solar cells: Energy performance and visual comfort assessment. 2017. URL https://www.sciencedirect.com/science/article/pii/S0306261917302258. Accessed on 16-07-2020.

[17] D. Chemisana, A. Moreno, M. Polo, C. Aranda, A. Riverola, E.Ortega, C. Lamnatou, A. Domènech, G. Blanco, and A. Cot. Performance and stability of semitransparent opvs for building integration: A benchmarking analysis. 2019. URL https://doi.org/10.1016/j.renene.2018.03.073. Accessed on 07-08-2020.

[18] L. Manzano Chávez. Optimization of a luminescent solar concentrator: Simulation and application in powerwindow design. 2017. URL http://resolver.tudelft.nl/uuid:832a9936-4817-4fbc-a677-234337db68d9. Accessed on 11-07-2020.

[19] C. Cornaro, G. Basciano, V.A. Puggioni, and M Pierro. Energy saving assessment of semitransparent photovoltaic modules integrated into nzeb. 2017. URL https://www.mdpi.com/2075-5309/7/1/9/htm. Accessed on 16-07-2020.

[20] C. Cornaro, L. Renzi, M. Pierro, A. Di Carlo, and A. Guglielmotti. Thermal and electrical characterization of a semi-transparent dye-sensitized photovoltaic module under real operating conditions. 2018. URL https://www.preprints.org/manuscript/201712.0046/v1. Accessed on 16-07-2020.

[21] TSEC Corporation. Tss63tn 6" mono c-si solar cell, 2016. URL http://www.tsecpv.com/upload/media/download_center/Cell_en/4BB/TSS63TN-VCELL%204pad_M2.pdf. Accessed on 18-03-2020.

[22] European Solar Shading Database. European reference glazing standards, 2018. URL https://es-so-database.com/index.php/knowledge. Accessed on 10-06-2020.

[23] N. C. Davy, M. Sezen-Edmonds, J. Gao, X. Lin, A. Liu, N. Yao, A. Kahn, and Y.L. Loo. Pairing of near-ultraviolet solar cells with electrochromic windows for smart management of the solar spectrum. 2017. URL https://doi.org/10.1038/nenergy.2017.104. Accessed on 20-07-2020.

[24] S.K. Deb, S.H. Lee, C. Edwin Tracy, J. Roland Pitts, B.A. Gregg, and H.M. Branz. Standalone photovoltaic-powered electrochromic smart window. 2001. URL https://www.sciencedirect.com/science/article/pii/S0013468601003905. Accessed on 31-05-2020.

[25] E. L. Didoné and A. Wagner. Semi-transparent pv windows: A study for office buildings in brazil. 2013. URL https://www.sciencedirect.com/science/article/pii/S0378778813004982. Accessed on 16-03-2020.

[26] Duracell. Duracell oplaadbare batterij solar rechargeable 400 mah, 2 stuks. URL https://www.hornbach.nl/shop/DURACELL-Oplaadbare-batterij-Solar-Rechargeable-400-mAh-2-stuks/6010848/artikel.html. Accessed on 27-06-2020.

[27] Building Performance Institute Europe. Europe's buildings under the microscope. 2011. URL http://bpie.eu/wp-content/uploads/2015/10/HR_EU_B_under_microscope_study.pdf. Accessed on 03-03-2020.

[28] Building Performance Institute Europe. Activities. impact. achievements. biennial report 2016-2017. 2018. URL http://bpie.eu/wp-content/uploads/2018/07/ANNUAL-REPORT-2016-1017_Digital_Final.pdf. Accessed on 03-03-2020.

[29] Efficient Windows Collaborative (EWC). Window technologies: Glazing types - double low-e glazing with roomside (4th surface) low-e. URL https://www.efficientwindows.org/gtypes_2lowe4.php. Accessed on 11-03-2020.

[30] F. Fiorito, A. Cannavale, and M. Santamouris. Development, testing and evaluation of energy savings potentials of photovoltachromic windows in office buildings. a perspective study for australian climates. 2020. URL https://doi.org/10.1016/j.solener.2020.05.080. Accessed on 17-07-2020.

[31] Center for Big Data Statistics of the Netherlands (CBS). Renewable electricity; production and capacity, 2019. URL https://opendata.cbs.nl/statline/#/CBS/en/dataset/82610ENG/table?ts=1583852558664. Accessed on 10-03-2020.

[32] Center for Big Data Statistics of the Netherlands (CBS). Renewable energy; final use and avoided use of fossil energy, 2020. URL https://opendata.cbs.nl/statline/#/CBS/en/dataset/83109ENG/table?ts=1592946848768. Accessed on 23-06-2020.

[33] T. Gao, T. Ihara, S. Grynning, B.P. Jelle, and A.G. Lien. Perspective of aerogel glazings in energy efficient buildings. 2016. URL https://www.sciencedirect.com/science/article/pii/S0360132315301402. Accessed on 27-05-2020.

[34] Y. Gao. Photovoltaic windows: Theories, devices and applications. 2019. URL https://doi.org/10.4233/uuid:7aa8438c-6106-4c0f-a33f-0ceb8782ad23.

[35] A. Ghosh and T.K. Mallick B. Norton. Daylight characteristics of a polymer dispersed liquid crystal switchable glazing. 2018. URL https://doi.org/10.1016/j.solmat.2017.09.047. Accessed on 23-03-2020.

[36] A. Ghosh and T.K. Mallick B. Norton. Influence of atmospheric clearness on pdlc switchable glazing transmission. 2018. URL https://www.sciencedirect.com/science/article/pii/S0378778818300756. Accessed on 23-03-2020.

[37] A. Ghosh and T.K. Mallick. Evaluation of colour properties due to switching behaviour of a pdlc glazing for adaptive building integration. 2018. URL https://www.sciencedirect.com/science/article/pii/S0960148117312983. Accessed on 23-03-2020.

[38] A. Ghosh and B. Norton. Optimization of pv powered spd switchable glazing to minimise probability of loss of power supply. 2019. URL https://www.sciencedirect.com/science/article/pii/S0960148118309121. Accessed on 25-05-2020.

[39] A. Ghosh, B. Norton, and A. Duffy. Measured overall heat transfer coefficient of a suspended particle device switchable glazing. 2015. URL https://www.sciencedirect.com/science/article/pii/S0306261915010892. Accessed on 03-06-2020.

[40] A. Ghosh, B. Norton, and A. Duffy. First outdoor characterisation of a pv powered suspended particle device switchable glazing. 2016. URL https://www.sciencedirect.com/science/article/pii/S0927024816301088. Accessed on 25-05-2020.

[41] A. Ghosh, B. Norton, and A. Duffy. Daylighting performance and glare calculation of a suspended particle device switchable glazing. 2016. URL https://www.sciencedirect.com/science/article/pii/S0038092X16001602. Accessed on 13-07-2020.

[42] Binswanger Glass. Switchable glass, 2017. URL https://www.binswangerglass.com/blog/switchable-glass. Accessed on 08-08-2020.

[43] Vitro Architectural Glass. How low-e glass works. URL http://glassed.vitroglazings.com/topics/how-low-e-glass-works. Accessed on 16-03-2020.

[44] J. E. Hay and J.A. Davies. Calculation of the solar radiation incident on an inclined surface. 1980.

[45] P. Heinstein, C. Ballif, and L.E. Perret-Aebi. Building integrated photovoltaics (bipv): Review, potentials, barriers and myths. 2013. URL https://www.researchgate.net/publication/272528840_Building_Integrated_Photovoltaics_BIPV_Review_Potentials_Barriers_and_Myths. Accessed on 07-08-2020.

[46] A. Hemaida, A. Ghosh, S. Sundaramand, and T. K. Mallick. Evaluation of thermal performance for a smart switchable adaptive polymer dispersed liquid crystal (pdlc) glazing. 2020. URL https://www.sciencedirect.com/science/article/pii/S0038092X19311247. Accessed on 23-03-2020.

[47] Ltd. InnoGlass Technology (Qingdao) Co. Switchable pdlc film specification, 2020. URL https://www.inno-glass.com/products/switchable-pdlc-film-glass/. Accessed on 18-03-2020.

[48] S. Jansen and E. van den Ham. Warmtebalans en warmte- en koudebehoefte van een gebouw. 2016. URL https://klimapedia.nl/wp-content/uploads/2018/01/Module-warmtebalans-tbv-BK2TE3_V201603b.pdf. Accessed on 25-06-2020.

[49] D.L. King, W.E. Boyson, and J.A. Kratochvill. Photovoltaic array performance model. 2004. URL https://prod-ng.sandia.gov/techlib-noauth/access-control.cgi/2004/043535.pdf. Accessed on 04-05-2020.

[50] E. Kort. Bouwbesluit energiezuinigheid. URL http://www.ekbouwadvies.nl/bouwbesluit/energiezuinigheid/vervangenkozijnen.asp. Accessed on 07-08-2020.

[51] M. Kwon. Energy-efficient office renovation - developing design principles based on user-focused evaluation. 2020. URL http://resolver.tudelft.nl/uuid:a09ca0a2-a53d-49f4-b6af-015609663518. Accessed on 16-03-2020.

[52] Sandia National Laboratories. An industry and national laboratory collaborative to improve photovoltaic performance modeling, 2018. URL https://pvpmc.sandia.gov/. Accessed on 15-12-2019.

[53] B. Lee, J. Z. Liu, B. Sun, C. Y. Shen, and G. C. Dai. Thermally conductive and electrically insulating eva composite encapsulants for solar photovoltaic (pv) cell. 2008. URL http://www.expresspolymlett.com/articles/EPL-0000613_article.pdf. Accessed on 28-05-2020.

[54] E.S. Lee and D.L. DiBartolomeo. Application issues for large-area electrochromic windows in commercial buildings. 2002. URL https://www.sciencedirect.com/science/article/pii/S0927024801001015. Accessed on 13-07-2020.

[55] E.S. Lee, S.E. Selkowitz, R.D. Clear, D.L. DiBartolomeo, J.H. Klems, L.L. Fernandes, G.J. Ward, V. Inkarojrit, and M. Yazdanian. Advancement of electrochromic windows. 2006. URL https://www.osti.gov/servlets/purl/899732. Accessed on 27-05-2020.

[56] D. H. W. Li and J. C. Lam. Measurements of solar radiation and illuminance on vertical surfaces and daylighting implications. 2000. URL https://www.sciencedirect.com/science/article/pii/S0960148199001263. Accessed on 26-06-2020.

[57] B. Y. H. Liu and R. C. Jordan. The interrelationship and of direct, diffuse and characteristic distribution total solar radiation. 1960. Accessed on 26-04-2020.

[58] Sunthru LLC. Aerogel window. URL https://www.sunthru.biz/product-development/. Accessed on 08-08-2020.

[59] N. Lolli and I. Andresen. Aerogel vs. argon insulation in windows: A greenhouse gas emissions analysis. 2016. URL https://www.sciencedirect.com/science/article/pii/S0360132316300713. Accessed on 27-05-2020.

[60] A. Martinez Lopez. Enhancing solar energy integration with innovative mini-modules. 2019. URL http://resolver.tudelft.nl/uuid:44932b07-20d4-4d1f-bd74-f7e02e1077f4. Accessed on 18-03-2020.

[61] L. Lucera, F. Machui, H.D.Schmidt, T. Ahmad, P. Kubis, S. Strohm, J. Hepp, A. Vetter, H.-J. Egelhaaf, and C.J. Brabec. Printed semi-transparent large area organic photovoltaic modules with power conversion efficiencies of close to 5 2017. URL https://www.sciencedirect.com/science/article/abs/pii/S1566119917301167. Accessed on 21-06-2020.

[62] C.S. Polo López and M. Sangiorgi. Comparison assessment of bipv façade semi-transparent modules: further insights on human comfort conditions. 2013. URL https://www.sciencedirect.com/science/article/pii/S1876610214004226. Accessed on 23-06-2020.

[63] P.H. Meijer and R. Verweij. Energieverbruik per functie voor senternovem. 2009. URL http://docplayer.nl/18150687-Energieverbruik-per-functie-voor-senternovem.html. Accessed on 16-03-2020.

[64] M. Meshkinkiya, R.C.G.M. Loonen, R Paolini, and J.L.M Hensen. Calibrating perez model coefficients using subset simulation. 2019. URL https://iopscience.iop.org/article/10.1088/1757-899X/556/1/012017/pdf. Accessed on 12-03-2020.

[65] R. J. Mortimer. Switching colors with electricity. 2013. URL https://www.americanscientist.org/article/switching-colors-with-electricity. Accessed on 07-08-2020.

[66] RVO Netherlands Enterprise Agency. Building regulations, 2012. URL https://business.gov.nl/regulation/building-regulations/. Accessed on 16-03-2020.

[67] NREL. Best research-cell efficiency chart, 2020. URL https://www.nrel.gov/pv/cell-efficiency.html. Accessed on 16-03-2020.

[68] National Renewable Energy Laboratory (NREL). URL https://energyplus.net/. Accessed on 24-04-2020.

[69] National Renewable Energy Laboratory (NREL). System advisor model, 2019. URL https://sam.nrel.gov/. Accessed on 26-05-2020.

[70] Government of the Netherlands. Central government encourages sustainable energy. 2020. URL https://www.government.nl/topics/renewable-energy/central-government-encourages-sustainable-energy. Accessed on 10-03-2020.

[71] M. Oh, S. Roh, M. Jang, and J. Park. Evaluation of heating and cooling load according to applying electrochromic glass to office building envelope in south korea. 2018. URL http://www.sbt-durabi.org/articles/xml/KKMv/. Accessed on 27-05-2020.

[72] M. Oh, C. Lee, J. Park, K. Lee, and S. Tae. Evaluation of energy and daylight performance of old office buildings in south korea with curtain walls remodeled using polymer dispersed liquid crystal (pdlc) films. 2019. URL https://www.mdpi.com/1996-1073/12/19/3679/htm. Accessed on 27-05-2020.

[73] L. Olivieri, E. Caamaño-Martín, F.J. Moralejo-Vázquez, N. Martín-Chivelet, F.Olivieri, and F.J.Neila-Gonzalez. Energy saving potential of semi-transparent photovoltaic elements for building integration. 2014. URL https://www.sciencedirect.com/science/article/pii/S0360544214009906. Assessed on 16-03-2020.

[74] I. Papathanasiou. Smart window integration into the building envelope: Implementation of a smart window integrated by luminescent solar concentrators into the building envelope– large-scale application: main facade of civil engineering building of tu delft. 2016. URL http://resolver.tudelft.nl/uuid:75b6d07c-0a6d-43a6-a6f4-0966f4d8fb95. Accessed on 23-06-2020.

[75] M. Cordoba Parra. Dimmable fenestration and incorporated photovoltaic design: Smart window design with pdlc and al-bsf cells. 2019. URL http://resolver.tudelft.nl/uuid:e60ae39e-6044-4acd-b577-31726bfb858c. Accessed on 20-01-2020.

[76] J. Peng, D.C. Curcija, L. Lu, S.E. Selkowitz, H. Yang, and W. Zhang. Numerical investigation of the energy saving potential of a semi-transparent photovoltaic double-skin facade in a cool-summer mediterranean climate. 2016. URL https://www.sciencedirect.com/science/article/pii/S0306261915016475. Accessed on 22-06-2020.

[77] J. Peng, H. Goudey, A. Thanachareonkit, D.C. Curcija, and E. Lee. Measurement verification of the performance of solaria bipv in flexlab test facility. 2017. URL https://flexlab.lbl.gov/sites/default/files/solaria-bipv-flexlab.pdf. Accessed on 21-06-2020.

[78] J. Peng, D.C. Curcija, A. Thanachareonkit, E.S. Lee, H. Goudey, and S.E. Selkowitz. Study on the overall energy performance of a novel c-si based semitransparent solar photovoltaic window. 2019. URL https://doi.org/10.1016/j.apenergy.2019.03.107. Accessed on 27-05-2020.

[79] R. Perez, P. Ineichen, R. Seals, J. Michalsky, and R. Stewart. Modeling daylight availability and irradiance components from direct and global irradiance. 1990. URL https://www.sciencedirect.com/science/article/pii/0038092X9090055H. Accessed on 27-05-2020.

[80] Philips. Master ledtube 1500mm ue 21.5w 840 t8, 2020. URL https://www.lighting.philips.com/main/prof/led-lamps-and-tubes/led-tubes/master-ledtube-em-mains-t8/929001377002_EU/product. Accessed on 17-03-2020.

[81] A. Piccolo and F. Simone. Performance requirements for electrochromic smart window. 2015. URL https://www.sciencedirect.com/science/article/pii/S2352710215300073. Accessed on 11-03-2020.

[82] C.F. Reinhart, J.A. Jakubiec, and D. Ibarra. Definition of a reference office for standardized evaluations 2 of dynamic facade and lighting technologies. 2013. URL http://web.mit.edu/sustainabledesignlab/publications/ReferenceOffice_BuildingSimularion2013.pdf. Accessed on 27-12-2019.

[83] S.D. Rezaei, S. Shannigrahi, and S. Ramakrishna. A review of conventional, advanced, and smart glazing technologies and materials for improving indoor environment. 2017. URL https://www.sciencedirect.com/science/article/pii/S0927024816303178. Accessed on 11-03-2020.

[84] SageGlass. Sageglass climaplus classic 42.1ec-12-4. electronically tintable glazing for curtain walls, windows and skylights, 2017. URL https://www.sageglass.com/sites/default/files/sageglass_datasheet_climaplus_42.1ec-12-4_classic_en.pdf. Accessed on 20-07-2020.

[85] Sanko. Sanko solar product- advantages. URL https://www.sanko-solar.nl/nl/downloads. Accessed on 17-06-2020.

[86] S. Shreea. Modeling the energy yield of the powerwindow. 2018. URL http://resolver.tudelft.nl/uuid:c26a5edd-5c45-4e1a-bc1c-22b745be19fb. Accessed on 23-06-2020.

[87] A. Smets, K. Jäger, O. Isabella, R. van Swaaij, and M. Zeman. *Solar Energy: The Physics and Engineering of Photovoltaic Conversion, Technologies and Systems*. UIT Cambridge, 2016.

[88] Onyx Solar. Onyx solar csi specifications example ii double laminated crystalline glass, 2011. URL http://www.onyxsolardownloads.com/docs/Onyx-Solar-CSI-Specifications-Example-II-double-laminated-Crystallyne-glass-f.pdf. Accessed on 09-07-2020.

[89] D. Suszanowicz. Internal heat gain from different light sources in the building lighting systems. 2017. URL https://www.e3s-conferences.org/articles/e3sconf/pdf/2017/07/e3sconf_eems2017_01024.pdf. Accessed on 11-03-2020.

[90] Engineering ToolBox. Metabolic heat gain from persons, 2004. URL https://www.engineeringtoolbox.com/metabolic-heat-persons-d_706.html. Accessed on 04-06-2020.

[91] Engineering ToolBox. Metals and alloys - densities, 2004. URL https://www.engineeringtoolbox.com/metal-alloys-densities-d_50.html. Accessed on 27-06-2020.

[92] Engineering ToolBox. Air - specific heat at constant pressure and varying temperature, 2004. URL https://www.engineeringtoolbox.com/air-specific-heat-capacity-d_705.html. Accessed on 10-08-2020.

[93] Engineering ToolBox. Air - density, specific weight and thermal expansion coefficient at varying temperature and constant pressures, 2004. URL https://www.engineeringtoolbox.com/air-density-specific-weight-d_600.html. Accessed on 10-08-2020.

[94] Engineering ToolBox. Water vapor - specific heat, 2005. URL https://www.engineeringtoolbox.com/water-vapor-d_979.html. Accessed on 10-08-2020.

[95] Express Toughening. URL http://www.expresstoughening.com/. Accessed on 11-08-2020.

[96] Climate Action Tracker. Temperatures, 2019. URL https://climateactiontracker.org/global/temperatures/. Accessed on 28-06-2020.

[97] A. C. van der Linden, A. C. Boerstra, A. K. Raue, S. R. Kurvers, and R. J.de Dear. Adaptive temperature limits: A new guideline in the netherlands: A new approach for the assessment of building performance with respect to thermal indoor climate. 2006.

[98] P. A. Waide and B. Norton. Variation of insolation transmission with glazing plane position and sky conditions. 2003. URL https://doi.org/10.1115/1.1563630. Accessed on 24-04-2020.

[99] M. Wang, J. Peng, N. Li, H. Yang, C. Wang, X. Li, and T. Lu. Comparison of energy performance between pv double skin facades and pv insulating glass units. 2017. URL https://www.sciencedirect.com/science/article/pii/S0306261917302374. Accessed on 22-06-2020.

[100] R. Weegink. Next generation shade-tolerant reconfigurable pv modules for urban landscapes. 2019. URL http://resolver.tudelft.nl/uuid:b5a9c63a-c692-4cf8-ba64-363002323040. Accessed on 10-06-2020.

[101] W. Zhang and L. Lu. Overall energy assessment of semi-transparent photovoltaic insulated glass units for building integration under different climate conditions. 2019. URL https://www.sciencedirect.com/science/article/pii/S0960148118313636. Accessed on 18-06-2020.

A

Yearly energy consumption and generation

Here the yearly energy consumption and generation for different locations and orientations are plotted. The smart windows are optimized for the lowest total energy consumption.

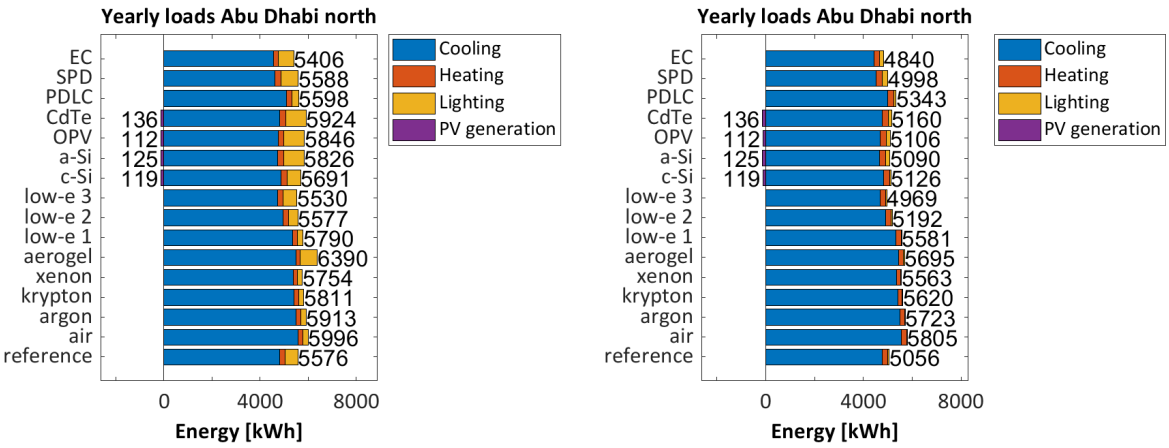

(a) Constant light source.

(b) Adjustable light source.

Figure A.1: The yearly cooling, heating and lighting loads and energy generated for an office room in Abu Dhabi with an orientation towards north when optimizing for lowest energy consumption.

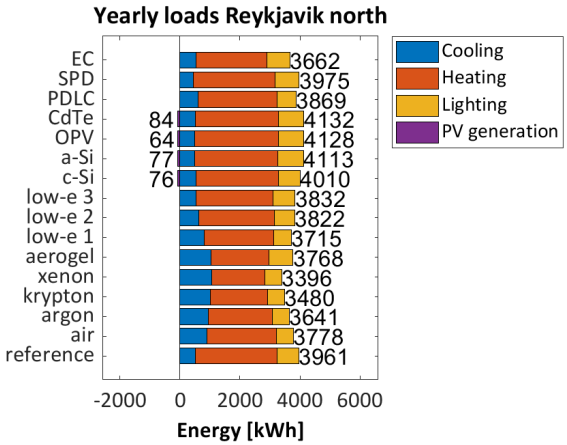

(a) Constant light source.

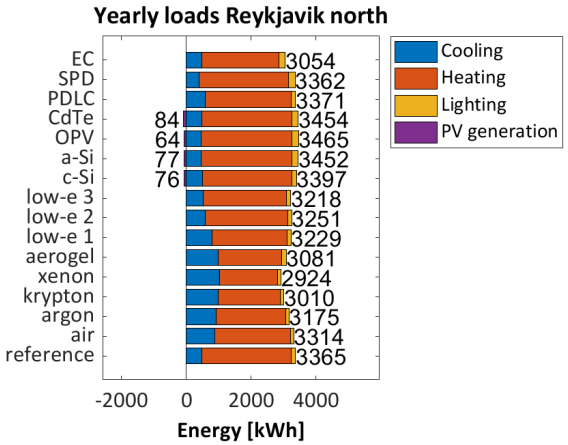

(b) Adjustable light source.

Figure A.2: The yearly cooling, heating and lighting loads and energy generated for an office room in Reykjavik with an orientation towards north when optimizing for lowest energy consumption.

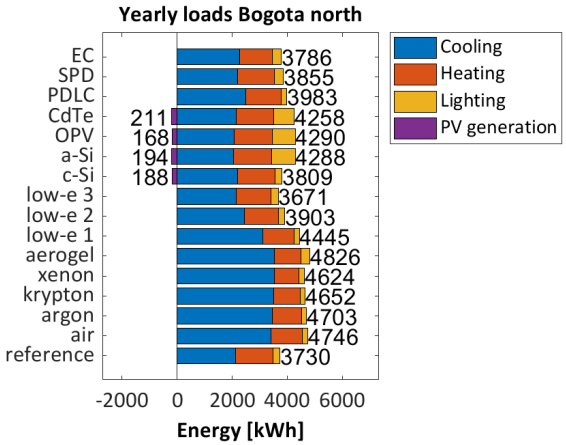

(a) Constant light source.

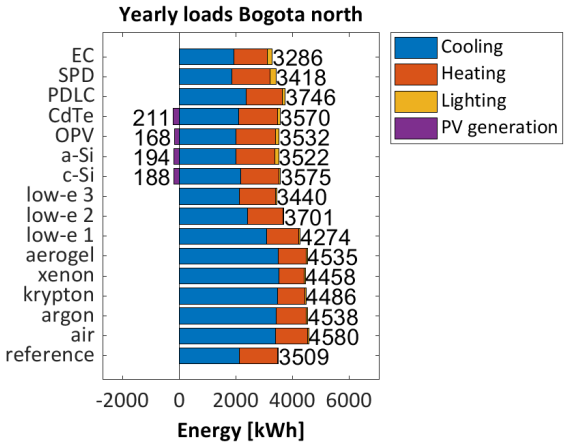

(b) Adjustable light source.

Figure A.3: The yearly cooling, heating and lighting loads and energy generated for an office room in Bogota with an orientation towards north when optimizing for lowest energy consumption.

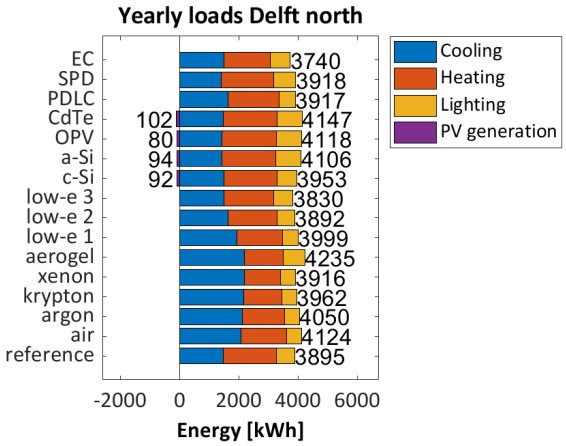

(a) Constant light source.

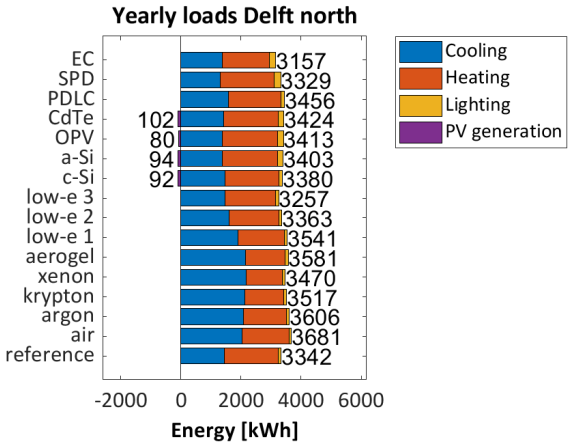

(b) Adjustable light source.

Figure A.4: The yearly cooling, heating and lighting loads and energy generated for an office room in Delft with an orientation towards north when optimizing for lowest energy consumption.

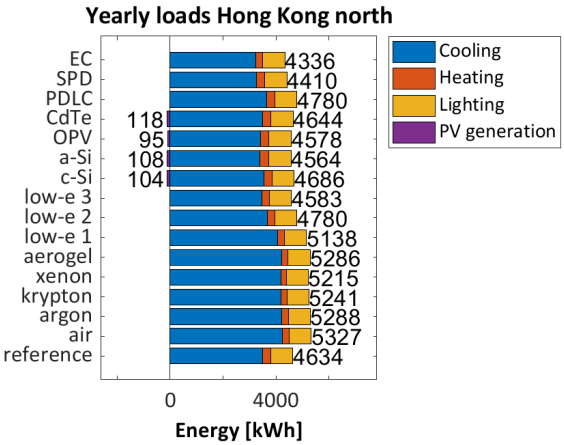

(a) Constant light source.

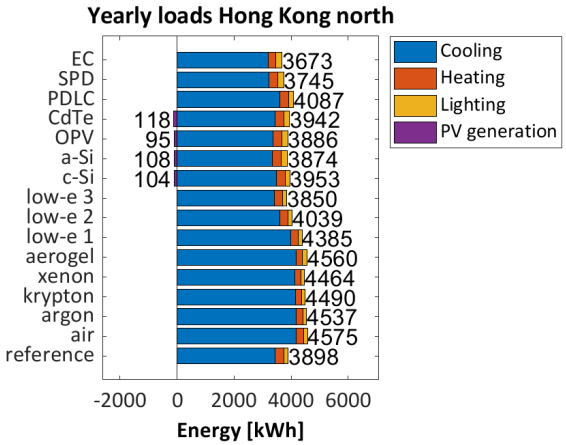

(b) Adjustable light source.

Figure A.5: The yearly cooling, heating and lighting loads and energy generated for an office room in Hong Kong with an orientation towards north when optimizing for lowest energy consumption.

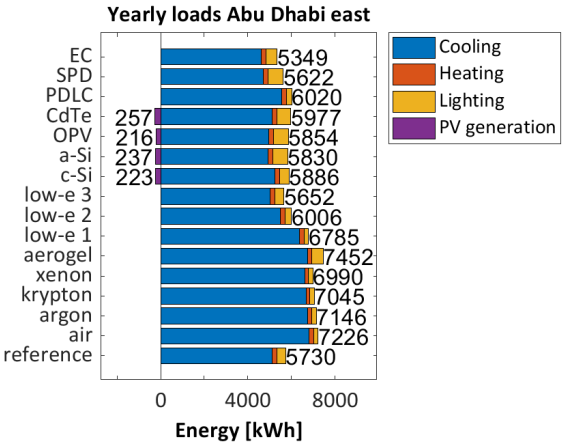

(a) Constant light source.

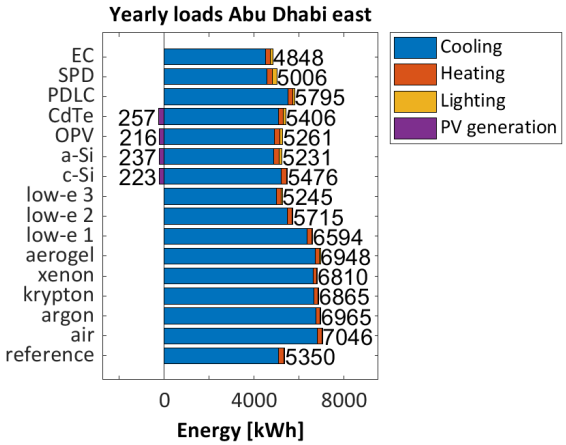

(b) Adjustable light source.

Figure A.6: The yearly cooling, heating and lighting loads and energy generated for an office room in Abu Dhabi with an orientation towards east when optimizing for lowest energy consumption.

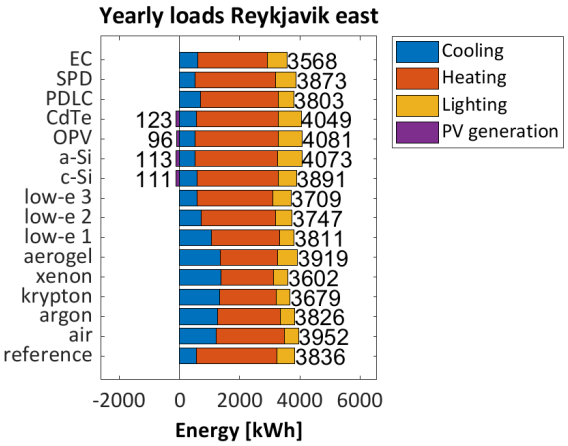

(a) Constant light source.

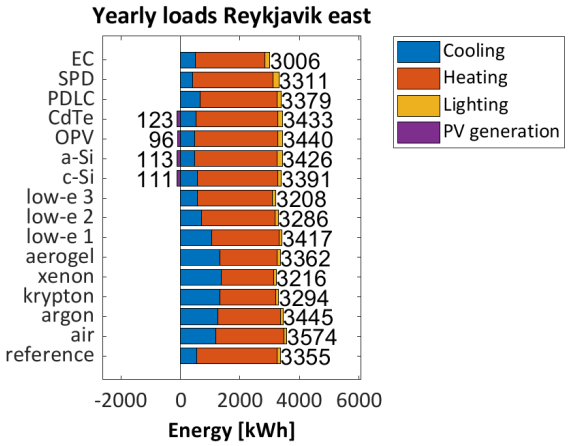

(b) Adjustable light source.

Figure A.7: The yearly cooling, heating and lighting loads and energy generated for an office room in Reykjavik with an orientation towards east when optimizing for lowest energy consumption.

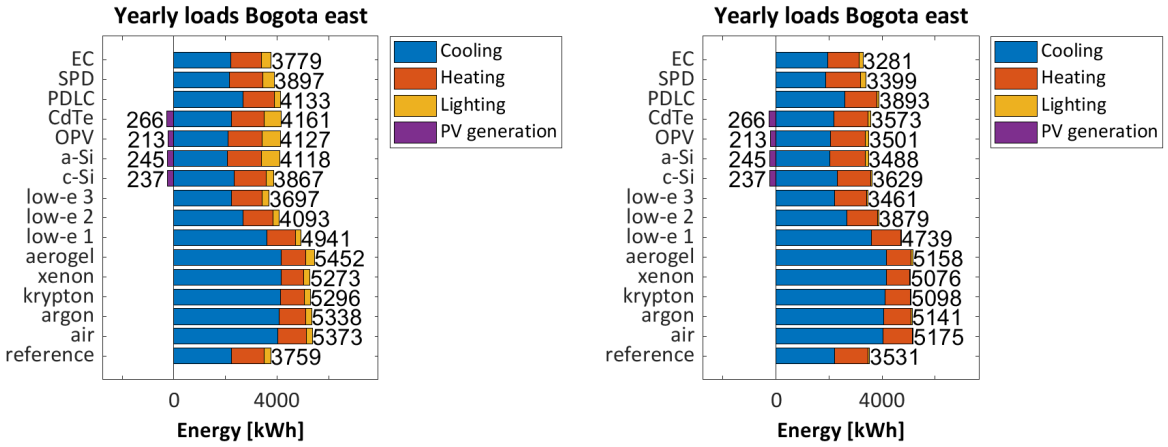

(a) Constant light source.

(b) Adjustable light source.

Figure A.8: The yearly cooling, heating and lighting loads and energy generated for an office room in Bogota with an orientation towards east when optimizing for lowest energy consumption.

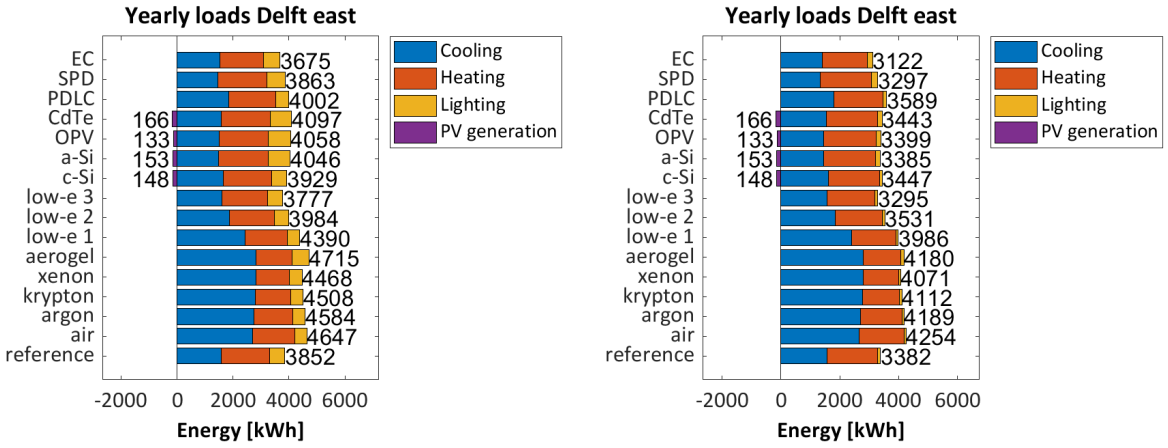

(a) Constant light source.

(b) Adjustable light source.

Figure A.9: The yearly cooling, heating and lighting loads and energy generated for an office room in Delft with an orientation towards east when optimizing for lowest energy consumption.

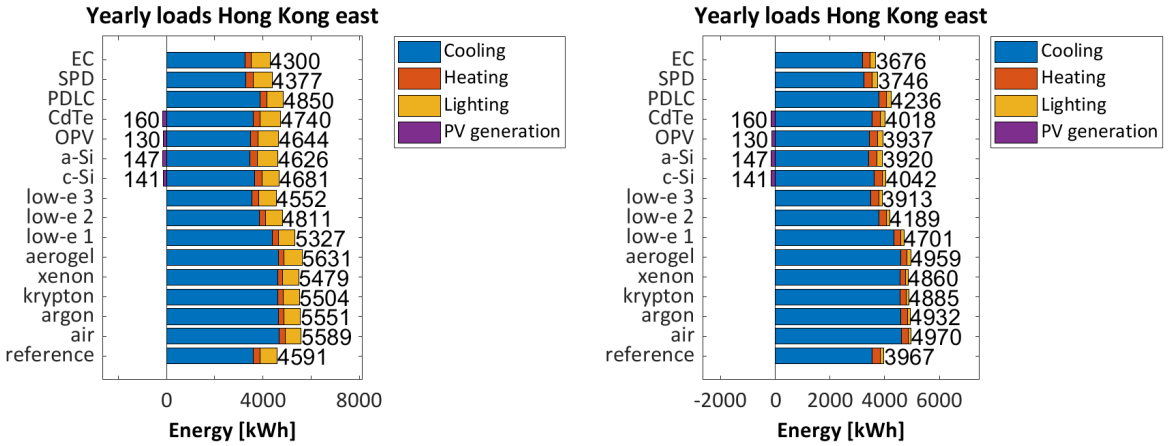

(a) Constant light source.

(b) Adjustable light source.

Figure A.10: The yearly cooling, heating and lighting loads and energy generated for an office room in Hong Kong with an orientation towards east when optimizing for lowest energy consumption.

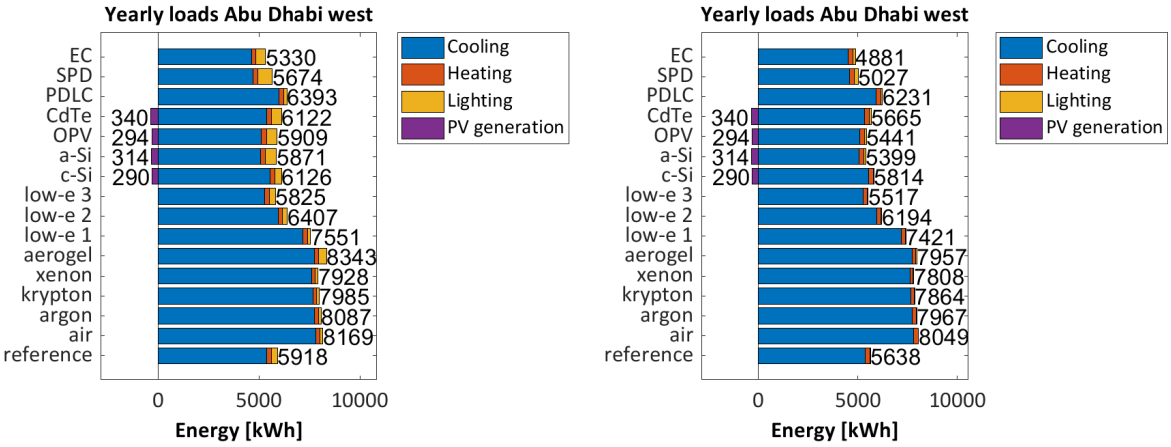

(a) Constant light source.

(b) Adjustable light source.

Figure A.11: The yearly cooling, heating and lighting loads and energy generated for an office room in Abu Dhabi with an orientation towards west when optimizing for lowest energy consumption.

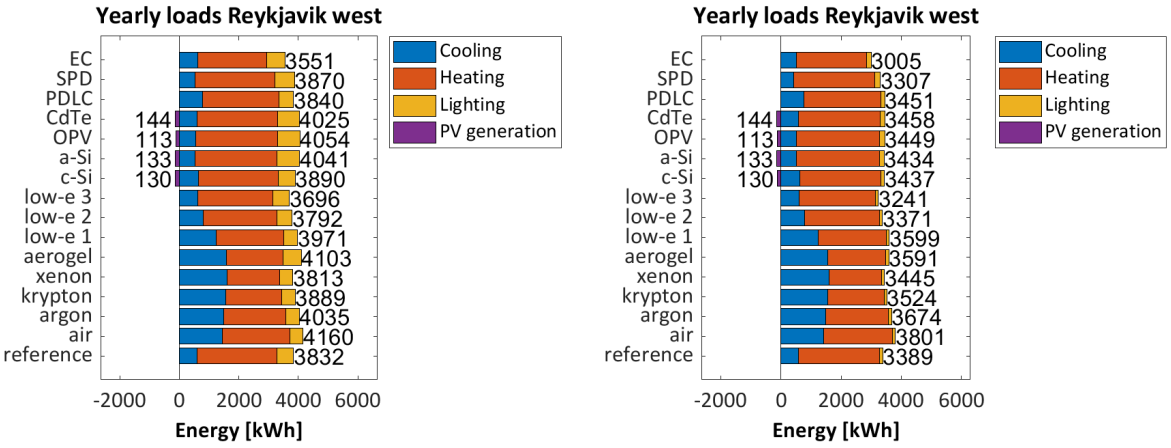

(a) Constant light source.

(b) Adjustable light source.

Figure A.12: The yearly cooling, heating and lighting loads and energy generated for an office room in Reykjavik with an orientation towards west when optimizing for lowest energy consumption.

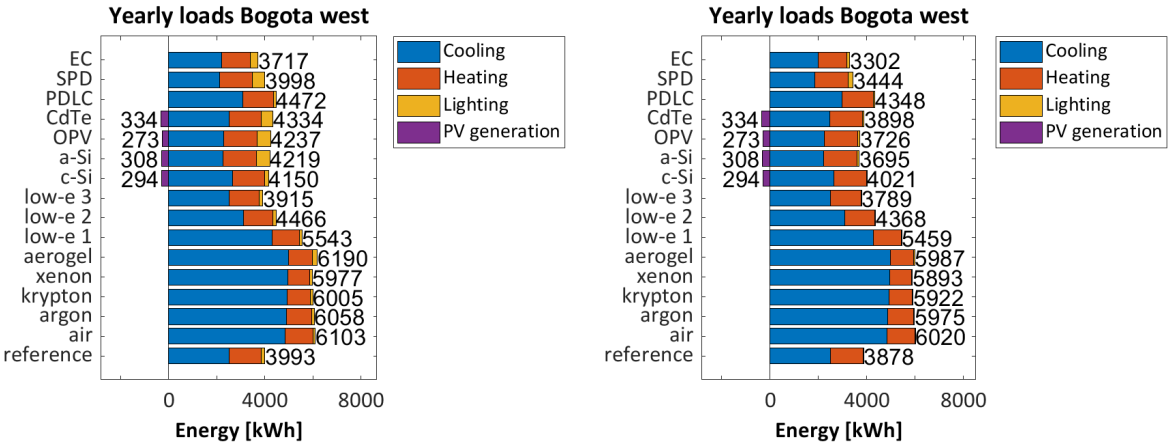

(a) Constant light source.

(b) Adjustable light source.

Figure A.13: The yearly cooling, heating and lighting loads and energy generated for an office room in Bogota with an orientation towards west when optimizing for lowest energy consumption.

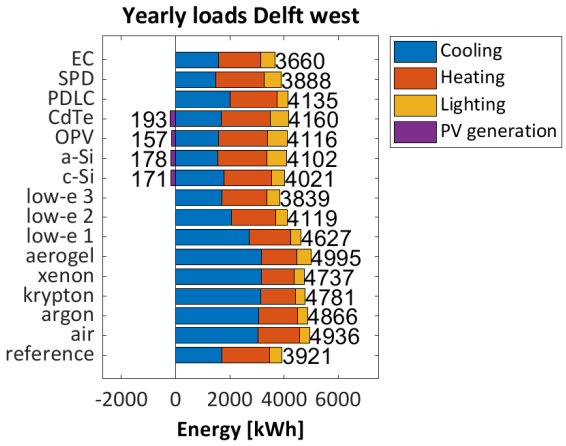

(a) Constant light source.

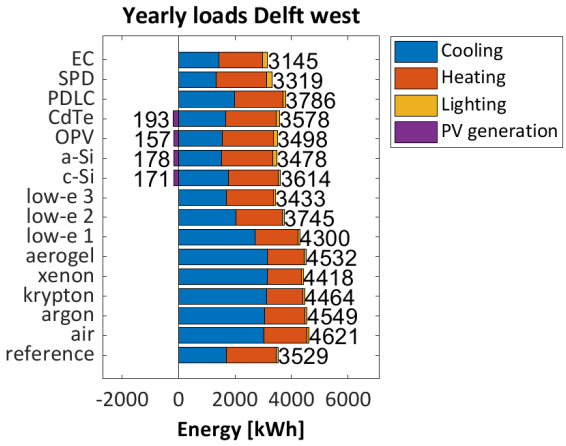

(b) Adjustable light source.

Figure A.14: The yearly cooling, heating and lighting loads and energy generated for an office room in Delft with an orientation towards west when optimizing for lowest energy consumption.

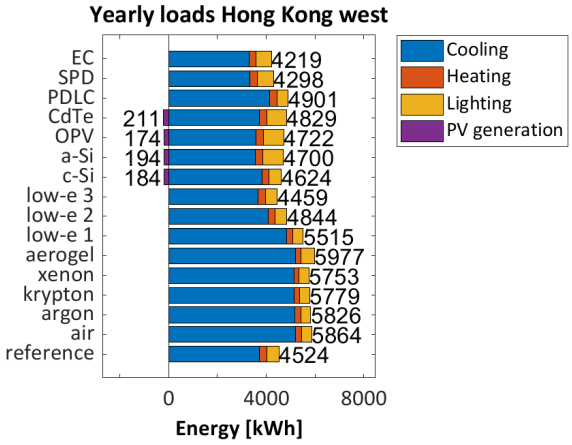

(a) Constant light source.

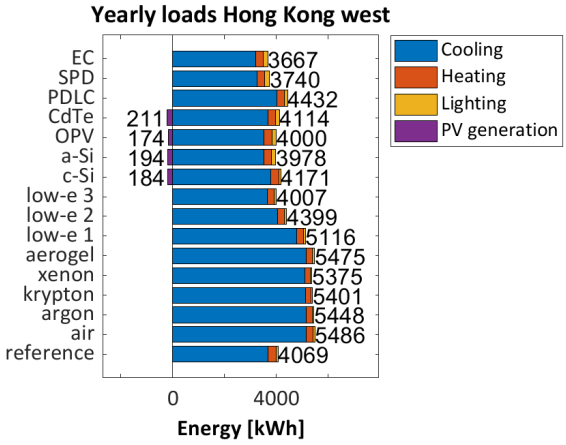

(b) Adjustable light source.

Figure A.15: The yearly cooling, heating and lighting loads and energy generated for an office room in Hong Kong with an orientation towards west when optimizing for lowest energy consumption.

B

Potential energy savings

Here the potential energy savings of different window technologies with respect to a reference window are plotted. This is done for different orientations and locations. The smart windows are optimized for the lowest total energy consumption.

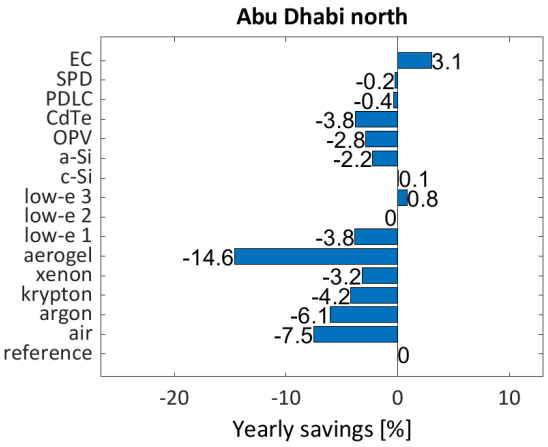

(a) Constant light source.

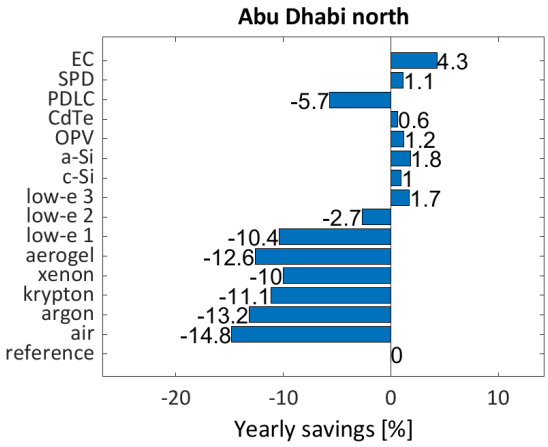

(b) Adjustable light source.

Figure B.1: The yearly potential energy savings for an office room in Abu Dhabi with an orientation towards north.

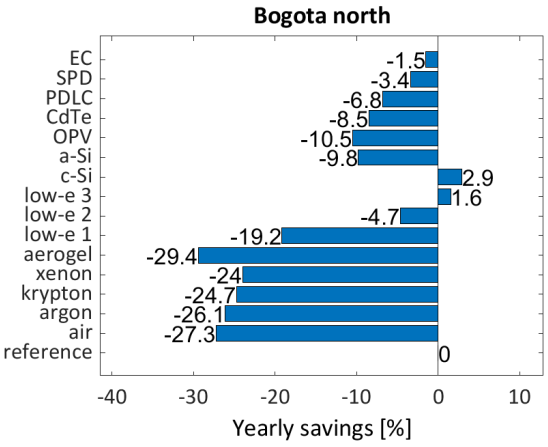

(a) Constant light source.

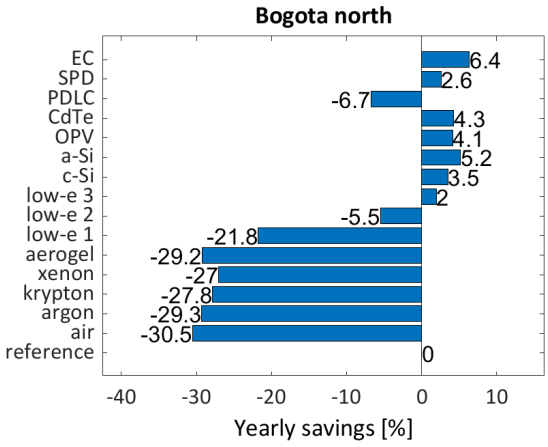

(b) Adjustable light source.

Figure B.2: The yearly potential energy savings for an office room in Bogota with an orientation towards north.

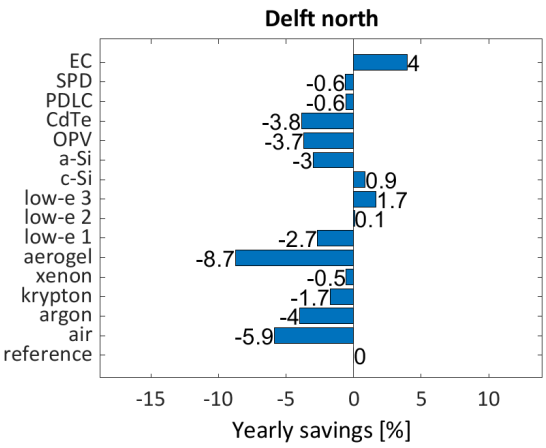

(a) Constant light source.

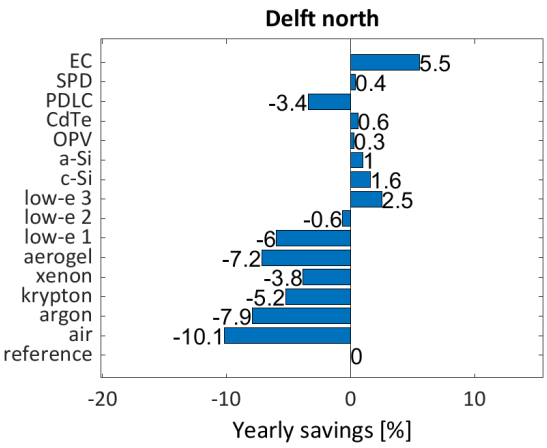

(b) Adjustable light source.

Figure B.3: The yearly potential energy savings for an office room in Delft with an orientation towards north.

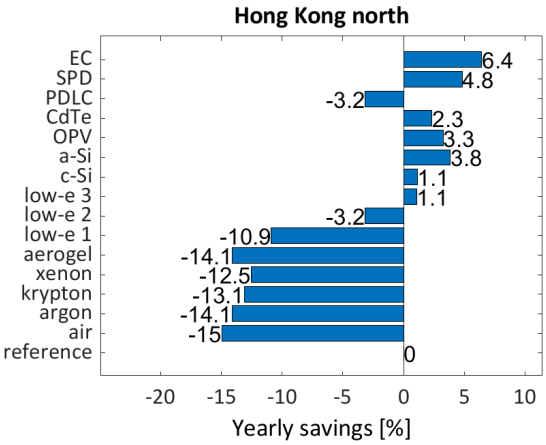

(a) Constant light source.

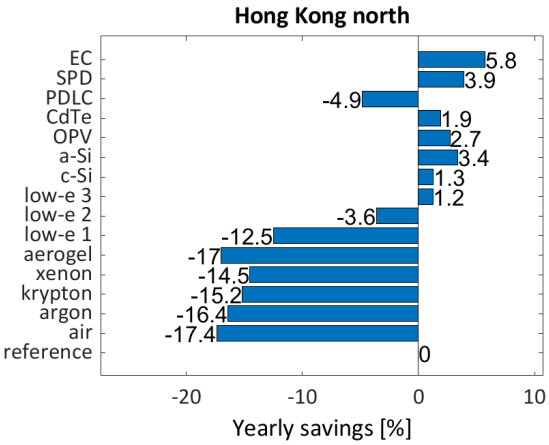

(b) Adjustable light source.

Figure B.4: The yearly cooling, heating and lighting loads and energy generated for an office room in Hong Kong with an orientation towards north.

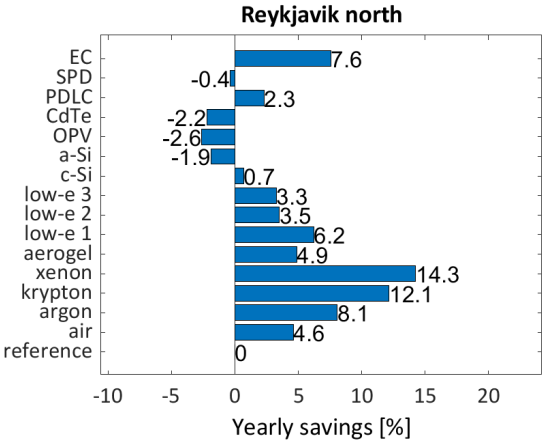

(a) Constant light source.

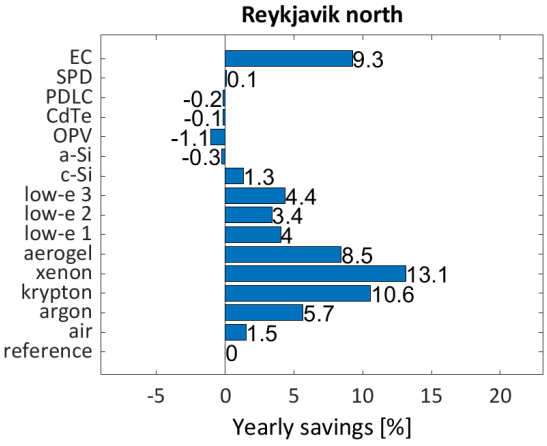

(b) Adjustable light source.

Figure B.5: The yearly potential energy savings for an office room in Reykjavik with an orientation towards north.

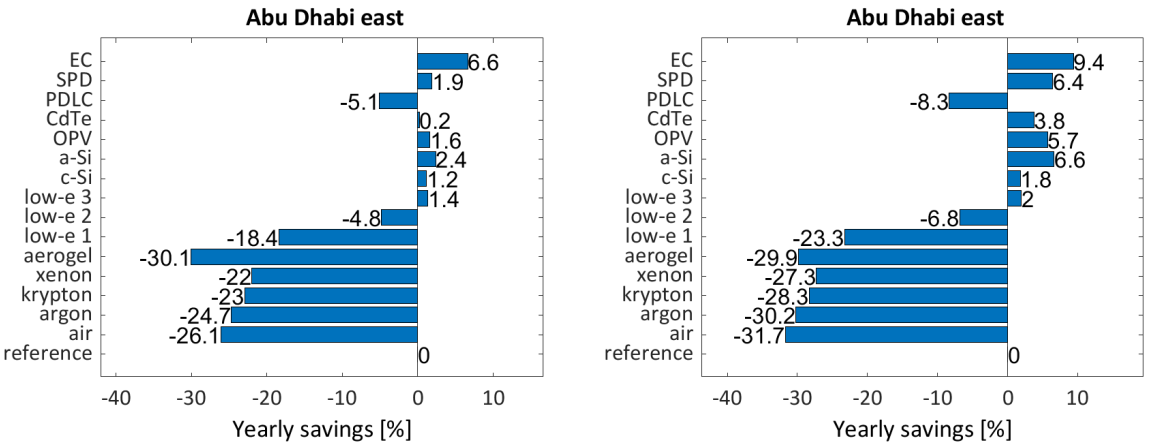

(a) Constant light source.

(b) Adjustable light source.

Figure B.6: The yearly potential energy savings for an office room in Abu Dhabi with an orientation towards east.

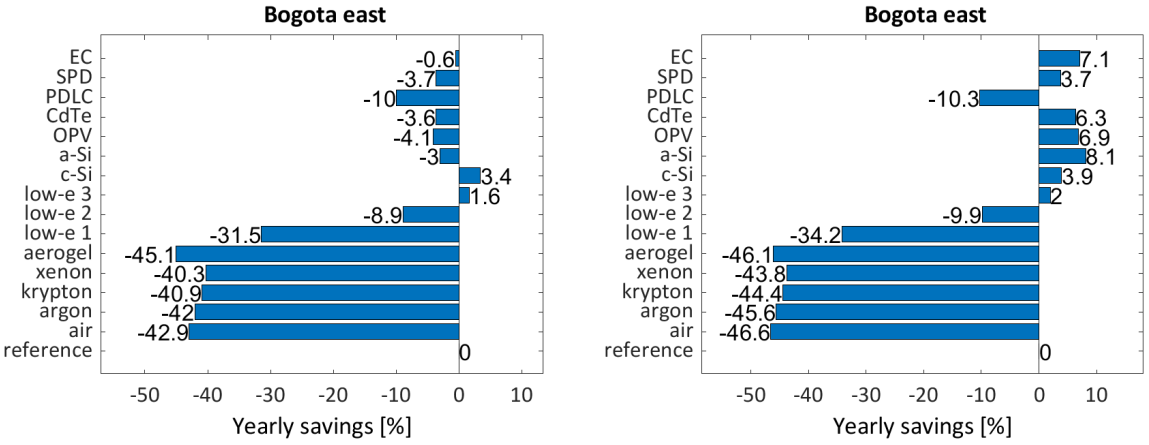

(a) Constant light source.

(b) Adjustable light source.

Figure B.7: The yearly potential energy savings for an office room in Bogota with an orientation towards east.

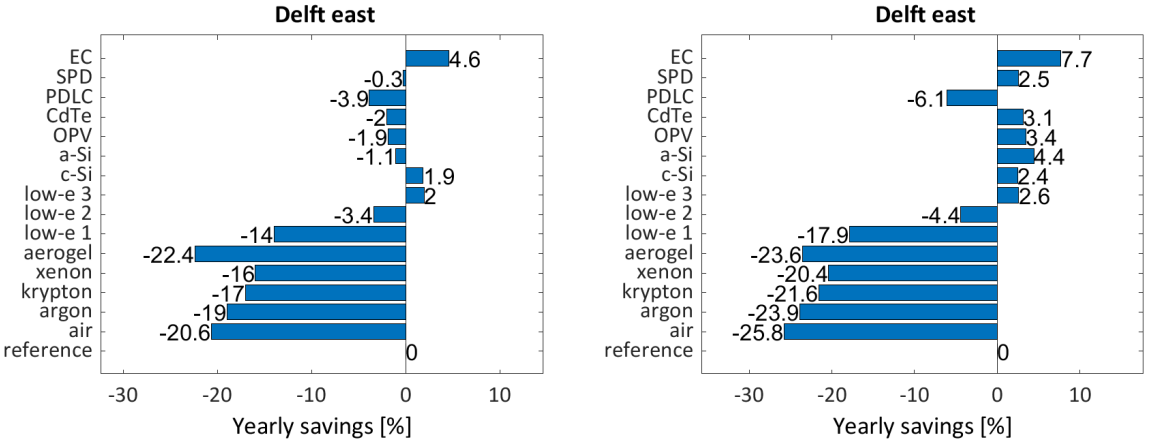

(a) Constant light source.

(b) Adjustable light source.

Figure B.8: The yearly potential energy savings for an office room in Delft with an orientation towards east.

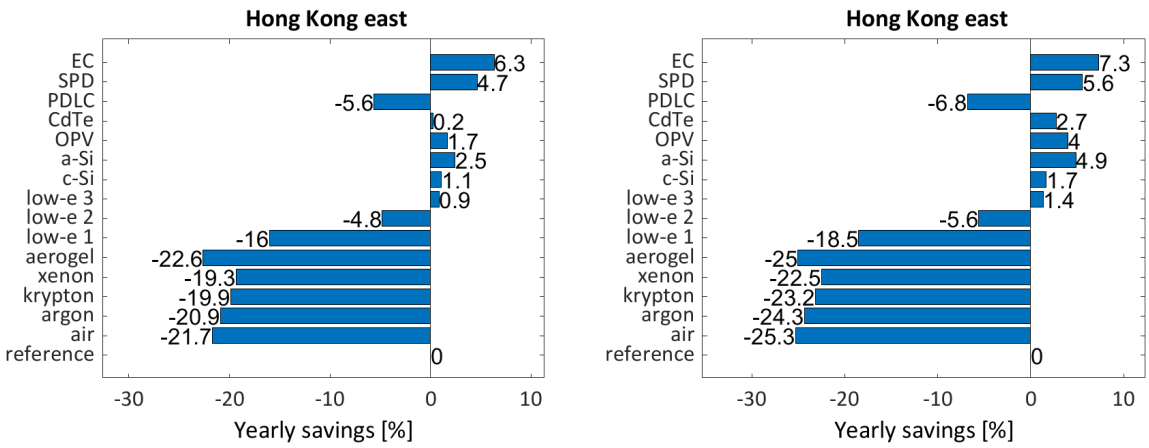

(a) Constant light source.

(b) Adjustable light source.

Figure B.9: The yearly cooling, heating and lighting loads and energy generated for an office room in Hong Kong with an orientation towards east.

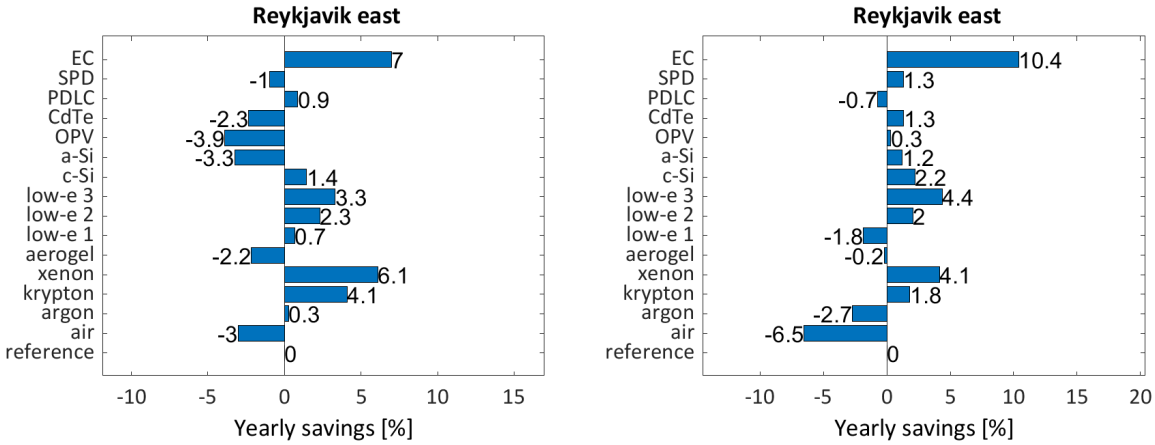

(a) Constant light source.

(b) Adjustable light source.

Figure B.10: The yearly potential energy savings for an office room in Reykjavik with an orientation towards east.

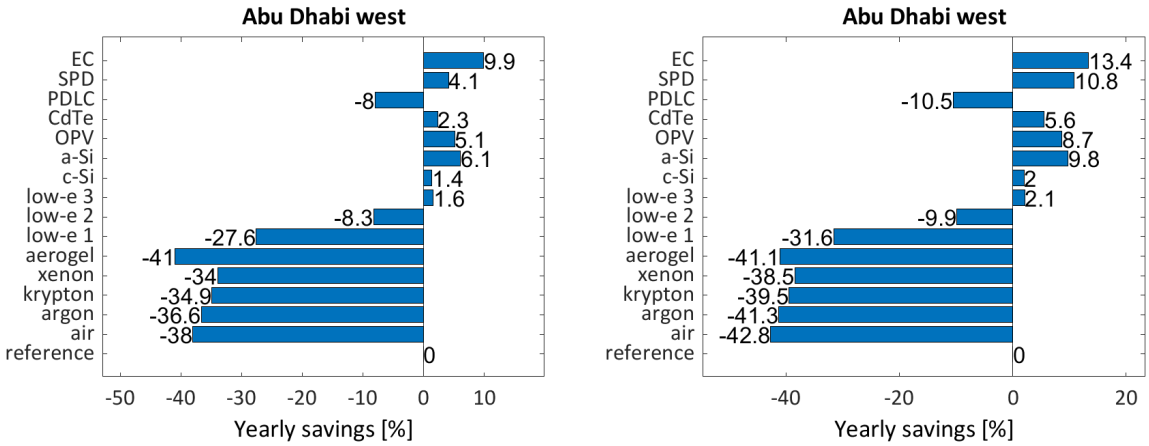

(a) Constant light source.

(b) Adjustable light source.

Figure B.11: The yearly potential energy savings for an office room in Abu Dhabi with an orientation towards west.

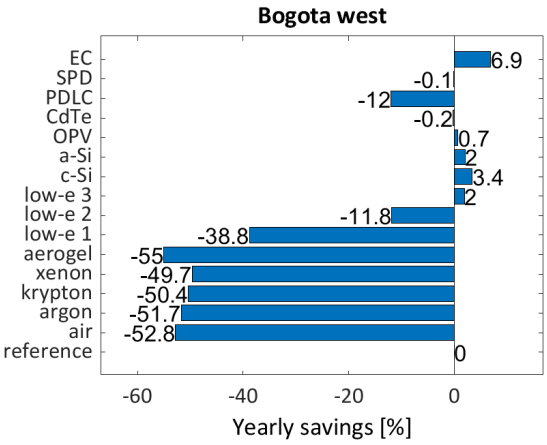

(a) Constant light source.

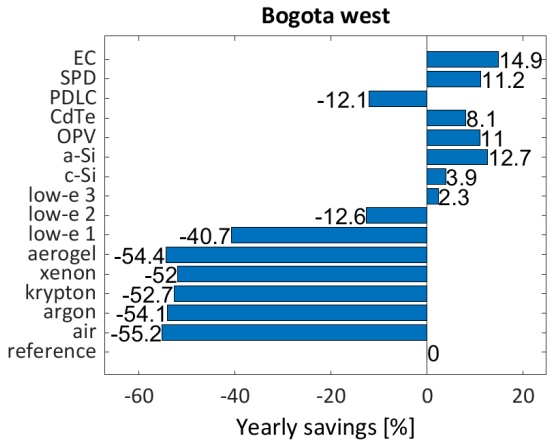

(b) Adjustable light source.

Figure B.12: The yearly potential energy savings for an office room in Bogota with an orientation towards west.

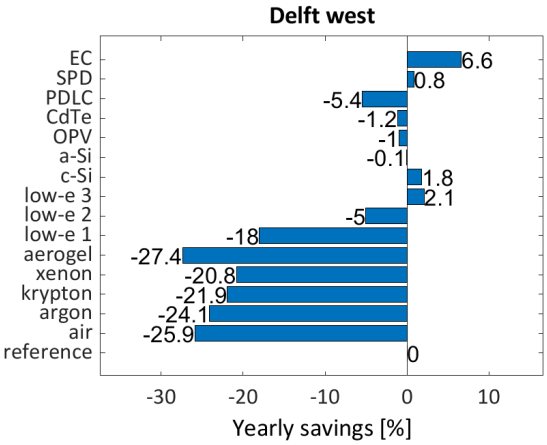

(a) Constant light source.

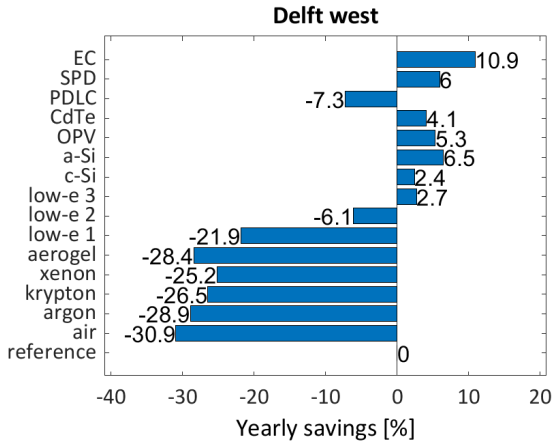

(b) Adjustable light source.

Figure B.13: The yearly potential energy savings for an office room in Delft with an orientation towards west.

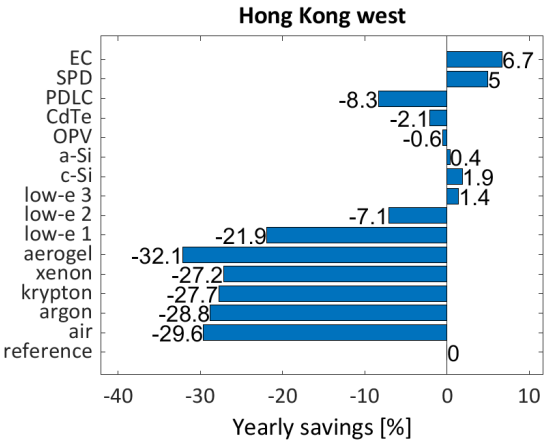

(a) Constant light source.

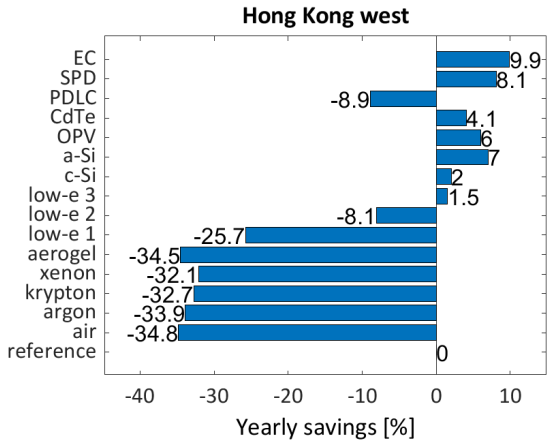

(b) Adjustable light source.

Figure B.14: The yearly cooling, heating and lighting loads and energy generated for an office room in Hong Kong with an orientation towards west.

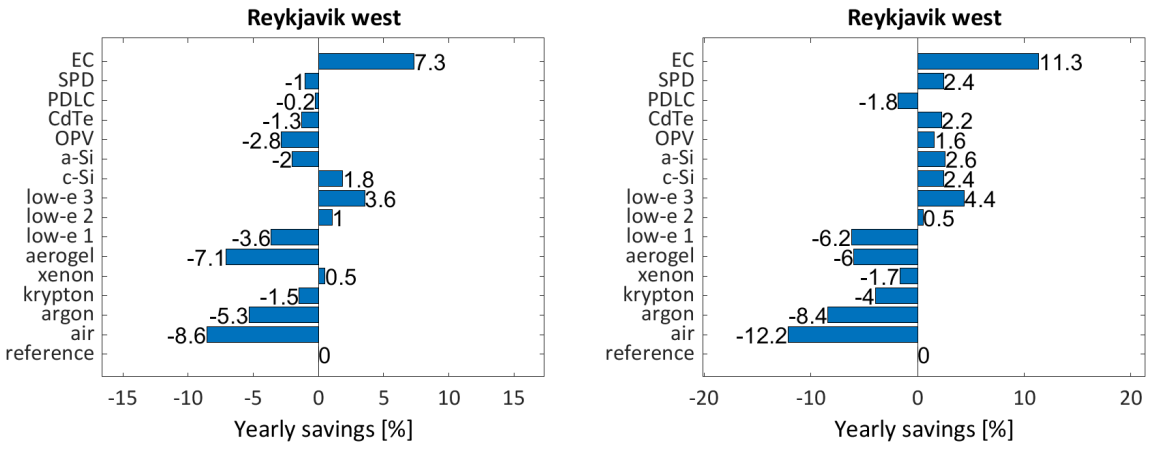

(a) Constant light source.

(b) Adjustable light source.

Figure B.15: The yearly potential energy savings for an office room in Reykjavik with an orientation towards west.